CRANFIELD UNIVERSITY

ABDULMAJID ADDALI

MONITORING GAS VOID FRACTION IN TWO-PHASE FLOW WITH ACOUSTIC EMISSION

SCHOOL OF ENGINEERING

PhD THESIS
Academic Year: 2009 - 2010

Supervisor: Dr. David Mba
April 2010

CRANFIELD UNIVERSITY

SCHOOL OF ENGINEERING

PhD THESIS

Academic Year: 2009 - 2010

ABDULMAJID ADDALI

Monitoring gas void fraction in two-phase flow with Acoustic Emission

Supervisor: Dr David Mba

April 2010

Doctor of Philosophy

© Cranfield University 2010. All rights reserved. No part of this publication may be reproduced without the written permission of the copyright owner.

ABSTRACT

The two-phase gas/liquid flow phenomenon can be encountered over a range of gas and liquid flow rates in the chemical engineering industry, particularly in oil and gas production transportation pipelines. Monitoring and measurement of their characteristics, such as the gas void fraction, are necessary to minimise the disruption of downstream process facilities. Thus, over the last decade, the investigation, development and use of multiphase flow metering system have been a major focus for the industry worldwide. However, these meters suffer from several limitations in some flow conditions such as Slug flow regime.

This research presents experimental results correlating Acoustic Emission measurements with Gas Void Fraction (GVF) in a two-phase air / water flow. A unique experimental facility was modified to accommodate an investigation into the applicability of the Acoustic Emission (AE) technology in monitoring two-phase gas\liquid flow. The testing facility allowed for investigations over a range of superficial liquid velocities (0.3 to 2.0 ms-1) and superficial gas velocities (0.2 to 1.4 ms-1). The influence of several variables such as temperature, viscosity and surface roughness were also investigated. Measurements of AE for varying gas void fractions were compared to conductive probe measurements and results showed a direct correlation between the AE energy and the gas void fraction.

It is concluded that the GVF can be determined by measurement of Acoustic Emission and this forms the major contribution of this thesis.

Keywords:

AE, slug flow, gas void fraction, process monitoring

ACKNOWLEDGEMENTS

In the name of God, the most Gracious, the most Compassionate

I would like to express my deep sincere gratitude to my supervisor Dr. David Mba, for his guidance and support throughout the time of this research project. His wide knowledge suggestions, comments and experience contributed significantly in this research work and my way of thinking.

I would like to thank Libyan government for supporting my tuition and fees during this Doctorate study.

I would like to thank my friends, Dr Salem Allababidi and Dr Firoz Khan for their valuable support and advice to undertake this research work.

I would also like to express my sincere thanks to Josh Redmond for his administrative support.

This would be incomplete without sincere thanks to my Late Father who always encouraged me to achieve the best, and to my Mother and my wife for their support and faith in me during the hardship…

To my beloved sons, Abdulrahman and Annas

April 2010

TABLE OF CONTENTS

LIST OF FIGURES

LIST OF TABLES

NOMENCLATURE

Symbol	Denotes
V_{SL}	Liquid superficial velocity
V_{SG}	Gas superficial velocity
V_M and V_{mix}	Mixed velocity
Q_L	Liquid flow rate
Q_G	Gas flow rate
A	Cross section area of the pipe
GVF and ε	Gas void fraction
E_L	Liquid hold-up
M	Total mass flow rate
$\rho_G, \rho_w, and\ \rho_O$	Densities of gas, liquid and oil phases respectively
$V_G, V_w, and\ V_O$	Velocities of gas, water and liquid phases respectively
$\alpha_G, \alpha_w, and\ \alpha_O$	Gas, water and oil phase fractions respectively
R_{XY}	Cross correlation function
V	Velocity of the flow
L	Distance between two sensors
τ	Lag time between two correlated signals
Z_e	Electrical impedance
R_m	Electrical resistance

C_M	Electrical capacitance
C_P	Steel pipe electrical capacitance
ω	Signal frequency
f_c	Sensor frequency
σ_w	Water conductivity
ε_w	Water permittivity
V_i	Reference voltage and equal to 1µ-Volt
V_o	Output voltage
f_0	Natural frequency of oscillation for zeroth mode
f_n	Frequency for the *n*th mode
P_0	Static pressure of the bubble
γ	Ratio of the specific heat of the gas in the bubble
R_0	Mean radius of the bubble
ρ	Density of the liquid
T	Surface tension of the liquid
H_{LSB}	Slug body holdup
C_c	Dimensional coefficient
A_i	Pipe internal diameter
Bo	Bond number

D	Pipe diameter
d_{bubble}	Bubble diameter
g	Gravitational acceleration
L_{LSB}	Liquid slug body length
L_{EB}	Eelongated bubble length
μ_G	Gas viscosity
μ_L	Lliquid viscosity
ρ_G	Gas density
ρ_L	Liquid density
σ	Interfacial surface tension
Fr	Froude number
G	Normalised probe output voltage
$E_{surface}$	Total surface free energy of the discrete gas bubbles
a,b,c and d	Constants
AE	Absolute energy of the acoustic emission level
PE	Percentage error
APE	Average percent error
SD	Standard deviation

Chapter 1 : Introduction and thesis structure

1.1 Introduction

Multiphase flow is one of the most commonly encountered phenomena in various industrial processes. Multiphase systems involve presence of more than one phase, which can be either solids or gas in liquid or all the three phases coexist. The presence of the second phase affects the fluid dynamics of the main flow. Depending on the amount of the other phase present, the flow conditions present in the system may vary significantly. For example, in liquid/gas multiphase flows, the flow can be configured in different flow patterns or regimes in horizontal pipeline such as stratified, wavy, annular, bubble, slug, and dispersed flow. Therefore it is very important to characterise such flow systems.

One of the main industries where the accurate characterisation of multiphase flow system is important is the oil and gas industries. Slug flow has been known as the most common in oil and gas production pipeline and because it is intermittent flow, it is difficult to control and accurately measure online, Also slug flow can be very destructive to downstream equipments. In the oil and gas industry, accurate metering of multiphase flow could lead to greater benefits in terms of production allocation, production monitoring, capital expenditure and operational expenditure, following are few examples:

- Reduction in the capital cost as the outputs of several wells can be grouped together after being metered at the well discharge.

- Reduction in capital cost of new offshore platforms by replacing the bulky and heavy test separators.

Better reservoir management, production allocation and optimisation of total oil production over the lifetime of the field. This could mean the continued production for otherwise uneconomical wells rather than abandonment leaving behind a high proportion of the oil untapped.

Many researchers have investigated the accuracy of the measurements of multiphase slug or mixture flow. Various techniques and technologies are currently available for measuring multiphase flows though the selected method can be dependent on the amount of second phase present or the intrusive and invasive nature of the measuring probes.

Whilst the development of Acoustic Emission (AE) technology to monitoring of various asset types has been growing over the last 50years, its application to monitoring and characterising multiphase flows is new and this investigation forms the foundation on which future research will be based.

1.2 Thesis Objectives

The main objectives of this thesis are:

- Formulate mechanisms for the generation of Acoustic Emission (AE) in two-phase flow.
- Establish an experimental programme for assessing the feasibility of employing AE for measurement of Gas Void Fraction (GVF).
- Measuring the Gas Void Fraction (GVF) of two-phase air/liquid flow by non-invasive and non-intrusive Acoustic emission sensors.
- Investigate the effect of operational and design parameters on the AE measurements

- Develop a correlation between experimentally measured GVF and AE generated from two-phase flow.

Based on the outcome from the last objectives, a set of proposal for future study is presented.

1.3 Main contributions of the present work

- First known attempt at applying AE technology to GVF assessment
- Correlation between AE energy and GVF over defined flow regimes
- Investigating the influence of operating variables such as pipe material, sensor orientation, temperature, viscosity and surface roughness on AE energy for two-phase flow condition

1.4 Thesis structure

Chapter 2 deals with the introduction to the multiphase flow in pipes and the different parameters used to characterise two-phase flows. This chapter describes various flow patterns and flow regimes generated by the gas-liquid mixture in horizontal pipeline. Also, inferential and direct flow measurement techniques used for two-phase flow measurement are reviewed. Direct measurement techniques for phase fraction, phase velocity and phase density are summarised at the end.

Chapter 3 covers current techniques used to measure gas and liquid phase fractions. Both the intrusive as well as non-intrusive techniques are described along with their accuracy and limitations. The literature describing application of these techniques in multiphase systems is briefly discussed.

The details of acoustic emission technique are covered in **chapter 4** and **5**. Chapter 4 provides background to AE technique, covering various components of AE device and data acquisition by AE method. Chapter 5 covers detailed literature review of the AE technique and sources of AE signal generation in the flows, concentrating on the AE signal generation due to the gas bubble through bubble break-up and coalescence. AE energy generation through some other mechanisms such as cavitation, chemical reaction and solid/liquid flows is also briefly covered. Slug flow mechanism and how AE generated is detailed, and several GVF correlations are reviewed.

The experimental rig used in this work is described in **chapter 6**. The 50 mm (2”) test facilities and various component used are detailed. The air and water supply system and AE system used in this work is described. The data acquisition system and the calibration process is also covered in the same chapter. The procedure involved in test rig design, set-up and measurements is discussed.

Chapter 7 presents main results and observations, followed by detailed discussion of the investigated parameters that was described in chapter 6. Also AE is correlated to GVF of two-phase flow and compared to other correlations

A brief description of the main findings of the above work is included in **chapter 8**. In order to extend the present work, recommendations for future work are made in the same chapter.

Chapter 2 : Introduction to the two-phase flow

This part of the thesis introduces multiphase flow in pipes and the different parameters used to characterise two-phase flows. Flow patterns and flow regimes generated by the gas-liquid mixture in horizontal pipeline are also discussed. In addition, inferential and direct flow measurement techniques used for two-phase flow measurement are reviewed. This is followed by a summary of direct measurement techniques for phase fraction, phase velocity and phase density.

2.1 Two-phase Flows

Flows can generally be classified into; single, two and multi-phase. Single phase flow describes any flow of a single liquid, gas or solid; the most common two-phase flows are gas-liquid, liquid-liquid, liquid-solid or gas-solid; multi-phase flow is any flow characterised by more than two phases. Two-phase flow is of great industrial significance and is commonly found in the chemical, process, nuclear, hydrocarbon, and food industries. The study of two-phase flows has received widespread research attention, with most emphasis on gas-liquid flow because of its enormous importance for the power generation, nuclear and automotive industries, and chemical and petroleum processes such as sewage treatments, oil and gas transport, boilers, heat exchangers, condensers, …*etc*.

In two-phase flow, the flow behaviour is much more complex than for single-phase flow. The phases tend to separate because of differences in densities, viscosities and relative speeds of the phases which lead to different shear stresses at the pipe wall for each phase, thus adding even more complexity to the flow behaviour.

2.1.1 Two-phase Flow Parameters

Important parameters commonly used to describe two-phase flow are (Clayton, 2005):

- Superficial Phase Velocity, V_{SL}

The term superficial phase velocity is the phase velocity calculated for each individual phase: it is the volumetric flow rate, *Q,* of that phase divided by the cross-sectional area of the pipe, *A,* neglecting any other phase within the pipe. Thus:

Superficial liquid velocity

$$V_{SL} = \frac{Q_L}{A} \qquad (ms^{-1}) \qquad 2\text{-}1$$

Superficial gas velocity

$$V_{SG} = \frac{Q_G}{A} \qquad (ms^{-1}) \qquad 2\text{-}2$$

It can be seen that algebraic sum of the gas and liquid superficial velocities, will determine the mixture velocity (V_M)

$$V_M = V_{SG} + V_{SL} \qquad (ms^{-1}) \qquad 2\text{-}3$$

- Gas Volume Fraction

The gas volume fraction (GVF) is the ratio of the volumetric flow rate of the gas to the total volumetric flow-rate:

$$GVF = \frac{Q_G}{Q_L + Q_G} = \frac{V_{SG}}{V_{SG} + V_{SL}} \qquad 2\text{-}4$$

- Liquid Hold-up

The term hold-up (E_L) is defined as the ratio of liquid/total volume flow:

$$E_L = \frac{Q_L}{Q_L + Q_G} \qquad 2\text{-}5$$

And

$$E_L + GVF = 1 \qquad 2\text{-}6$$

2.1.2 Gas-liquid Flow Regimes in Horizontal Flow

The most distinguishing characteristic of multi-phase flow is the variation in the physical distribution of the phases in the flow conduit, known as the flow pattern or flow regime. The flow pattern that exists depends on the relative magnitudes of the forces that act on the fluids. These forces will depend on the properties of the fluids; density, viscosity, surface tension: the angle of inclination and diameter of the conduit carrying the flow: and the flow itself, most particularly, the degree of turbulence. Thus, the hydrodynamics of the flow, as well as the flow mechanisms, change significantly from one flow pattern to another.

Several investigations, (Al-Sheikh et al.,1970; Dukler et al.,1964; and Govier and Aziz, 1972), have shown that classification and description of the flow distributions into flow regimes or patterns is still often a very subjective process.

There is no single theory or correlation that can satisfactorily predict the pressure gradient or liquid hold-up over all possible flow regimes encountered in two-phase gas--liquid flow in pipes. However, there are some generally accepted descriptions

Flow patterns are often displayed using a flow pattern map, which is a graphical representation of the flow regime transition boundaries for a particular system. Theoretically, dimensionless parameters are to be preferred for representing the different flow regimes but in practice the superficial velocities are much more commonly used. Baker (1954) was amongst the first to publish a horizontal flow regime map to describe flow regimes based on the mass velocities of gas and liquid phases. A commonly accepted example is the map that was proposed by Mandhane et al, (1974) which is shown in Figure 2-1.

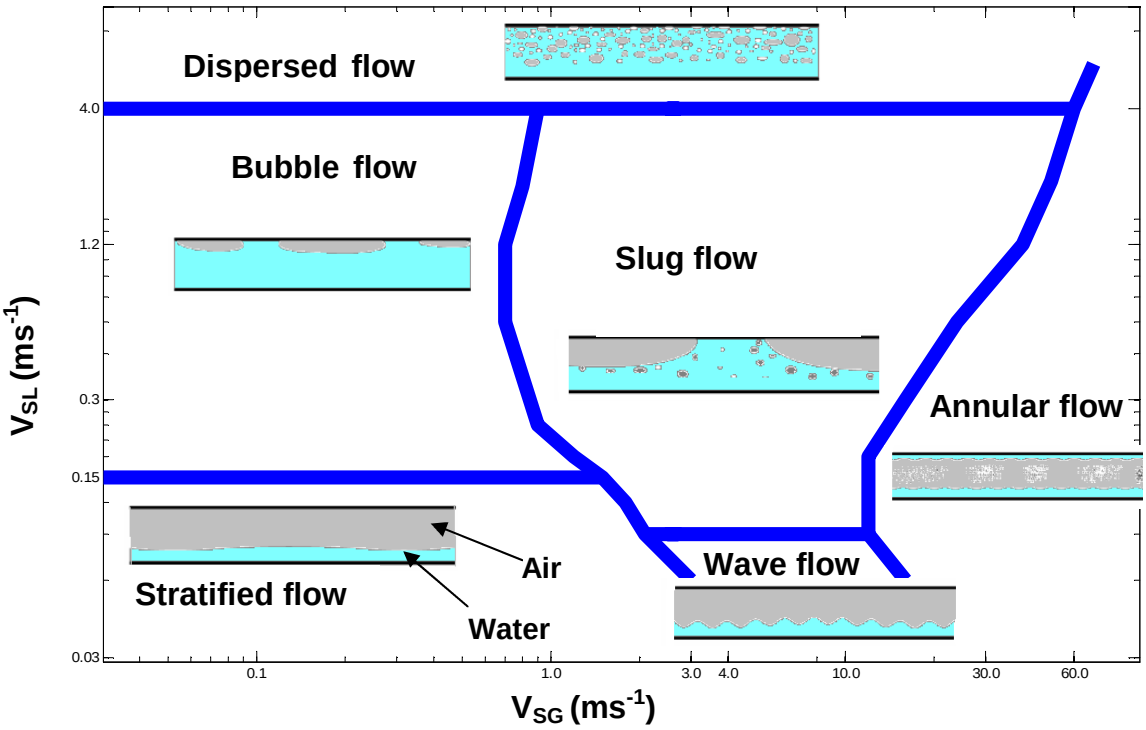

Figure 2-1: Horizontal Flow Regimes Map, Mandhane et al, (1974)

The flow regime map is fully dependent on the superficial liquid velocity (V_{SL}) and superficial gas velocity (V_{SG}). Two-phase flow regimes are normally

characterized by a series of flow patterns that are designated as stratified, wavy, bubble, slug, and annular flow in horizontal pipes, see Figure 2-1. These patterns excluding stratified and wavy flows are also found in vertical pipes (Hewitt, 1982). Following is a brief description of each regime:

- Stratified Flow

At low velocities of both gas and liquid, due to gravitational separation the liquid flows along the bottom side of the pipe and the gas flows on the top side filling the space above the liquid. The contact area between gas and liquid is typified by very smooth and gentle activities.

- Wavy Flow

Increasing the gas velocity in the stratified flow will increase the activity of the gas-liquid contact area (free surface), the higher relative velocities between the phases generates a wave-like texture.

- Annular Mist Flow

This regime occurs at high gas velocities. A thin film of liquid is present around the internal wall of the pipe but, typically, most of the liquid is entrained in the form of droplets in the gas. Some droplets appear on the bottom of the pipe as a result of gravity.

- Slug Flow

Slug flow is the occurrence of periodic large, coalesced gas bubbles in a liquid process. The gradual increase in liquid velocity will result in converting the wavy

flow to what is described as slug flow, in this flow pattern large waves of liquid form a slug that can fill the whole cross-section of the pipe leading to blocking of the downstream gases. These slugs can be generated by surge waves on a thick layer of liquid on the bottom of the pipe. Slugs are usually not intentional and can be disruptive to flow and density measurement. Slug flow is commonly found in long-distance piping that does not fill properly. It may occur as a result of leaks in pump suction or tank agitation, allowing air to be pulled into a line (McAllister, 2009).

- Bubble Flow

This flow type is characterised by the presence of a layer of elongated bubbles travelling at the top of the pipe, liquid dominates this flow type.

- Dispersed Flow

In this flow pattern the gas phase is distributed within a pipe entirely filled with liquid. Discrete gas bubbles tend to move towards of the top region of the pipe while gravity holds the liquid in the bottom of the pipe.

2.2 Multiphase flow measurement

2.2.1 Inferential Measurement Strategies

The ideal multiphase flow meter would determine the mass flow rate of each phase in the multiphase flow. However, such devices do not exist for multiphase flows and are not common for two phase flows. The practical alternative is to simultaneously measure the instantaneous velocity, volume fraction and density of each phase across the cross-section of the conduit and infer the individual

and total mixture mass flowrates (Thorn et al, 1997). Figure 2-2 shows a schematic of such an approach.

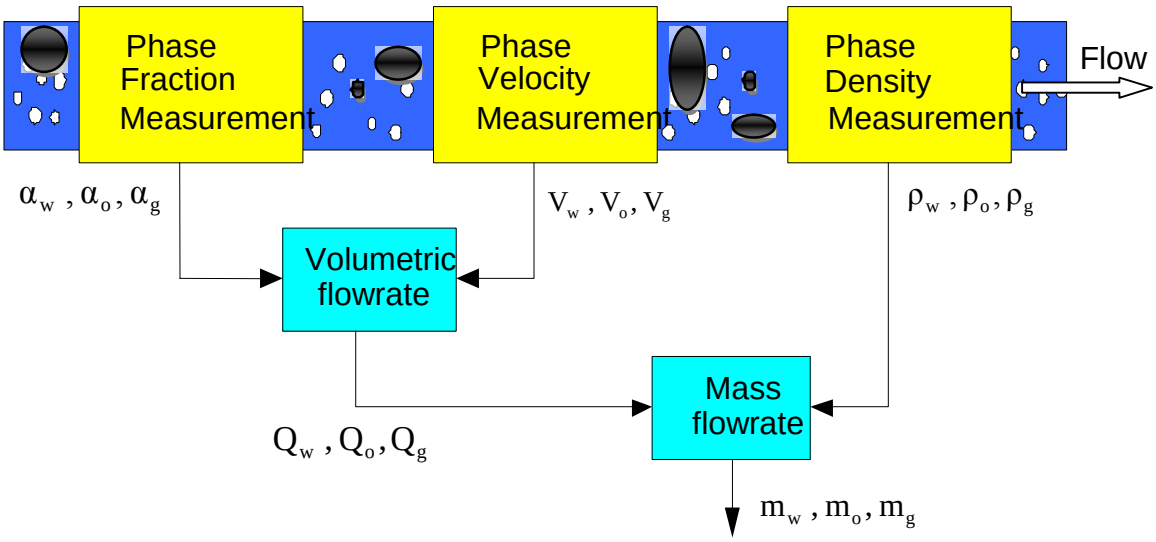

Figure 2-2: Schematic of an Inferential Multiphase Flow Measurement Strategy, (Thorn et al., 1997)

The two categories of parameter in inferential multiphase metering systems are: primary and secondary.

1. Primary parameters:
    - Phase fraction (e.g. void fraction, water cut);
    - Phase velocity; and
    - Phase density
2. Secondary parameters:
    - Flow regime;
    - Phase viscosity;
    - Phase salinity; and
    - Phase permittivity/ conductivity

Fortunately, data on the density of oil, water and gas phases is readily available, e.g. densitometer readings or estimated from Pressure,Volume and Temperature (PVT) diagrams using measured pressure and temperature. In practice the problem is usually the measurement of the phase velocities and volume fractions of the gas and water. The oil fraction is deduced from the fact that the sum of the three phase fractions is equal to one.

$$M = \alpha_G * V_G * \rho_G + \alpha_W * V_W * \rho_W + \alpha_O * V_O * \rho_O \qquad 2\text{-}7$$

Where M is the total mass flow rate, $\rho_G, \rho_W, and \rho_O$ are the densities of gas, water and oil respectively.

2.3 Direct Measurements Techniques in Multiphase Flow

2.3.1 Phase Fraction Measurement

Electrical impedance techniques and gamma-ray attenuation are two very common methods for measuring gas and liquid fractions in a multiphase flow. Other, less commonly used, techniques which are available include microwave attenuation and nuclear magnetic resonance (NMR). The details of phase fraction techniques will be explained and reviewed in the next chapter.

2.3.2 Phase Velocity Measurement

2.3.2.1 Differential Pressure Meters

Olsen (1993) stated that several types of multiphase meters use the differential pressure to determine the total speed of the multiphase mixture. The types employed most frequently are Venturi meter and the orifice plate, (Zhang et al. 2005). The principle of an orifice meter is based on the difference between the upstream and downstream pressure across an orifice plate. The difference in pressure in a Venturi meter is not immediate as in as orifice, but it takes place with change in internal area of the pipe.

2.3.2.2 Positive Displacement

The operating principle of positive displacement meters is based on separating the flowing liquid into its component phases and accurately measuring the discrete and identical volumes. Electronic or mechanical triggers are generally used for counting the number of these discrete volumes; the flow rate can then be calculated. Several types of positive displacement meters are available, depends on the techniques used to separate the fluid such as vanes, gears, rotating valve, pistons or diaphragms.

Commercial multiphase flow systems using this technique have been well reviewed by Tuss *et al*. (1996). It was found that the positive displacement can only measure the total volumetric mixture of the gas and liquid phases but not the gas flow rate, see Jama (2004).

2.3.2.3 Cross-correlation Technique

Cross-correlation techniques are well-known and are becoming widely used in both industry and laboratory for pipeline flow velocity measurement. In gas/liquid two-phase flow, the presence of gas bubbles and the formation of liquid slugs can be detected non-invasively by various types of transducer, such as ultrasonic transducers, microwave or gamma ray devices, and capacitance, (Yang and Beck. 1997). Several researchers have adopted this technique to measure bubble and slug translational velocities (Reis and Goldstein 2005; Dong *et al.* 2005 ; Cheng *et al*. 2005 and Al-lababidi, 2006).

The main principle of this method is shown in figure (2-3). Two similar sensors placed axially at defined distance from each other (L), are used to detect the flow pattern (slugs and/or bubbles). The signals from the two sensors (x (t) and y (t- τ)) are cross-correlated using the following equation.

$$R_{XY} = \frac{1}{T}\int_0^T x(t)y(t-\tau)\,dt \qquad 2\text{-}8$$

Knowing the lag time between the two correlated signals (τ), the velocity of the flow can then be calculated as follows: $V = \frac{L}{\tau}$

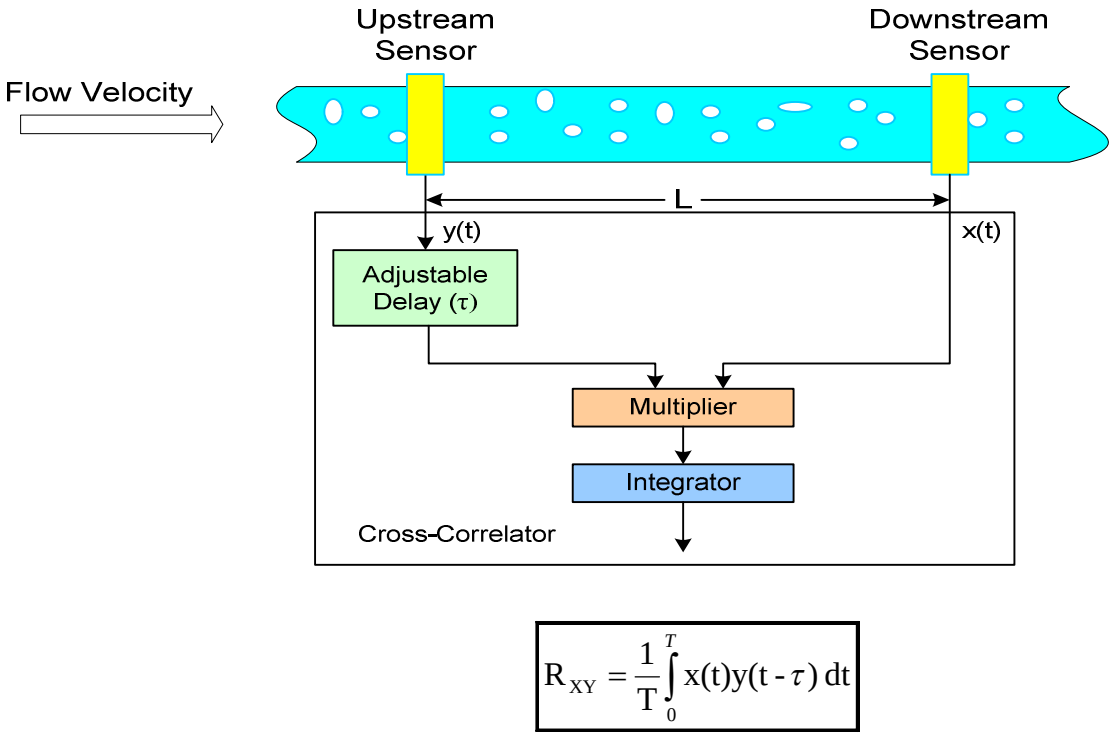

Figure 2-3: Cross-Correlation Technique, (Thorn et al., 1997)

2.3.3 Phase Density Measurement

As shown in Figure 2-1, to convert the phase volumetric flow rates into mass flow rates, measurement of individual phase densities is required. However, the phase density measurement is well established and it is readily available from other parts of the production process such as gamma densitometers, or from the PVT diagrams and that by using the measured temperature and pressure. The principle of the gamma-ray densitometer is explained in the next chapter.

Chapter 3 : Phase Fraction Measurement Techniques

Unfortunately, separating the phases for individual measurement requires bulky and expensive equipment. A multiphase flow metering system is required which measures the line conditions of the individual phases without separation or sampling. For testing flow from oil wells, multiphase flow metering would be the simultaneous measurement of the flow rates of the oil, water and gas produced by the well, without the necessity of either a two-phase or a three-phase separator, Hewitt et al. (1995). This chapter provides a background on current techniques for measuring gas and liquid phase fractions. Multiphase flows in pipelines have been widely investigated by researchers such as (Thorn,et al.,1997; Corneliussen et al. 2005).

In the literature there were numerous reviews devoted to the subject of gas and liquid phase fraction measurements such as Shearer and Nedderman (1965), Hewitt (1972), Gregory and Mattar(1973), Jones and Delhaye (1976),Sharma and Sachdeva (1976), Thorn,et al.,(1997), Ismail et al.,(2004), Xie, (2005), Al-lababidi, (2006) and many others.

The next section details the two most commonly used techniques for phase fraction measurements; gamma-ray attenuation and electrical impedance, and very briefly summarises other available techniques.

3.1 Methods of Void Fraction/hold-up Measurement:

Measuring hold-up is important and necessary for two-phase flow measurements. There are various models available to predict hold-up, but it is not always possible to know all the different model parameters for a given situation. Thus, it is always necessary that hold-up measurements are carried out.

Several techniques are commercially available for measuring gas void fractions in two and multiphase flows; however, this measuring process is always combined with a degree of difficulty due to the natural complexity of two-phase flows. Separation is the most traditional method used for void fraction measurements, where an expensive separator facility is employed to physically separate and then measure the two-phase flow components. Gamma-ray attenuation and electrical impedance are the most commonly adopted techniques but other, alternative, techniques include microwave transducers, X-ray and gamma-ray tomography, magnetic resonance imaging and nuclear magnetic resonance (Clayton, 2005).

3.1.1 Gamma Ray Attenuation Measurement

When any collimated beam of radiation passes through the multiphase mixture it is attenuated and the degree of attenuation can be directly related to the composition of the flow. A detailed analysis of the principles and practical determination of the void fraction in multiphase flow is given in (Pan, 1996), and the limitations of this technique are discussed in Fournier and Jeandey (1993). Gamma ray attenuation measurement is applicable to all possible combinations of two-phase and three-phase flows (Corneliussen *et al*. 2005).

There are different gamma ray systems that are used for multiphase flow metering, including single-beam and dual-beam gamma ray systems. Although the procedures and the principles are similar, single-beam gamma ray system can only be used for two-phase flows, whereas the dual-beam system can be used for three-phase flows.

3.1.1.1 Single-Beam Gamma Ray Attenuation

This method is one of the most widely employed for hold-up measurement in two-phase systems It depends on the difference in gamma-ray absorption between the two phase components of the flow (gas, oil, water). The absorption is exponentially dependent on the thickness and density of the mixture. A single energy gamma ray beam is directed at the pipe from a source placed diametrically opposite the receiver on the other side as shown in Figure 2-4. Single energy gamma ray attenuation can be used conveniently in liquid/liquid (oil/water) or liquid/gas systems. In a pipe, with inner diameter *d*, the intensity of the beam of radiation after it has passed through the mixture of two-phase flow is given by:

$$I_m(e) = I_v(e).\exp[-\sum_{i}^{2} \alpha_i.\mu_i(e).d] \qquad 3\text{-}1$$

Where $I_m(e)$: is the measured count rate, $I_v(e)$: is the count rate when the pipe is empty, μ_i: represents the linear attenuation coefficients for the two phases. Apart from fractions of the phases α_i, the attenuation coefficients μ_i are also initially unknown. However, the latter can be found by calibrating the system by subsequently filling the pipe with the individual fluids, when:

$$I_{Water} = I_v.\exp[-\alpha_{Water}.\mu_{Water}.d] \qquad 3\text{-}2$$

$$I_{Gas} = I_v.\exp[-\alpha_{Gas}.\mu_{Gas}.d] \qquad 3\text{-}3$$

These two calibration points together with the relation $\alpha_w + \alpha_g = 1$ can be rewritten as an expression for the water fraction in two-phase liquid/gas mixture (or the water cut) as:

$$\alpha_w = \frac{\ln(I_{Gas}) - \ln(I_m)}{\ln(I_{Water}) - \ln(I_{Gas})} \qquad 3\text{-}4$$

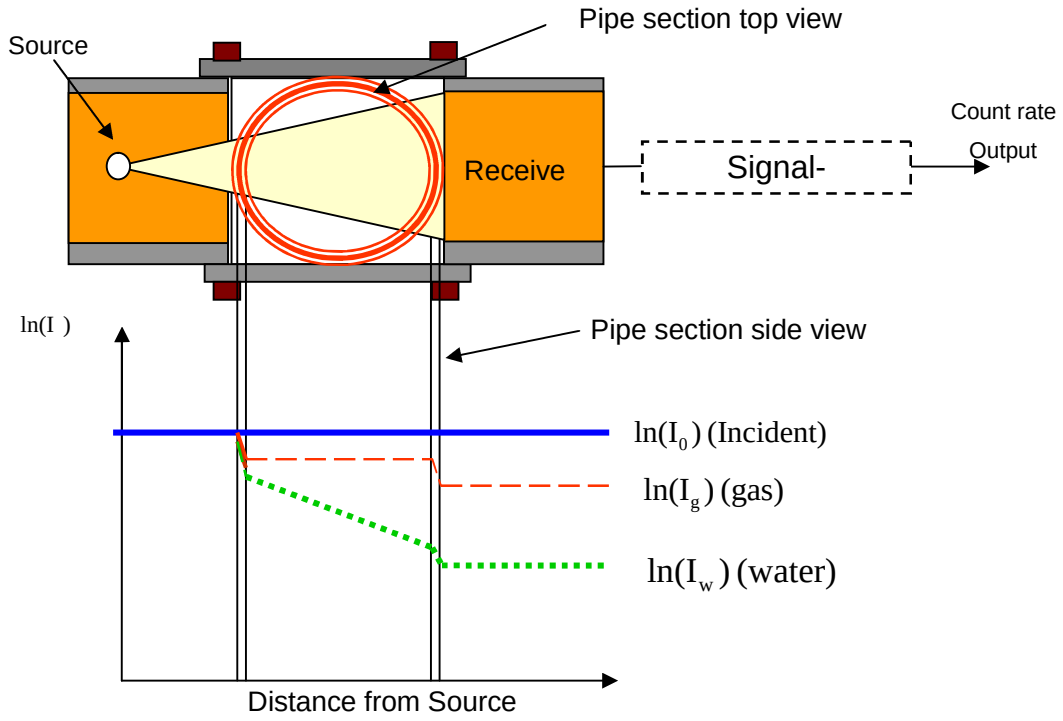

Figure 2-4: Single-Beam Gamma Ray Densitometer (Thorn et al., 1997)

3.1.2 Electrical Impedance Measurements

The main principle of electrical impedance methods for component fraction measurements is that the fluid flowing in the measurement section of the pipe is characterised as an electrical conductor. By measuring the electrical impedance across the pipe diameter (using e.g. contact or non-contact electrodes), properties of the fluid mixture like conductance and capacitance can be determined. The measured electrical quantity of the mixture then depends on

the conductivity and permittivity of the oil, gas and water components, respectively. Figure 2-5 shows the basic principles of the impedance method used to measure component fraction.

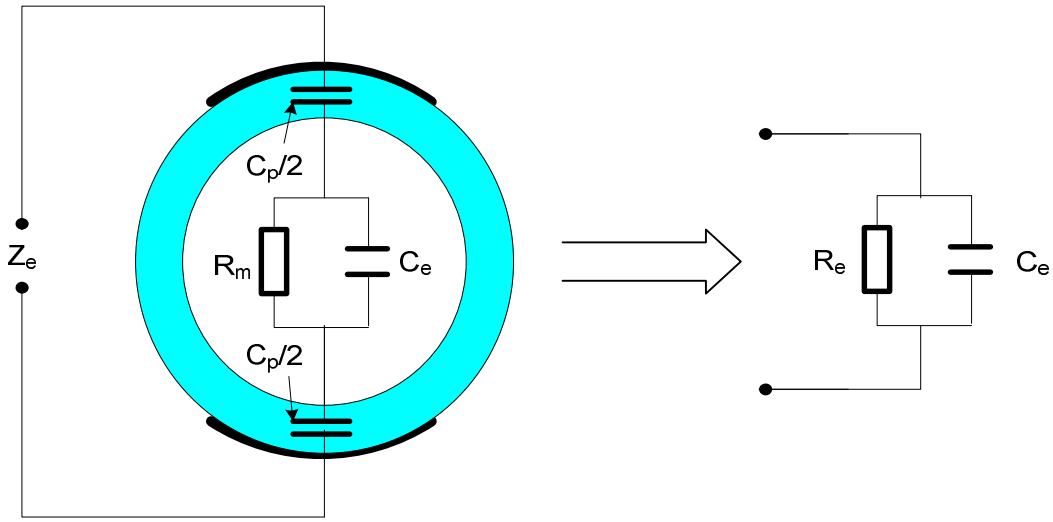

Figure 2-5: Impedance Method of Component Fraction Measurement (Thorn et al, 1997)

In Figure 2-5, the electrical impedance (Z_e) is measured across the two outer electrodes. Simply to demonstrate the principles, it is initially assumed that the capacitors may be assumed parallel plate. It is also assumed that the multiphase flow inside the pipe and between the electrodes can be represented by a resistance R_m in parallel with a capacitance C_M, and that the (steel) pipe itself can be assumed to have negligible resistance but a capacitance C_P (which is shown in the figure as two capacitances $C_P/2$ in parallel for convenience). The measured impedance (Z_e) and capacitance (C_e) is given by:

$$R_e = \frac{1+\omega^2 R_m^2 (C_m + C_P)^2}{\omega^2 R_m C_P^2} \qquad 3\text{-}5$$

$$C_e = \frac{[1+\omega^2 R_m^2 C_m (C_m + C_P)^2] C_P}{1+\omega^2 R^2 m (C_m + C_P)^2} \qquad 3\text{-}6$$

The relative volume fractions of oil, gas and water will determine the values of R_m and C_m of the mixture in the pipe. The measured impedance, Z_e, and capacitance, C_e, will obviously depend on the frequency ω of the applied signal and, in reality, will also depend on the geometry and construction of the sensor. For a given geometry and construction (C_P fixed), the measured impedance, Z_e, and capacitance, C_e, will be direct functions of the relative volume fractions of the flow.

In oil continuous mixtures (Z_e) is large and can be difficult to measure reliably. For the flows in which water is the continuous phase, a short circuiting effect will occur caused by the conductive water if the sensor excitation frequency, f_c, is less than:

$$f_c < \frac{\sigma_w}{2\pi\varepsilon_o\varepsilon_w} \qquad 3\text{-}7$$

Where σ_w and ε_w are the conductivity and permittivity of the water component respectively. For process water this would mean frequency below that of microwave frequencies. Therefore, the impedance method is limited to oil or gas in continuous phase.

For air-water, Costigan and Whalley (1997) used two conductance sensors to determine both liquid hold up and phase velocity. The PDF (probability density function) of the signal (sampled at 200Hz) showed characteristics patterns for

bubble, slug and annular flows. The bubble and slug velocities were determined using a correlation technique.

However, impedance based methods suffer from two important limitations; they cannot be used over the full component fraction range and are flow regime dependent. This dependency is eliminated by one of two methods: (1) homogenisation of the phase, before the measurement is made; and (2) development of electrodes which minimise the dependency upon the flow geometry.

Various methods have been used to reduce the flow regime dependency effects of impedance sensors as shown in figure 2-6. In this figure four different designs of non-intrusive sensor are illustrated. These styles were developed to minimise the flow geometry dependency.

1. Arc electrodes (Xie et al., 1990), for resistive and capacitive cross-section measurement, figure 2-6 (a). In this design the guard electrodes are installed at either side of the electrodes, and that to reduce the sensitivity to axial flow variations.
2. Ring electrodes (Fossa, 1998; Andreussi et al, 1988), for resistive measurement, and to achieve a more uniform electric field structure within the sensing volume, a ring electrodes trades-off a localised cross-section measurement, see figure 2-6 (b).
3. Helical electrodes (Abouelwafa et al, 1980), figure 2-6 (c). In this model, a pair of continuous helical electrodes are mounted on and twist round the outside wall of the pipe, to overcome flow geometry dependence.
4. Rotating field electrodes (Merilo et al., (1977)), as shown in figure 2-6(d), this design achieves a similar effect to helical electrodes. Here, three electrode pairs are driven at 120° phase intervals, to produce a rotating field vector in the pipe centre.

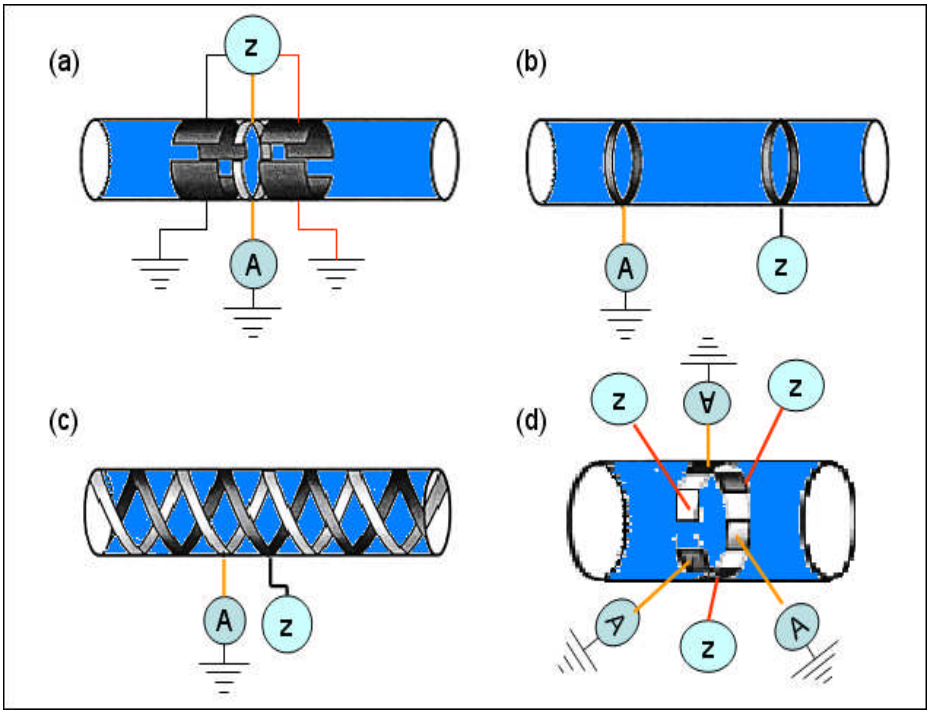

Figure 2-6: Non-Intrusive Impedance Measurement

3.1.3 The nuclear magnetic resonance method

This method involves measuring NMR signal from a ^{1}H nuclei in the liquid which can be related to the two-phase mixture density. Callaghan (1991) provides a detailed background to this technique. Lynch and Segel (1977) used this technique and claimed that the method provides linear relations for void fractions from zero to unity. One of the main drawbacks is that it requires a non-metallic pipe section close to the measurement point to allow penetration of the radio frequency field.

3.1.4 Microwave technology

Microwave measurements are also dielectric measurements, but are significantly different from the capacitive measurements techniques as both the frequencies are higher (several hundred MHz) and the operation principles of

the sensor devices are different. Microwave sensors are based on the fact that the interaction between microwaves and the medium of propagation (liquid and gas phases) is completely determined by the relative permittivity. For liquid and gas flows in pipelines; Microwave Resonator sensors is the suitable choice. The operation principles of this technology have been reviewed by Nyfors (2000).

3.1.5 Ultrasound Probes:

This technique is based on ultrasound propagation in the multiphase system. Depending upon the way ultrasound signals are used, it is divided into two main categories; ultrasound attenuation where the attenuation of the ultrasound transmitted is used to obtain gas hold-up or the time-averaged local interfacial area, while the other technique, called the Doppler technique, uses the waves reflected back from the bubble surface to obtain bubble size or bubble velocity.

Ultrasound techniques have been applied to measure multiphase flows (mainly gas-liquid). Ruffer et al. (1995) used ultrasound method in an external loop airlift to measure bubble velocity. Allababidi and Sanderson (2004) used an ultrasound Doppler technique to investigate gas-liquid multiphase flows in a horizontal pipe, where the ultrasound signals were used to measure the gas void fraction. Although this technique is non-invasive and allows quicker multiphase flow measurement, the accuracy of the measurement deteriorates at higher gas holdup conditions. Broring et al. (1991) suggested that the measurement accuracy of the ultrasound technique is very poor when the gas holdup is >20%. However, more recent work from Allababidi and Sanderson (2004) has shown that this technique can be effective even at very high gas fractions.

3.1.6 Tomography techniques

Tomography is a completely non-intrusive method that measures conductivity or other properties (e.g. radiation attenuation) over an entire cross-section of the pipe or column. The sensors are placed around the pipe or column section which measures the physical property being investigated and a reconstruction algorithm is then used to obtain phase fraction image over the cross-section. The tomography results are entirely time averaged. The tomography technique can be broadly divided into three categories depending upon the property being measured: γ-ray attenuation, electrical tomography and ultrasound tomography.

With γ-ray attenuation measurement based tomography, the attenuation is proportional to the density of the material for a given energy. The reconstructed image provides the distribution of phase fraction across the column or pipe cross-section. Kumar et al. (1995) and Froystein (1997) used this method to investigate multiphase systems such as packed beds or bubble columns.

Electrical tomography is relatively cheaper to install. The electrodes measure resistance or impedance at the wall of a column or a pipe. This technique has been investigated very widely and used for bubble columns, and in pipe flows (Schmitz and Mewes, 2000; George et al., 2000).

Ultrasonic tomography is based on the fact that the ultrasonic wave propagation depends on the phase fraction, dispersed phase size and flow regime. Very little information is available on the applicability of this technique in the multiphase systems (e.g. Warsito et al., 1999).

3.1.7 The Beta-ray attenuation method

This method works on the same principle as the previous method, the only difference is that β-rays are absorbed more readily than γ-rays and so will often be effected for strongly than γ-ray and therefore can be effective for measurement in small channel cross-sections. Cravarolo and Hassid (1965) used this method.

3.1.8 X-ray method

The principle is same as for γ-ray or any other radiation method. The attenuation of the X-ray varies with the density along the radiation path or the interfacial area. More detailed information on the basic principle of this technique and its limitations are described by Fournier and Jeandey (1993). Pike et al. (1967) and Nevstrueva and Tyutyaev (1975) were among the first to use this method for phase void measurement for different flow regimes.

3.1.9 Gamma-neutron reaction method

Neutrons are emitted when γ-rays pass through heavy water. The neutron emission depends on the amount of heavy water. Hewitt (1972) and Shearer and Nedderman (1965) used this as a basis for void fraction measurement. This technique has very limited application as the liquid phase must be heavy water.

3.1.10 Laser-Doppler Anemometry

Laser Doppler Anemometry (LDA) is a result of developments in laser technology. In this technique, laser light illuminates the flow, and light scattered from gas or solid phase in the flow is collected and processed. In practice, a single laser beam is split into two equal-intensity beams, which are focused at a common point in the flow field. An interference or fringe pattern is formed. Because of the movement of gas bubbles or solids across the intersection volume, the frequency of the light is shifted slightly (Doppler shift), in proportion to the velocity of the bubbles or particles. There is, however, a directional ambiguity, in interpreting the signal, since particles moving in either the forward or the reverse direction will produce identical signals and frequencies. Therefore, in practice, the frequency of one of the beams is slightly shifted, using a Bragg cell: with this frequency shift in one beam relative to the other the

interference fringes appear to move and thus negative and positive velocities can be distinguished.

This method can provide velocity measurements in the individual phases of gas-liquid flows. Mahalingham et al (1976) used this method to study bubbly flow. This method suffers from measurement errors at higher gas fractions in the flow. Liquid velocities measured by LDA may be contaminated by bubble velocities, as observed by Bendjaballah-Lalaoui (2000).

3.1.11 Hot-wire anemometry

This technique depends on the sensing and measurement of the rate of cooling of an electrically-heated fine wire or probe. The wire is usually made of platinum coated tungsten, and the diameter is typically 5μm. If only the fluid velocity varies, then the heat loss can be interpreted as a measure of that variable. These anemometers have a high frequency response and thus are well suited to the measurement of unsteady flows. This method has been used widely for the single phase flow, but when used to two-phase flow; it leads to gas fraction and liquid phase mean and RMS velocities. This technique has been widely used to study turbulence in the gas and liquid flows. Serizawa et al., (1975) Delhaye (1969) and Carvalho and Bergles (1991) have used this technique for hold-up measurements in two-phase systems. Utiger et al., (1999) used this technique in a gas-liquid system with gas of up to 20% hold-up; however, no limitation in gas hold-up is reported in the literature. One of the main drawback of this technique is it is intrusive; the presence of the probes may disturb the flow.

3.1.12 The void needle

Void needles are classified into two main types; optical and resistive probes:

- **Optical probes**

Optical probes are generally made of quartz. This method is described in detail by Lockett at al., (1977), and exploits the difference in the refractive index of liquids and gases to measure void fraction. Infra red light is sent through the probe to the tip. When the tip is in the liquid the tip transmits the light beam, but reflects the light back when it is surrounded by the gas phase (Chabot et al., 1998). This method is useful even when the flowing mixture is non-conducting electrically.

- **Resistive probes**

These are very thin and sharp needles mounted in the flow such that it pierces as many bubbles present in the flow as possible. They are made of oxidation resisting materials such as nickel, platinum and stainless steel (Hogsett and Ishii, 1997). Different versions of void needle have been described and reviewed by Boyer et al. (2002). In general, it consists of an insulated needle with an exposed tip electrode facing upstream. The needle tip measures the time it is in the liquid phase, provided there is a continuous liquid phase present between the wall and the needle. Some variations involve more than one needle or even very small concentric electrodes in which high frequency potential is applied and the output signals shows whether a gas or liquid phase is present around the electrodes, this can be related to the void fraction. These types of probes can be used as a single tip probe to measure gas fraction or double-tip probes to facilitate bubble velocity measurement. The needle probes have many limitations due to their invasive nature. To obtain reliable results the needle size should be very small compared to the bubble size. Some of the factors that may limit the accuracy of this method are: errors due to the bubble-probe interactions, probe orientation in the flow, bubble shape, errors in the signal treatment.

3.1.13 Dilation Method

The dilation method, as described by Hewitt (1972), is a closed circuit system in which voids are generated in a voidless system result in some liquid being expelled. The method involves collecting and measuring the volume of the expelled liquid and determining the void fraction. The main disadvantage of this method is that it does not provide local void fraction but measures the void fraction for the whole circuit.

3.1.14 Quick Shutting Valve Method

This method involves a pair of synchronised quick shutting valves placed at both ends of a test section where the void fraction is to be measured. By assessing the liquid phase trapped in the test section, the other phase fraction can be measured. Hewitt (1972) claims this is the most accurate method if the valves are properly adjusted and the experimental error greatly reduced if the closing time elapse of the valves is reduced to 0.01sec. Lockhart and Martinelli (1949) were among the first to use this method for void fraction determination.

3.1.15 Void fraction by measuring shear-stress and pressure drop

Cravarolo and Hassid (1965) determined void fraction by measuring shear stress and pressure drop simultaneously in the vertical flow. Assuming negligible momentum variation in the flow direction, the mixture density could be obtained mathematically provided that densities of liquid and gas phases are known.

3.1.16 Void fraction measurement by sampling

This method requires taking a sample from the flow stream and measuring the weight or the volume of the liquid phase, the gas phase can be then determined. Measurement rate is completely dependent on the sampling rate.

3.1.17 Photographic method

This method involves determining size and velocity of bubbles in two-phase flow, and is always used in conjunction with other methods such as X-rays. Bendjaballah et al. (1999) used this method for void fraction measurement. One of the limitations of this method is that it requires a transparent wall and transparent liquid, and the visualisation is usually possible only close to the wall. Use of this technique in conjunction with radiography allows measurements even in non-transparent fluid systems. Heindel (2000) used this technique with the flash X-ray radiography to determine bubble size and shape.

3.2 Conclusions

The various void fraction measurement methods described above fall into two general categories, intrusive and non-intrusive. Techniques such as γ, β and X-ray and dilation method do not affect the flow whereas void needle method, turbine method and sampling method do interfere with the flow. However, the radiation method requires the construction of complicated, dedicated facilities, and the ultrasonic method cannot easily be applied to a variety of flow patterns.

Depending on the technique used the accuracy of void fraction measurement will also vary. Some methods such as quick acting valves and the dilation method can measure only overall average void fraction, while void needles or sampling probes can provide point measurement. Also quick-closing valves cannot measure the void fraction in real time. Other techniques such as gamma-ray densiometer and conductivity rings suffer from a saturated output

signal at higher gas void fractions and require the construction of complicated, dedicated facilities.

The impedance method is a real-time technique requiring relatively simple equipment. The conductance method, using non-intrusive walls probes such as shown in Figure 2-6, will give a void fraction measurement that is an average over the cross-section of the pipe. However, the signal from conductance probe shows a high sensitivity and dependency on temperature, a $1^{o}C$ increase of the temperature of the flow can raise the conductivity by 2.5% (Kim at al., 2009). Techniques such as the dilation and photographic methods are suitable for laboratory and research use only. Thus proper consideration is required when choosing the method/ technique to be used for void fraction measurement.

Chapter 4 : AE Technology

4.1 Acoustic Emission History

Acoustic Emission (AE) refers to the transient elastic waves naturally generated by the abrupt release of stored energy in a material or structure, and exists in nature in the form of audible and sensible phenomena generated by such occurrences as earthquakes and the creaks of a wooden beam before it breaks. As practical tool, the first manmade applications of AE dated back as early as 6500 BC when pottery makers, used the sound generated from clay vessel to identify defective products as they cooled in the oven. The observation of AE in metal-working first took place around 3700 BC during twining of pure tin, which was called “tin cry”, but this was not documented until the eighth century by an Arabian alchemist Jaber ibn Hayyan (Miler, 1987). Jaber described the audible tin-cry as a “harsh sound” or “crushing noise”. He also used the term “sounding much” to describe iron during the forging process, which is believed to be produced by martensite formation during the cooling process (Miler, 1987). Comprehensive summaries of the history and discoveries of AE have been detailed in many textbooks and articles [see Drouillard, 1996] and, for example, it has been found that most common structural materials: e.g. ceramics, cement, glass, metals and polymers will exhibit some form of AE

It was not until the late 1930s that AE technology began to be systematically investigated. One of the earliest known AE experiments was performed in Germany by Foerster and Scheil (1936) who built a system to convert the mechanical vibrations caused by martensite transformations into electrical voltages. The AE phenomena generated in a wire-shaped nickel-steel specimen were detected by the minute electrical resistance variations they generated.

However modern AE had its beginning in 1950 with the publication of Kaiser's dissertation (Kaiser, 1950) on the testing of tensile materials and the effect named after him (that an acoustic emission will not re-occur for loads less than the maximum previously applied load). Schofield developed Kaisers's work and in 1961 published his report in which the term "Acoustic Emission" was used for the first time (Schofielde 1961).

4.2 Types of AE signal:

Generally AE signals are categorised as either continuous or burst:

(a) Obviously because an AE signal is the abrupt release of stored energy there cannot be any truly continuous AE signals. A continuous AE signal is said to be one in which the average time between bursts of emission is less than the duration of the emission itself (Lingrad, 1993). The signal has a random oscillatory appearance because it results from the overlapping of many burst type signals. Thus continuous AE signals are characterised in terms of statistical parameters such as amplitude RMS. Usually continuous emissions are of low energy and are not singularly distinguishable.

(b) If the pulses that form the AE signal are detectable above background noise and are sufficiently well enough separated in time so that each is identifiable, the emission is called burst emission (Matthews, 1983). AE from crack growth falls into this category, and dislocation movement in a metal is a typical example. The waveforms of burst type AE signals where the signal can be identified as a discrete transient are often approximated by an exponentially decaying sinusoid.

Of course, if the burst rate is high and the time gaps between bursts is very short burst type emission becomes continuous, and vice versa. There is also mixed mode activity in which burst activity is superimposed on a background of continuous activity.

In the context of multiphase flow the AE signal generated from single bubble collapse is akin to a burst type signal. However, when hundreds or thousands of bubbles collapse in very short time the AE signal can be considered continuous.

As a condition monitoring (CM) tool, AE has the capability to detect failures at a very early stage and accurately monitoring the progression of faults or failures.(Mba et al., 2006). AE techniques are particularly effective for incipient failure detection (IFD), and may be considered an extension to the familiar vibration detection methods which use similar signal processing techniques, but with a higher frequency domain. Signals can also characterised by well-known statistical parameters such as Mean, RMS, Skewness, and Kurtosis. Mean and RMS parameters are explained in section 4-3. Skewness is the measure of the relative energy above and below the mean signal level. Kurtosis provides a sensitive indicator of shifts in the proportion of time the signal at higher amplitude (Holroyed, 2000).

AE monitoring is a passive, non-invasive technique, and the high frequency of AE signals offers a rapid spread of the wave throughout the surrounded media and the rapid formation of a multidirectional diffuse sound field which in turn facilitates the installation and positioning of suitable sensors at any convenient point in the vicinity of the AE source. AE methods have been successfully applied to monitor the condition of bearings, gears, pressure vessels, pipelines, pumps and turbines, and quality control in manufacturing. In research AE has been applied in investigations into composite materials such as advanced aerospace materials, fibreglass and reinforced plastics.

In the field of Condition monitoring, AE offers a number of advantages over the commonly used vibration technique. These include:

- AE is more sensitive to signal faults than normal running.
- AE signals are multidirectional; this means that AE sensor can be located anywhere in the vicinity of AE sources.

- The high signal to noise ratio (SNR) of AE signals is less affected by mechanical background noise giving a clearer and direct indication of the fault mechanism.
- AE can be applied to a wide range of rotating machines and industrial process irrespective of operational speed.
- AE is relatively sensitive and capable of detecting incipient failures because the sources are usually produced at microscopic level within the material.
- Structural resonances have no effect on the AE signal generated.
- AE has the potential to become a prognostic tool, due to its ability of identifying faults at early stages

The main drawbacks associated with AE are:

- AE are characterised by low amplitude signals, which require AE sensors to be placed closed to the sources of emission.
- By definition AE is unable to detect faults not produced within the material (such as misalignment, imbalance, etc.).
- AE requires highly specialised sensors and signal processing.
- AE suffers disturbance from high frequency signals sources such as turbulence, and interference from nearby electromagnetic sources.
- AE can only provide a qualitative but not quantitative assessment.
- AE requires highly skilled employees.

4.3 AE Parameters

AE testing is not only based on a few bursts, many thousands of bursts are recorded and certain important statistical features of the waveforms determined, see Figure 3-1:

- Peak amplitude of the pulse.

- Rise-time (time between initiation of signal and peak amplitude).
- Number of threshold crossings (counts) of the threshold of one polarity.
- Signal duration (time interval between first and last threshold crossing).
- Energy (integral of the square of the amplitude over duration of signal).
- RMS value of the continuous background noise in the absence of the burst.

The relevant measurements for each waveform have to be determined and recorded to usefully compare the results from a reference or defect-free object and the test specimen.

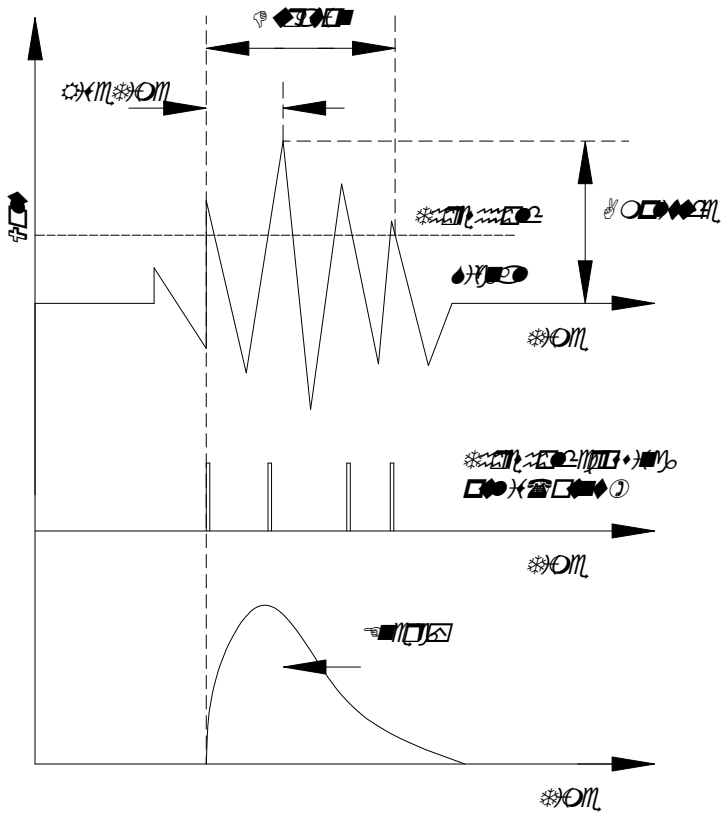

Figure 3-1: AE Signal Parameters

4.4 AE Transducers

Detection of AE events requires a sensor able to convert very small, very fast movements of a surface (displacements of the order of 10^{-12} m) into useful electrical signals. The frequency response of AE transducers is usually in the range 20kHz-1MHz. Because the signals are likely to be of low amplitude these transducers need to be very sensitive and to have a high signal to noise ratio to avoid problems due to background noise.

Several types of AE sensors and methods have been developed and used in the early 1960s, including phonograph needles, optical methods, accelerometers, microphones and quartz crystal based piezo-electric transducers (Drouillard, 1996). However, since then there have been considerable developments, piezo-electric polymer transducers (Stiffler,1983), microbeams (Schoess, 1998), laser interferometers (Nishinoiri and Enoki 2004), fibre optic sensors(Cho et al. 2004) and thin films (Imai et la., 1997 and Noma et al. 2006).

Piezo-electric AE sensors are considered to provide the best combination of ease of use, high sensitivity, low cost and range of frequency response. Piezo-electric is where an electric charge is produced in a material when it is mechanically strained, moreover the effect is reversible. Piezo-electric materials include (Holroyed, 2000):

- Certain natural crystal such as Quartz
- Specially formulated and processed ceramics such as Lead Zirconate Titanate (PZT)
- Specially formulated and processed polymers such as Polyvinylidene Fluoride(PVDF)

Due to its robustness and high sensitivity, Piezo-ceramic is most widely used in AE transducers. Two types of transducers are well established:

- Resonant piezo-ceramic, used when targeting certain frequencies.
- Broadband piezo-ceramic, used over a range of frequencies.

A typical AE sensor with, for example, a Lead Zirconate Titanate element will transform a displacement of 10^{-12}m (1picometer) into an electrical signal of about 1mV. Normally, the sensitivity of the AE broadband transducer is less than that of the resonance. Because PZT has a relatively low Curie point, sensors of this material have limited application at elevated temperatures.

4.5 Sensor couplant

An essential requirement in mounting a sensor is for there to be good acoustic coupling between the sensor's surface and the structure's surface because of the low amplitudes of AE signals. For good acoustic contact a thin layer of couplant is required. The couplant eliminates air gaps between the two surfaces and ensures good acoustic transmission: solvent-soluble resins, water-soluble glycols and proprietary ultrasonic couplants are used to match the impedance of the transducer to the impedance of the moving surface and so reduce loss of signal energy. Before positioning the sensor, the surface should be cleaned of all debris, including old layers of paint. The surface should be level and smooth where the sensor is to be positioned to obtain maximum adhesion.

The sensor must always be stationary with respect to the monitored surface, so in addition to the different means of coupling, there are various methods for fixing the sensors to the structure such as adhesives and cements. Some of these can act as a couplant but to prevent unwanted attenuation; care must be taken to avoid air bubbles and thick glue layers. In case of using glue, special care must be taken when removing the transducer. A number of less desirable ways exist to attach AE transducers, tapes, elastic bands, springs, magnetic hold-downs but none of these is as good as such Ethylcyanoacrylate based industrial super glue.

Electrical grounding of the transducer casing is necessary. Care should be taken that no mounting (or the transducer itself) should form an electrical bridging between the sensor case and the supporting structure. This arrangement will minimise the electronic noise generated from the monitored structure.

4.6 Preamplifier:

AE transducers require a pre-amplifier and amplifier. This is because the piezo-electric materials are high impedance sources producing small high frequency signals, and so cannot drive signals over long distances. The cables from sensor to pre-amplifies should be kept short (<1m) and be shielded (co-axial or BNC) to avoid electro-magnetic noise. The pre-amplifier matches the high impedance of the source (transducer) to the low impedance cable. Pre-amplifiers which minimize electronic noise and filter out unwanted frequencies should be used, and amplifiers with a flat response in the frequency range of interest are best. The gain of the amplifier is given by:

Gain = 20 log 10 (V_o/V_i) dB

Where V_i is the reference voltage and equal to 1µ-Volt ,and V_o and output voltage

4.7 Calibration of AE transducers by using Hsu-Nielsen method

The Hsu-Nielsen calibration method (Brüel & Kjaer,1981) is a simple and easy method that does not require any complex auxiliary apparatus. The calibrating device, see Figure 3-2, consists of an “automatic pencil” in which the “lead” is a sensitive graphite pin of hardness 2H and diameter 0.5mm. The calibration signal is generated at the moment of breaking the pin, which is cased in a properly adapted tip put on the “automatic pencil”. The “lead” is pulled out by a standard 3mm to ensure the same breaking angle at each test, which also

means generation of a repeatable acoustic surface waves. This method is classified as a pulse calibration method where the pulse results from the manual breaking of the marking point achieved by pressing on the pencil (Boczar and Lorenc 2004). Because of its simplicity it is frequently used for calibration of measuring systems installed in technical conditions and is standardized (French standard NF–A 09-350, 'Non-destructive tests, vocabulary used in AE')

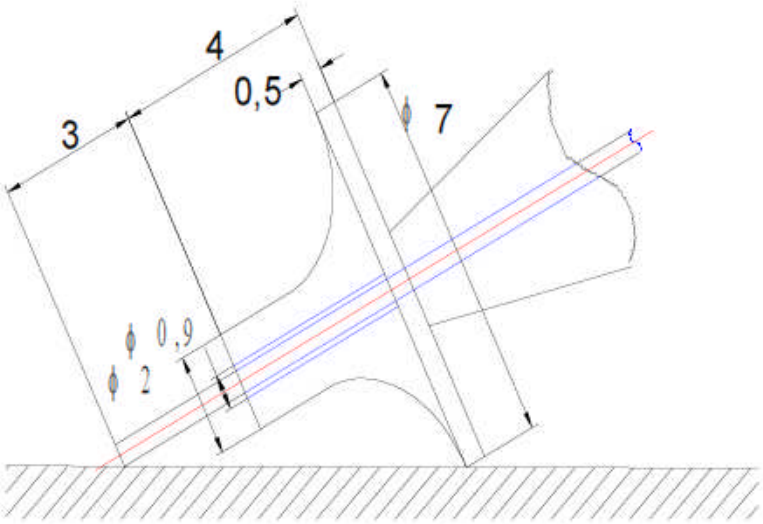

Figure 3-2: Hsu-Nielsen Calibration Head, (Boczar and Lorenc 2004)

4.8 Data Acquisition

The data acquisition board is the means by which the data enters the computer for analysis. Normally AE signals are processed directly, or in case of using pre-amplifiers, after the amplitude becomes larger than the threshold level. The board samples the analog signal and converts it to digital data. The major considerations are the triggering and speed of A/D conversion. Today A/D devices are so fast that a large number of events can be recorded and the A/D

converter can sample every channel of the recording unit. Anti-aliasing filters are required to ensure that signals can be accurately transformed to the frequency domain. The monitoring system can be used to analyze the signal to produce such information as arrival-time, count, duration, event rise time, peak amplitude, RMS value and frequency spectrum.

4.9 Review of existing AE technology

The detailed review of existing AE technology is reported by Sikorska (2006) The following section provides a brief description of some of them.

1. Stress Wave Analysis- Swantech Ltd

Swantech Ltd have developed stress wave analysis as a process for examining the data collected by its patented stress wave sensory technology to identify the operating condition of an item of plant or equipment. Depending on the mechanical complexity of a given machine, multiple sensors may be required to characterize the condition of the equipment (Jamaludin at al., 2001).

2. Spectral Emitted Energy (SEE)-SKF

SEE is a technique developed by SKF Engineering and Research Centre and used which uses envelope analysis for detection of bearing defects. The sensor is a wide band Piezo-electric transducer. The output is suitably filtered and enveloped. The envelope signal can be analysed using normal analysis equipment. SEE provides useful information on lubrication related problems (Jantunen ae al., (1993).

3. Acoustic Emission- Holroyd Instruments

Since the mid 1990s, Holroyd Instruments has released a number of products based on their patented acoustic emission/stress wave sensing technology.

Data acquired by special Holroyd sensors give results in terms of two parameters: Distress® and dB level dB level which are an indicator of the general health of the machine being monitored, typical data loggers facilitate a dB level range up to 80-92dB. Whereas Distress® is determined by taking the analogue dB level signal (Jiaa and Dornfeld, 1990).

Chapter 5 : AE in the Process Industries

In recent years much Acoustic Emission (AE) research has been concentrated on detecting initiation and propagation of cracks in materials (Roberts and Talebzadeh, 2003; Bouras et al., 2008). However, a significant amount of AE research has been into fault detection and the monitoring of plant, machines and structures (e.g. nuclear power plants, pipe leakage, and bridge and bearing failures). This latter aspect has been well reviewed elsewhere by such authors as David (2006). AE sources also exist in many chemical processes such as gas/liquid mixing, chemical reactions and particle transportation systems. This review will be devoted to describing AE as a tool for monitoring two-phase flow. Although air/solid and liquid/solid flows are mentioned in this review, the core will be gas/liquid mixtures.

5.1 Acoustic Emission definition:

AE is defined as a physical phenomenon occurring within and/or on the surface of materials (ISO 22096, 2007). The term AE describes the spontaneous elastic energy released by a process in the form of transient elastic waves. Acoustic emissions generated within a material will be manifest as elastic waves on the surface of the material and cover a broad frequency range, typically from 20kHz to 1MHz, which is outside the range of human hearing.

5.2 Sources of Acoustic Emission and sound emitted from fluid flow processes:

AE sources are divided into two main categories; Primary sources are those where the AE originates from mechanisms of deformation and fracture; in metals, sources of AE include crack growth, moving dislocations, slip, twining,

grain boundary sliding and fracture, and dislocation of inclusions. Secondary sources of AE include leaks, cavitation, liquefaction and solidification (Miller, 1987).

AE originating in industrial processes are usually generated from one of two main sources: mechanical or hydraulic. Mechanical sources would include; cracks that occurred within a moving part, or friction and rubbing between moving parts of a pump, valves, separators, gears or bearings associated with the process. Hydraulic sources considered to make a contribution to generating AE are listed below (Abouelwafa and Kendall, 1980; Merilo et al., 19977)

1. Cavitation - bubble formation, growth and collapse, (Leighton,1994 and Mba et al., 2006),
2. Turbulence noise produced by flow vortices (Derakhshan et al.,1989 and Brennen 1995),
3. Gas, solid and liquid mixture interaction in multiphase flows,(Boyd and Varley 2001)
4. Flow past restrictions and side branches in piping systems (McNulty, 1985),
5. Broadband turbulence energy resulting from high flow velocities, (McNulty, 1985),
6. Intermittent bursts of broadband energy caused by cavitation, flashing, recirculation, and water hammer (Neill et al., 1998),
7. Liquid drops impacting on a liquid surface (rain fall) (Pumphrey and Crum, 1989; Oguz and Prosperetti,1990),
8. Leakage from e.g. pipes (Lee and Lee, 2006),

9. Chemical reactions (Van Ooijen et al., 1978),

10. Foam break up (Lubetkin, 1989), and

11. Oceanic noise due to the breaking of waves (Leighton,1994 ;Vergniolle et al., 1996; Grant 1997)

In the above list, the AE emitted from liquid flow as a direct consequence of gas bubble formation and collapse is an important area for search, even though each source has a different formation mechanism.

5.3 The Mechanisms of Acoustic Emission and sound generated from bubbles

In the literature the earliest known reference relating to the sound emitted from water/air mixtures due to the presence of air bubbles was by Bragg (1921); the murmuring of a brook and the "plunk" of liquid droplets impacting on the water surface were both attributed to entrained air bubbles. The first person to relate the frequency of the sound produced by a bubble formed at a nozzle to the physical parameters involved was Minnaert (1933). Subsequently, a number of investigations were devoted to the sound emitted from two phase flow as a function of bubble size and bubble population, Schiebe (1969), Pandit et al., (1992), Terrill and Melville (2000), Manasseh et al., (2001) and Al-Masry et al., (2005).

Strasberg (1956) suggested that sound emitted by a bubble was the result of oscillatory motion of the bubble wall. He compared volume pulsation and shape oscillation of a bubble. Four orders of oscillation, corresponding to bubble wall oscillation modes are shown in Figure 5-1. The zeroth mode represents a simple volume pulsation with fixed shape. The first mode corresponded to translational oscillation about a fixed point with fixed volume and shape. The

second and third modes of oscillation show changes in shape of increasing complexity with a fixed volume. Strasberg (1956) calculated the natural frequency of the zeroth mode of volume pulsation from Minnaert's (1933) model, see equation 5-1. The natural frequencies of the other three oscillatory modes were calculated according to Lamb's (1945) model, see equation 5-2

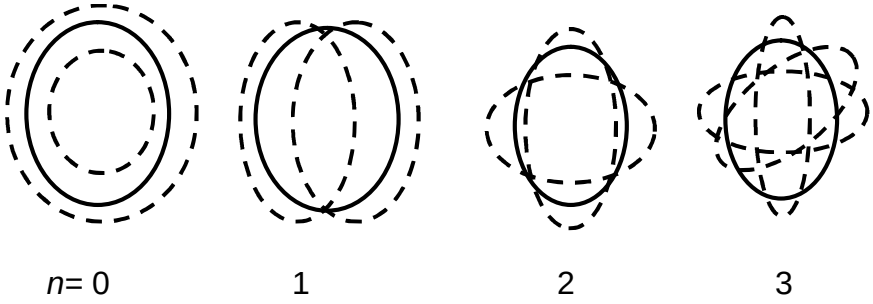

Figure 5-1: Four modes of oscillation of a spherical bubble

$$f_0 = \frac{\left[3\gamma P_0 / \rho\right]^{\frac{1}{2}}}{2\pi R_0} \qquad 5\text{-}1$$

$$f_n = \frac{\left[\left(n^2 - 1\right)\left(n + 2\right)T / \rho R_0\right]^{\frac{1}{2}}}{2\pi R_o} \qquad 5\text{-}2$$

Where:

f_0 is the natural frequency of oscillation for zeroth mode of volume pulsation

f_n is the frequency for the *n*th mode

P_0 is the static pressure

γ is the ratio of the specific heat of the gas in the bubble

R_0 is the mean radius of the bubble

ρ is the density of the liquid

T is the surface tension

Strasberg (1956) investigated factors influencing the amplitude of the bubble oscillations (the resulting sound pressure) when bubbles were exited by such mechanisms as; (a) bubble formation, (b) bubble coalescence and division and (c) the flow of a free stream of liquid with entrained bubbles past an obstacle and the flow of bubbles through a pipe past a constriction**.**

5.3.1 Bubble formation (Volume pulsation) ,

The pressure waves produced by gas bubbles as they form within the body of a liquid has been the topic of much research in order to separate sources of ambient sound in the oceans from that of marine traffic. Leighton (1994) is a good review of bubble acoustics. Minnaert (1933) showed theoretically that the pressure waves originated mainly from volumetric bubble oscillations when the bubble is formed and has not reached a state of equilibrium. The bubble undergoes initial oscillations which produce an acoustic pressure wave before reaching its equilibrium state. Meyer and Tamm (1939) showed experimentally that the sound emitted was mainly due to volumetric pulsations of the bubbles.

Minnaert's analysis was not concerned with why or how the bubbles were formed, but photographic studies by Richardson (1948), Strasberg (1956) and Franz (1959) showed that the commencement of the pressure pulse due to the impact of a liquid drop on the surface of a liquid occurred at the same instant as

a bubble is formed in the liquid. Pumphrey and Crum (1989) studied the impact of water drops on a free surface using a high-speed camera and found that when the impacting drop entrains an air bubble, the majority of the sound produced is due to volume pulsations of the bubble which generates sound pulses at a frequency characteristic of its radius, as shown in Equation 5-1. Strasberg (1956) and Manasseh et al., (1998) used high speed photography of the neck-breaking phases of the newly formed bubble from a nozzle, and correlated each phase to its corresponding emitted sound acquired by hydrophone. Kidin et al., (1984) used a stroboscopic Schlieren technique to confirm their theoretical model that a sudden volumetric expansion of a bubble gave rise to a pressure impulse.

Strasberg (1956) used Equation 5-1 to show that a bubble of 0.65mm diameter will oscillate at 10kHz due to volume pulsation in the zeroth mode. The same bubble will oscillate at 790Hz and 1500Hz due to shape pulsations in modes 2 and 3, respectively. He concluded that appreciable sound is radiated only when the bubble is in volume pulsation mode, and sound pressures associated with change of shape modes (higher modes) are relatively negligible (three orders of magnitude less), and translational oscillations emit no sound. He also found that smaller bubbles, with a smaller surface area radiate less energy for a given volume rate of bubble formation.

When two bubbles of equal radius undergo equal volume oscillations the amplitude of the resulting pressure wave is increased simply because there is now twice the sound energy, but the frequency of the sound is unchanged (Benjamin, 1954). Schiebe (1969) showed that the magnitude of the pressure pulse due to n similar bubbles is proportional to $\sqrt{n}$.

5.3.2 Bubble breakup and coalescence

Bubble breakup controls the maximum stable bubble size and will be greatly influenced by the balance of hydrodynamic stresses and surface tension forces (Hinze 1955). Walter and Blanch (1986) have pointed out that the existing hydrodynamic stresses in the region of the bubble itself will determine bubble breakup. In the case of laminar flow the break up will be determined by the stretching of the bubble due to viscous shear at the bubble surface. With turbulent flow the turbulence eddies will impact on the bubble surface causing it to breakup.

When bubbles split or coalesce, a decaying pressure pulse is emitted, as in bubble formation. In this case, the excitation of volume pulsation results from the difference in equilibrium pressure inside a large bubble and inside a small bubble. The pressure difference is due to the reduced surface tension pressure on the single larger bubble (Strasberg 1956).

However, a recent investigation was of sound emitted by air bubbles as they detach from an underwater orifice connected to a large volume of gas. Here a hollow needle injected air into a tank of water. The bubbles formed on the end of the needle and for a steady flow where bubbles detach singly very little noise is generated. However, above a certain flow rate two bubbles are generated in rapid succession, see Figure 5-2. The physics of the situation is such that the secondary, very much smaller bubble coalesces with the larger as shown in Figure 5-2, and a loud bubble-acoustic emission was generated. Furthermore, for a given primary bubble diameter, the amplitude of the sound due to coalescence increased as the size of the secondary bubble increased. The maximum sound was observed at the equalization of pressure in the coalescing bubbles. Moreover the sound created on coalescence has an order of magnitude greater amplitude than the sound created on pinch-off of the primary bubble, and the time of the acoustic emission was around 5ms (Manasseh et al., 2007).

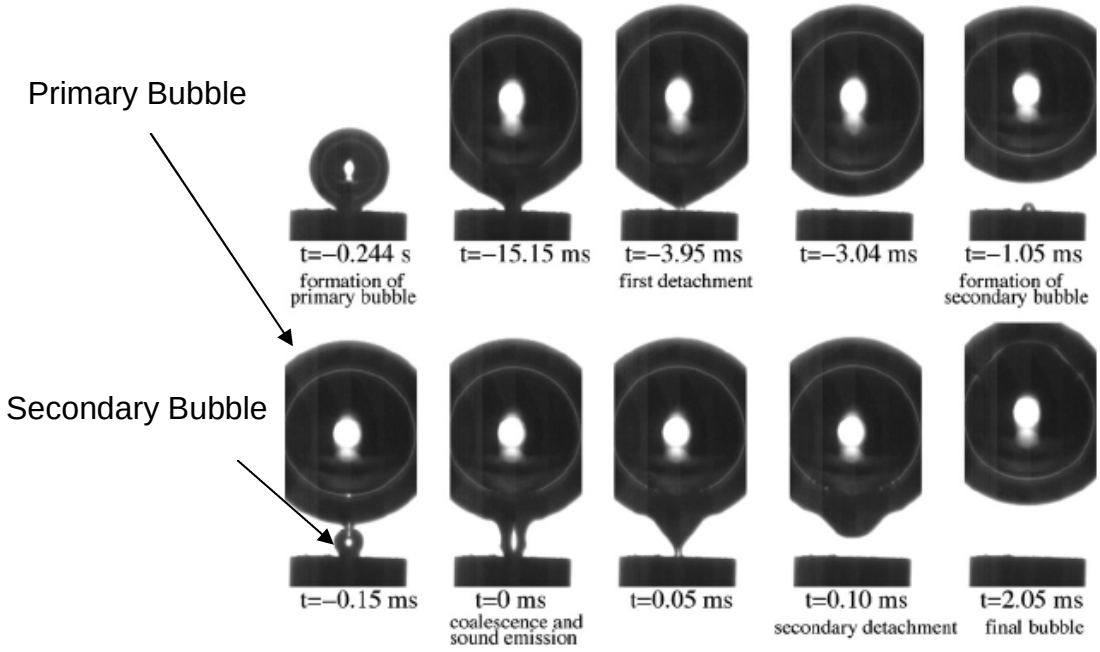

Figure 5-2: High speed video of bubble formation and coalescence sequence (Manasseh et al., 2007 – the air bubbles are white and the black background is the water into which the bubbles are being injected)

5.3.3 Hydrodynamic forces

This includes flow of a free stream of liquid with entrained bubbles past an obstacle, such as the flow of bubbles through a pipe past a constriction. The bubbles are subject to a transient pressure as they move past the constriction which causes them to pulsate and radiate a pressure wave. A similar phenomenon occurs when entrained bubbles flow past any non-uniformities in pipes, such as valves, bends, and changes in cross-section.

5.4 Previous work

5.4.1 AE and sound generated from two-phase air/liquid flow

Pandit et al., (1992) investigated sound emitted from bubbly two-phase flow. Firstly for different fluid velocities and void fractions using a horizontal pipe located downstream of centrifugal pump, where the sound emitted was measured by a hydrophone fitted into the pipe. The second was on using an axi-symmetric gas/liquid jet immersed in a rectangular Perspex water tank with the same hydrophone placed in front of the gas/liquid jet. These authors concluded that bubble size distribution could be determined from the frequency and amplitude of the measured pressure fluctuations.

Leighton at al., (1996) used acoustic techniques to characterise bubble populations within liquids. Principally they investigated the best way of measuring bubble size using “eight” (the title of the paper says eight, but the list of methods in the paper shows only seven) scattering techniques either individually or together, so that the limitations of any one technique were balanced by the strengths and advantages of the others. These techniques were; broadband scattering, scattering at the fundamental frequency of the bubble, scattering at the second harmonic of the bubble, scattering at the third harmonic of the bubble, geometric scattering, fundamental sum-and-difference scattering, sub-harmonic sum-and-difference scattering. Leighton at al., (1996) concluded that multiple acoustic techniques showed more accuracy than any single technique in classifying the bubble population. Some individual techniques showed good results for high density population, whereas others were more applicable for measuring small numbers of bubbles.

Manasseh et al. (2001) used an acoustic bubble sizing technique to measure void fraction inside an agitated vessel. It was assumed that only bubbles within a certain critical radius of the sensor were detected and that over the measurement period there was only one bubble in the relevant region. It was emphasised that these were severe limitations and thus the measured void fraction could only be taken as a qualitiative assessment. The initial frequency of oscillation of a bubble is determined by its radius, so if measuring the frequency of oscillation is restricted to the initial moments this is a method of measuring bubble volume. Manasseh et al. used a windowing technique which was triggered at a certain pressure threshold. The window ensured that only the initial portion of the pulse was captured and this gave the frequency of oscillation of the bubble and hence a measure of its volume.

Manasseh (2004) conducted an investigation using a passive bubble acoustic technique as part of a feedback loop to control and optimise aeration in a chemical process taking place within a 20000 litre bioreactor tank. A hydrophone with a subsequent high pass filter to eliminate unwanted background noise was inserted into the tank, close to the wall. The high pass filter was set for 400Hz because the lowest frequency of interest was about 700Hz, which corresponded to the largest bubbles in the process, about 10mm diameter. The typical bubble diameter was about 4mm which generated frequencies of about 1500Hz. The tank was operating at full production while measurements were made continuously over 24 hours. Manasseh concluded that this was a new sensing technique which could be used to improve aeration and increase bubble dispersion in industrial processes.

Lubetkin (1989) inferred the nucleation rates of bubbles being formed at a single site beneath the surface of a liquid by measuring the acoustic noise of bubbles bursting at a surface. Rzesotarska et al., (1998) measured the AE below short-lived static foam (Triton X-100, ethanol and water mixture) floating

on water. The bubble rupture which was part of the drainage process generated high intensity AE with emissions over the range 25 to 70kHz and it was found that AE increased as the proportion of ethanol was increased.

Morozov et al. (2007) performed an experimental study to simulate leak monitoring in a nuclear power plant using acoustic noise. However, the leak signals were distorted by background noise. In order to identify the main sources of acoustic noise, 53 narrow band sensors were used and placed in power plant facilities such as the heat exchangers (by means of waveguide), circulation pumps, injection and cooling system pipe lines, valves, etc. It was found that the main and strongest background acoustic source was the presence of free gas in the coolant, mainly as a result of pressure fluctuations driving volume oscillations of the bubbles. It was also found that the acoustic noise was proportional to the volume flow rate of the free gas (gas void fraction).

5.4.2 AE and sound generated from Cavitation phenomena

Derakhshan (1989) studied the attenuation of the pressure pulses from bubble collapse generated by a spark (electrode) system placed in a plastic water tank of 1m x 0.75m x 1m size at a depth of 152.2mm. A calibrated 10 to 125kHz broadband AE transducer was placed at a different distances from the electrode. It was found that the pressure pulse of bubble collapse did not follow the acoustic law for a spherical source (the energy attenuates with the square of distance from the source), and it was concluded the reason might be disturbance of the bubble growth (bubble cloud) by the transducer and/or the pressure front may not be fully developed.

Derakhshan also observed that RMS acquired from an AE transducer placed on a steel specimen exposed to a jet stream of water and bubbles, within the same tank, increased with increased pressure and bubble rate. On the other hand the RMS output from a tank wall transducer decreased with increasing pressure and bubble rate. The formation of a bubble cloud attenuated the AE signal prior to it reaching the transducer. He concluded that RMS is an effective way of monitoring bubble collapse intensity, provided that the signal is detected directly or by using steel rod which works as wave guide.

Hutton (1969) experimentally studied the viability of detecting and segregating AE signals emitted from solid material (carbon steel plate) which experience plastic deformation in the presence of hydraulic flow and pump noise (turbulent flow and cavitation). The plate was attached to a steel tube of an existing hydraulic loop. The hydraulic noise was introduced by changing the flow speed and cavitation generated by a gate valve about 3m upstream of the detecting sensors. Also a 2.2MHz shear-wave transducer was mounted on the edge of the plate and 1.0MHz longitudinal-wave transducer mounted on the surface of the plate.

Hutton (1969) concluded that cavitation was found to generate a significant increase in noise level up to 800kHz, and hydraulic noise including cavitation has spectral content that was mostly below 1MHz. It was found that the presence of cavitation in the system increased the AE noise by a factor of 50. Furthermore the AE burst emitted from the steel plate due to a seeded plastic deformation had a frequency of more than 1.5MHz, and so was unaffected by the hydraulic noise and cavitation. In addition the edge mounted shear-wave sensor produced a much sharper and shorter response to AE than the surface mounted longitudinal-wave sensors

Darling and Johnston (1991) conducted a qualitative comparative study between a vibration accelerometer and 500kHz resonant stresswave (AE) transducer, both mounted on the casing of high pressure hydraulic piston pump with seven cylinders. They observed that, under normal running condition, the time domain analysis of the accelerometer signal revealed that the pumping frequency component at 174Hz was buried by the noise and vibration caused by structural and hydraulic effects. Also, different results were reported for different accelerometer positions which was regarded as an indication of sensor position sensitivity. On the other hand the time domain results from the stresswave transducer showed very clearly the impulses in each cylinder during the pumping cycles. Although the AE amplitude changed with position and securing bolt torque, the relative size of each harmonic remained the same, concluding that stresswave sensors were less sensitive to their positioning.

Later in a cavitation test, Darling and Johnston reported that the AE mean signal output increased as cavitation was induced, but a decrease was noted during severe cavitation, and this was related to the absorption of the AE signal by a bubble cloud and a consequent increase in the attenuation of the AE signal through the two phase mixture. They also noted that collapse of the bubbles cause wideband noise up to 1MHz, and the AE strength depends upon the size of bubbles and the pressure of the pump. Conversely, the time domain analysis of the accelerometer signal showed little sign of the degree of cavitation, with only small changing from normal vibration signature.

Deeprose et al., (1974), studied sound levels generated by cavitation at three different frequencies; shaft frequency, blade frequency and at 40kHz. Piezo-electric hydrophones were used with a resonant frequency of 400kHz. They were placed in the suction and discharge lines, and a high pass filter of 4kHz was used to improve signal to noise ratio. Deeprose et al., reported that for early development of cavitation in a pump impeller, high frequency level (AE)

was generated, the main source being the growth and collapse of small vapour bubbles. The AE continued to increase with further development of the cavitation, until at a certain degree of cavitation the bubbles absorb so much energy that the AE decreased. The cavitation noise was detected at a frequency of 40kHz, but it was claimed that the observation can be readily and accurately repeated at frequencies much higher than 40kHz. Noise levels measured from several non-cavitating pumps have been shown to be substantially in excess of levels measured arising only from fluid flow.

Al-Maskari (1984) conducted experiments at different flow rates with a 22kW centrifugal pump at a speed of 300 rpm to study cavitation using AE techniques. Eight different flow rates were used, at each flow rate the test began for a non-cavitating condition and continued to a cavitating condition. An AE transducer was placed at the pump inlet and another on the pump casing. The output data were presented as amplitude distribution plots, number of events, number of counts and total vibration level.

Almaskari concluded that AE analysis was just capable of detecting developed, but not incipient cavitation. He observed an increase in total numbers of events and counts as well as the amplitude distribution just before the developed cavitation condition; however, no change was reported for any of these outputs for incipient cavitation. He also related the increase and decrease of the signal just before the developed cavitation at flow rate above $85m^3/h$ to the absorption of sound by the large number of bubbles present. The results obtained from the two different transducers locations were very similar, this was related to the characteristic of AE surface waves and its location insensitivity in the vicinity of the AE source.

Neill (1997) investigated the possibility of detecting incipient cavitation using AE techniques. Two single stage centrifugal pumps, one of 3kW and the other of

75kW were investigated under normal and cavitating conditions in the presence of background noise. The AE signals were acquired in unprocessed (raw) format at a sampling rate of 2.5MHz and processed RMS format at 50kHz. Neill reported that although the background noise was relatively high in the case of 75kW pump compared to the 3kW pump, incipient cavitation was detected as a drop in the RMS level for both pumps. The author concluded that the AE sensors were able to detect incipient cavitation prior to any significant change in hydraulic performance being detected. A remarkable increase in the high frequency energy band was observed at the beginning of cavitation, whereas developed cavitation showed a decrease in the high frequency energy band which was attributed to the formation and movement of a bubble cloud.

Neill (1998) in a separate work, investigated the possibility of using AE to detect recirculation in centrifugal pumps and how was it might be discriminated from cavitation in the presence of noise produced by normal flow and mechanical sources. The same two pumps and AE arrangements was used as in (Neill 1997). Recirculation is defined as a flow reversal at either inlet or the discharge tips of the impeller vane. The designed flow of the tested pump was 200m^3/h and recirculation become significant when flow rate fell substantially from the design flow. Neill (1998) concluded that the detection and discrimination between different fluid phenomena can be accomplished using AE measurements. Plots of raw AE signals showed clear differences in the AE signature associated with circulation, cavitation and, normal running. In the latter the AE signature was random continuous with disturbance pulses. In circulation the background noise to the pulses remains high, contrasting with cavitation where there was a considerable relative drop in the background noise. Board (2002) also confirmed that cavitation and circulation can be detected by stress wave energy levels.

Alfayez and Mba(2005); and Alfayez et al. (2005), studied the application of AE for detecting incipient cavitation on three centrifugal pumps. Several broadband AE sensors with flat rate response of 0.1 to 1MHz were placed on each pump;

however, the authors found out the AE sensor located in the vicinity of impeller of the pump casing had the strongest signal. It was observed that the highest RMS levels of AE signal were recorded at near zero flow rates, due to the high turbulence associated with the fully closing valve downstream the pump. Furthermore, they observed an increase in AE RMS levels with the onset (incipient) of cavitation, and a decrease in AE RMS with developed cavitation was noted, which was again attributed to attenuation of AE signal by bubble cloud formation.

Alhashmi (2005) investigated the acoustic signal acquired from centrifugal pump using a microphone as acoustic sensor in the audible frequency range 5Hz-20kHz. The experiment was performed at seven different flow rates. The author reported that there was no significant change in RMS levels of acoustic signal with increase inflow rate prior to the onset of cavitation. However with incipient cavitation a remarkable increase in RMS levels was reported.

Sikorska and Hodkiewice (2005) conducted a comparative study using AE, vibration and dynamic pressure analysis for detecting hydraulic changes on a double-suction centrifugal pump. The AE results compared well with the other methods. Three broadband sensors were magnetically mounted on the suction and discharge flanges and pump casing. Sikorska reported that for this particular pump, AE signals acquired from suction and discharge flanges can clearly identify the changes occurring within the pump associated with the onset of suction and discharge recirculation and incipient cavitation.

Duclose et al., (2004) used AE technology to continuously monitor the erosion rate in pipes due to particulate impact, and were able to separate them from AE signals originated from fluid flow and gas bubbles. Two AE sensors were placed on a sharp 90^{o} bend made from 26.7mm diameter stainless steel, opposite to the flow direction the surface was flattened in order to fix the sensors; the wall thickness was 3.1mm. Data was acquired at 1MHz. Sand particles and bubbles were introduced into the flow and controlled by means of 60ml syringe, placed

2m upper stream from the bend. Water was supplied and returned to a tank using a centrifugal pump. It was concluded that AE waveforms of air bubbles can be clearly distinguished from those of particle impacts; AE intensities for air bubbles were much lower, and the event duration was much longer compared to particle impacts. Also the AE energy increased as the air bubble volume increased and, regardless of the particle size, AE energy increased with amount of sand introduced into the flow.

5.4.3 AE and sound generated from two-phase solid/solid, solid/liquid, or solid/air flows

With particulate or powder flow, AE generation has generally been attributed to either friction or collision, either particle-particle or particle-wall interactions (Tsujimoto at el., 2000). Some of the kinetic energy of the moving particles will be transferred as soon as the particles impact on the conduit wall, if the particle slides along the wall some energy will be transferred by sliding friction with the wall, and translated into elastic waves in the conduit wall. The propagation of these elastic waves will depend on the elastic properties of the wall. To detect these waves a suitable AE sensor was fixed on the outer face of the wall (Buttle and Scruby, 1990).

In this context work has been carried out to study particle transportation phenomena as a source of AE. Folkestad and Mylvaganam (1990) detected the amount of sand carried as particles within the oil in a pipeline. The collisions of sand particles with the wall increased with the amount of sand in the oil and the AE signal also increased until at a certain threshold level the amount of sand is deemed unacceptable. A major advantage of this method is that the AE transducer is placed on the outside of the pipe and this does not disrupt flow or plant operations.

Albion et al., (2007) used AE techniques to experimentally investigate the flow regimes of powder in a horizontal 100mm ID, stainless steel, pneumatic transport pipe. Two AE sensors on the outside of the pipe, one on at the top and the other underneath, recorded the acoustic noise generated at different superficial gas velocities and mass flow rates. High speed cameras were used and the videos of the flow correlated with the AE signals. Albion et al., (2007) concluded that frequency analysis and various statistical parameters of the acoustic measurements recorded from the pipe provided a reliable means of identifying both dilute phase flow and flow over settled solids.

Withers (1996) investigated the build-up of fouling in the heat exchangers and pipe work of ultrahigh-temperature processing plants, e.g. for milk and milk products, which can lead to a reduction in both efficiency and product quality. Withers introduced a small piezo-electric transducer into the system at a point where fouling was worst. Thus the transducer would be most rapidly affected by the build-up of fouling film. The transducer, was excited by a signal which covered a narrow range of frequencies around its natural frequency. The application of the signal caused the piezo-electric crystal to vibrate. However the growth of fouling on the crystal damped the vibrations and shifted the natural frequency slightly. This shift in natural frequency is easily detectable and can be used as a measure of the thickness of the fouling film. Such sensors are temperature sensitive, but this does not pose a pose a serious problem as any shift can be compensated during signal processing.

Tily et al., (1987) used a readily available kitchen mixer with a metal bowl to simulate solid/solid mixing in an orbital mixer. A transducer was attached to the bowl and a number of two-phase solid/solid mixtures introduced. The signals from the transducer increased in amplitude with size of particles in the bowl and the mass of particles in the bowl. However, in all cases a point was reached at which the AE levelled off and this steady level could, in turn, be used as a measure of when the mixing process was completed. Initial investigation, by Tily

et al., of the mixing of solids and liquids showed a similar pattern of AE with time.

5.4.4 AE and sound generated from Chemical reactions

Chemical reactions with phase change often produce acoustical signals, and AE has been used to investigate particular chemical reactions. Van Ooijen et al., (1978) observed that if zinc chloride was added to a solution of dichloro(pyrazine)zinc(II) in water a loud cracking sound was heard, followed by precipitation of a fine white powder and then bright white crystals. Frequency analysis showed that the main proportion of the acoustic energy was concentrated in the region of 100kHz. The sound was claimed to be louder the more concentrated the reactants. If the mixture was shaken some time later cracking was again heard. Van Ooijen et al., considered that they had inadequate information to fully explain this phenomenon but suggested that the AE was generated by a phase transition as the precipitate crystals formed.

Betteridge et al., (1981) were the first attempt to use pattern recognition to classifying reactions by their AE signal. These researchers investigated 43 chemical reactions all of which took place in a glass beaker. A piezo-electric transducer whose output was band-pass filtered to between 100 and 300kHz, was attached to the underside of the bottom of the beaker. Three criteria were used and these differentiated the reactions into 8 possible clusters: the duration of the AE, intensity of the AE, and a heterogeneity factor of both reactants and products. However, the criteria used did not provide clear differences between the clusters and additional investigation was necessary; possibly statistical analysis of the AE signals in both the time and frequency domains.

The AE signals from an electrolytic cell with the formation of hydrogen and oxygen bubbles at the electrodes were investigated by Crowther et al., (1991). The anode and cathode were both circular rods 120mm long and 7mm diameter, the anode was of stainless steel and the cathode of nickel. The electrolyte was NaOH solution which varied in strength between 0.1M to 2.1M. A piezo-electric transducer was attached to the working electrode. The applied voltage ranged from 1.4V to 5.0V. It was found that bubble formation coincided with bursts of AE at frequencies of up to 800kHz. The strength of the AE signal depended on the concentration of the electrolyte and was a maximum at a concentration of 1.5M.

High pressure gas and liquid leaks can be significant sources of AE, and detectors based on this technique have been widely used in industry for many years. For example, Fowler (1992) has described such leak detection with super-heated, high pressure, steam heat exchangers in a sulphuric acid plant where wave guide probes were used to protect the sensors from the high temperatures. An alarm sounded if the sensors detected a leak.

5.5 Slug Flow Mechanism and Acoustic Emission

In oil and gas production process, multiphase slug flow regime is normally encountered for a range of pipe inclinations, and, over a wide range of gas and liquid flow rates. Slug flow is characterised by a complex dynamic structure, which consists of aerated slugs of liquid that travel down the pipeline at the local gas velocity. The mechanism of slug initiation has been experimentally investigated by many authors (Kordyban and Ranov, 1970; Graham et al., 1973; Taitel and Dukler,1976; Mishima and Ishii, 1980; Nydal et al. 1992; Barnea and Taitel, 1993; Fan et al., 1993a; Hale, 2000).

One approach of predicting slug initiation is based on studying and analysing the stability of a stratified flow in pipeline as investigated by several researchers. Kordyban et al (1970) suggested that the transition from stratified flow to a slug flow might be described by a classical linear stability analysis. Graham et al. (1973) examined the growth of linearly unstable long wavelength disturbances on a flowing liquid whilst others (Mishima and Ishii, 1980; Fan et al., 1993a; Hale, 2000) considered the evolution of a slug from a finite amplitude wave, with a wavelength in a range that would be stable by the inviscid Kelvin-Helmholtz (IKH) mechanism. However a viscous Kelvin–Helmholtz (VKH) analysis, including the effects of wall and interfacial shear stress, generally gives better predictions for the initiation of slug flow (Nydal et al. 1992; Barnea and Taitel, 1993). In their slug phenomena description, Taitel and Dukler (1976) presented the development of gas and liquid flow in a pipeline. Figure 5-3 shows various stages of slug development. Near to the entrance, due to pipe wall shear stress, gravitational force and the pressure, the liquid decelerates and small perturbations results into the stratified layer. These could lead to growing waves as shown in figure 5-3 (b). The increased gas velocity over these regions could lead to suction effect and could increase the liquid height covering the whole pipe cross-section, see figure 5-3 (c). This process blocks the flow of gas, see figure 5-3 (c), and so the upstream pressure builds causing the blockage to be accelerated to the gas velocity.

Along the way, the fluid blockage picks up slow moving liquid and thus increases the volume and forms slug, figure 5-3 (d).Velocity differences between the slug front and the liquid film results into the gas entrainment and the dispersion of small bubbles which may be transported through the body of the liquid slug. Meanwhile, at the slug tail, liquid and previously entrained gases are released (shedding process) from the slug body. The “shed” liquid decelerates to a velocity determined by the shear stresses at the wall and the interface and becomes a stratified layer as illustrated in figure 5-3(e). The

"shed" gas mainly passes into the elongated bubble (EB) region above this layer, although a fraction may remain entrained within the liquid film. As long as the volumetric "pick-up" rate is larger than the "shedding" rate, the slug continues to grow. However, eventually the "pick-up" rate becomes equal to the "shedding" rate and the slug becomes fully developed so that the slug length stabilises "stable slug". Nydal et al. (1992) experimentally investigated the length of the pipe required to reach quasi-stable flow conditions (slug development distance) and found that it is between 300 and 600 pipe diameters. Once the quasi-stable conditions are reached, the slug length has a mean value between 12 to 15 pipe diameters. Based on the shedding and pick-up processes, slug flow might be classified into three main states. The pick-up rate is greater than the shedding rate; the slug in this case continues to grow. The "pick-up" rate equals to the "shedding" rate, the slug becomes fully developed so that the slug length stabilises. Finally, when the "pick-up" rate is less than the "shedding" rate, the slug under this condition dissipates.

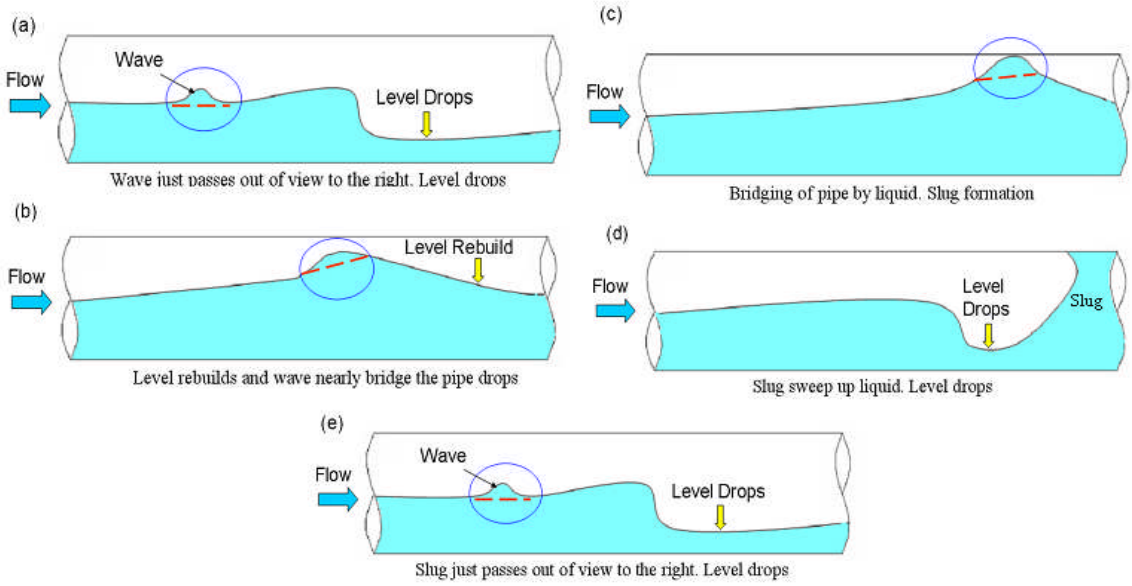

Figure 5-3: The process of slug formation by Taitel and Dukler (1976)

The idealised picture of a “stable slug” flow in horizontal pipe is presented in figure 5-4. The section ‘F’ represents the front region of the liquid slug body (LSB) and section ‘T’ represent the tail region of the liquid slug body. In a stable slug flow, the liquid slug body length, L_{LSB} and the elongated bubble (EB) length (L_{EB}) remain essentially constant in the downstream direction.

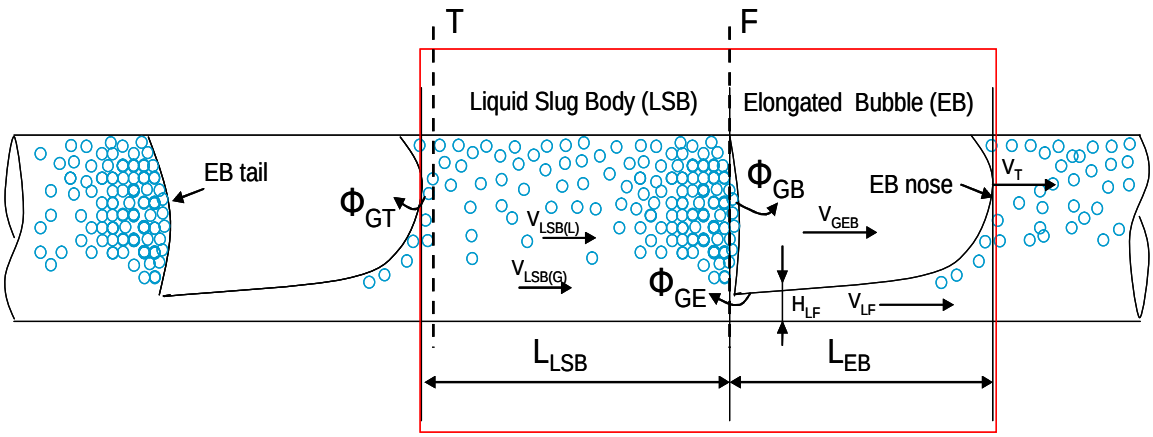

Figure 5-4: Schematic description of the EB and LSB in idealised developed slug flow

The gas in the elongated bubble moves at a velocity, V_{GEB}, which is faster than the average mixture velocity, V_{mix} in the liquid slug body. As a result, the liquid is shed from the back of the liquid slug body to form the liquid film layer along the elongated bubble. The liquid in the film at the EB nose may be aerated. Also, bubbles in the liquid slug body coalesce with the elongated bubble interface and are gradually absorbed, which in the fullness of time results in the liquid film becoming un-aerated. The mixture velocity is the sum of the liquid velocity and the gas velocity ($V_{SL} + V_{SG}$).

At the same time, the gas bubbles are fragmented from the tail of the elongated bubble and re-entrained into the front section of liquid slug body ‘F’ at a rate

Φ_{GE}. The fragmentation of the elongated bubble tail and the entrainment of the bubbles into the front section of the liquid slug body are due to the dispersing forces induced by the flow of the liquid film as it plunges into the liquid slug front. However, some of the gas bubbles that are entrained into the front section of the liquid slug body may re-coalesce with the elongated bubble tail at Φ_{GB} rate, resulting in a net gas flow rate of Φ_{GE} - Φ_{GB} out of the elongated bubble tail. The Φ_{GT}= Φ_{GE} - Φ_{GB} is the constant gas flow rate which is entrained to the elongated bubble EB, and eventually is absorbed into the successive elongated bubble. Therefore, the net rate of gas entrainment in the slug body is the result of a balance between bubble injection and rejection.

The gas bubbles entrainment from the elongated bubble tail and their re-coalescence at the successive nose result in an effective elongated bubble translation velocity, V_T, which is higher than the gas velocity in the elongated bubble, V_{GEB}. From the description of the slug flow formation, dispersed gas bubbles can be generated in the liquid slug body region through the formation, coalescence, breakage and collapse of bubbles processes. The entrained gas bubbles in the liquid experience a transient pressure as they move through the hydrodynamic pressure field of the liquid. The transient pressure causes the gas bubbles to oscillate at their natural frequencies; one consequence of which is the generation of sound (Strasberg, 1956).

5.6 Gas Void Fraction (ε) in Slug Flow

The liquid holdup in the slug body or gas void fraction (ε) is an important parameter for the design of multiphase pipelines and associated separation equipment. The definition of the liquid holdup is “the flowrate of the liquid phase divided by the total flowrate of both the gas and liquid flowrates”. And the definition of the gas void fraction is “the flowrate of the gas phase divided by the

total flowrate of both the gas and liquid flowrates". Several gas void fraction correlations were developed, however, the majority of these correlations were obtained based on the slug body liquid holdup. In multiphase flow, the extensively-used correlation developed by Gregory *et al*. (1978) was obtained from the measurements of liquid holdup, using electrical capacitance probes, in air-water and oil-water flow in horizontal pipes with diameter of 0.0258 m and 0.0512 m. The correlation gives slug body holdup as a function of the mixture velocity V_{mix} only:

$$H_{LSB} = \frac{1}{1+\left(\frac{V_{mix}}{8.66}\right)^{1.39}} \qquad 5\text{-}3$$

where V_{mix} is the slug mixture velocity in ms^{-1} and is equal to the sum of the superficial gas and liquid velocities.

Malnes (1982) proposed an alternative correlation also based on the same data of Gregory et al. (1978) as:

$$H_{LSB} = 1 - \frac{V_{mix}}{C_C + V_{mix}} \qquad 5\text{-}4$$

Where, the dimensional coefficient C_c is measured as following:

$$C_C = 83\left(\frac{g\sigma}{\rho L}\right)^{0.25} \qquad 5\text{-}5$$

Beggs and Brill, (1973) developed their correlation for the whole spectrum of flow situations using 1" and 1.5" pipe sizes at various angles from the horizontal. The correlation passed on Froude number and the slug body length for the intermittent flow as following;

$$\varepsilon = \frac{0.845 E_{LSB}^{0.5351}}{Fr^{0.0173}} \qquad 5\text{-}6$$

where *Fr* is the Froude number, defined as a dimensionless number comparing inertia and gravitational forces, and calculated as

$$Fr = \frac{V_{mix}^2}{gD} \qquad 5\text{-}7$$

Hughmark (1962) proposed correlation for the gas void fraction based on slug mixture velocity and superficial gas velocity, given by:

$$\varepsilon = \frac{V_{SG}}{1.2 V_{mix}} \qquad 5\text{-}8$$

Gregory and Scott (1969), developed similar correlation to the one proposed by Hughmark (1962), as following:

$$\varepsilon = \frac{V_{SG}}{1.19 V_{mix}} \qquad 5\text{-}9$$

Ferschneider (1983) developed a more complex correlation for slug body holdup H_{LSB} using data obtained from natural gas and a light hydrocarbon oil facility. The facility loop comprised a 0.15 m diameter with 120 m long test section loop and operated at elevated pressure of between 10 and 50 bar. The correlation proposed by Ferschneider (1983) took account for surface tension of

the fluids in terms of Bond number (Bo). Bo is a measure of the importance of the surface tension forces compared to gravitational forces.

$$H_{LSB} = \frac{1}{\left\{1+\left[\left(\frac{V_{mix}}{\sqrt{\left(1-\rho_G/\rho_L\right)gD}}\right)\times\left(\frac{Bo^{0.1}}{25}\right)\right]^2\right\}^2} \qquad 5\text{-}10$$

Bo is Bond number and is given by:

$$Bo = \frac{(\rho_L - \rho_G)\times g\times D^2}{\sigma} \qquad 5\text{-}11$$

Nickline (1962) proposed correlation for the gas void fraction based on the measured liquid holdup for air-water flow in 0.05m and 0.09 m horizontal pipe. The correlation is given by the expressions:

$$\varepsilon = \frac{V_{SG}}{(1.2V_{mix} + 0.35\sqrt{gD}} \qquad 5\text{-}12$$

Abdul-Majeed (2000) developed a new correlation to compute the slug void fraction, which only depends on the fluid viscosities and mixture velocity: a data bank set contained several hundreds of slug hold-up points, gathered from

seven different resources were used in this correlation, only mixture velocity V_{mix} and liquid and gas viscosities μ_L and μ_G were utilised as following;

$$H_{LSB} = 1.009 - \left(0.006 + 1.3377 \frac{\mu_G}{\mu_L}\right) V_{mix} \qquad 5\text{-}13$$

Al-lababidi and Sanderson (2005; 2007) investigated the measurement of the slug body liquid holdup and film liquid holdup using the non-intrusive ultrasonic pulse-echo mode system. The system consists of an ultrasonic pulser–receiver which was used to excite the ultrasonic transducer (2.25 MHz), to receive and amplify the reflected signals and an electronic circuit to measure the time of transmitted and reflected ultrasound wave in liquid phase. The authors concluded that the liquid holdup measurements were validated against the non-intrusive conductivity transmitter and compared with correlations from the literature. However, as the gas void fraction increases, the attenuation and distraction of the transit time ultrasonic signals increases. As a result, the transit time ultrasonic can be considered a good technique for the measurement of the slug body and film liquid holdup at low gas void fraction.

Woldesemayat and Ghajar (2007) performed an intensive literature review of the slug body holdup in multiphase flow in pipeline. However, the majority of the gas void fraction (ε) correlations reviewed in this work and in Woldesemayat and Ghajar (2007) intensive review was experimentally developed based on the direct measurement of the liquid holdup in the slug body rather than measuring the gas void fraction.

Most, if not all, of the available correlations for the average slug void fraction in liquid slugs were found to be unsatisfactory when applied to different geometries from those used in extracting the empirical correlations (Paglianti et

al., 1993).This is perhaps not surprising since the above mentioned correlations are derived from fully developed slug flow, and do not account for the transient behaviour of slug growth and collapse (Bonizzi and Issa, 2003).

5.7 Conclusion

The formation, collapse, coalescence and break-up of bubbles all relate to changes of one or more gas/liquid interfaces. Energy from such processes, channelled through mechanisms involving surface tension and hydrostatic and hydrodynamic forces, will generate bubble oscillations and pressure pulses which radiate outwards in all directions as acoustic waves (Leighton et al. 1998). Generally, the frequency of oscillation depends on bubble diameter; Minnaert (1933) stated that "*bubbles with diameters of 3–6 mm would give sounds with frequencies beyond the limit of human audibility*". The decay of a typical AE signal was investigated by Strasberg (1956) and is shown in Figure 5-5**.** It is evident that maximum amplitude is generated by the newly formed bubble, and begins at the moment the bubble closes ('necks'). From the scale provided the duration of the process was tens of microseconds.

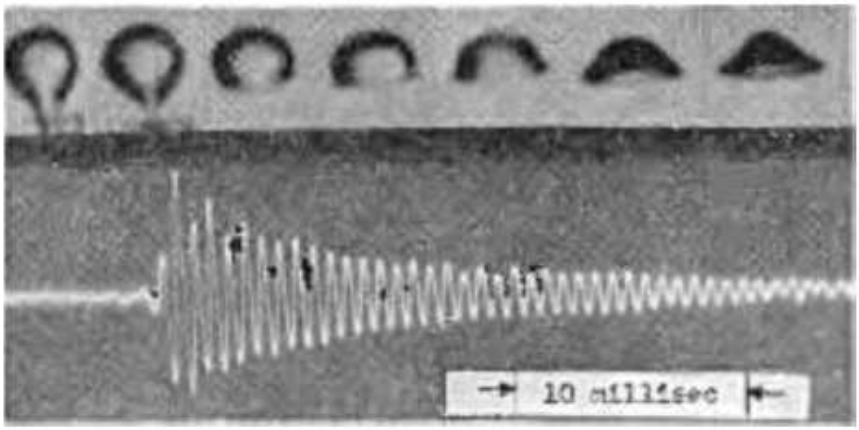

Figure 5-5: Sound pulse signal from an individual gas bubble leaving a nozzle, correlated to sequential photos of the process Strasberg (1956)

The above review of previous research using AE has demonstrated its potential as a monitoring tool for multiphase flows. In all the reviewed research, the AE signals were created by the process itself. The AE signals accompanied physical and chemical events, occurring within the processes and were detected by several different means. Piezo-electric transducers were used when the AE signal was transmitted along the body of the structure (e.g. pumps, pipes and tanks); hydrophones were used in case of the AE signal travelling through the bulk of a liquid, and microphones were used in case of an airborne AE signal. Piezoelectric transducers were generally used to acquire AE signals as this type of sensors can be arranged to be non-intrusive and few special arrangements were needed when installing these sensors. Due to the multidirectional nature of the AE signal, the AE sensor position is not normally important as long as it in the vicinity of the AE source.

The mechanisms of AE generation in two-phase gas/liquid flow have been reviewed and explained. These mechanisms will be used to justify and explain how AE was generated from two-phase air/water flow in bubbly and slug regimes in this investigation (see chapter 7). The mechanisms discussed included; incipient cavitation, developed cavitation, recirculation, bubble formation, bubble collapse and bubble coalescence and break-up. Although, bubble activities are a major AE source, bubbles clouds will attenuate and scatter the AE signal.

Chapter 6 : Experimental Setup and Procedures

This chapter describes the two closed loop test rig facilities, and test procedures, used in this research study;

1. An Initial investigative 50mm (2”) internal diameter (ID) multi-phase water/air test facility, see Figure 6-1.
2. Advanced 50mm (2”) ID multi-phase water/air test facility, see Figure 6-4.

Design details of each test facility will be discussed in the following sections, including water and air supply systems, other devices and measuring instruments.

6.1 Initial investigative 50mm (2”) test facility

The primary objective of this rig was to carry out a preliminary investigation of the applicability of AE technology to the monitoring of two phase flow; to investigate the effects of varying AE sensor orientation/ position on the pipe, and pipe material type on the characteristics of the measured AE signal. The test facility was designed to simulate two phase water/air flow at different water and air velocities, Figure 6-1 shows the general arrangement of the test rig. A description of the test facility including air and water supply systems, pipe lines and instruments will be given in the following sections.

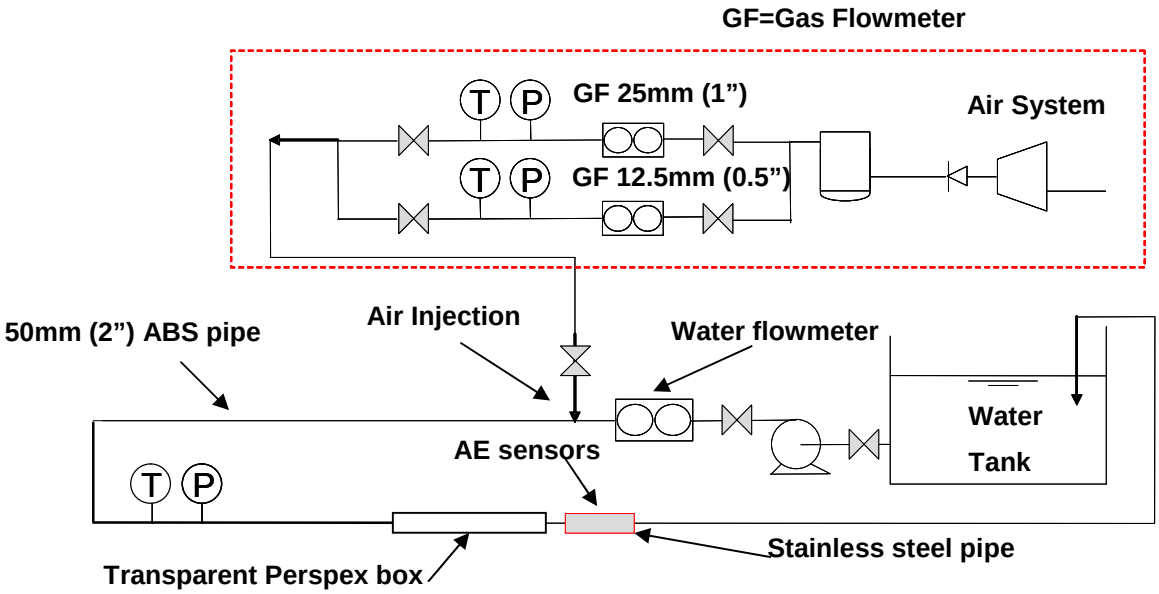

Figure 6-1: Two-phase water/air preliminary test rig

6.1.1 Liquid supply system

Water was used as the working liquid, supplied from, and returned to, a fibreglass tank with capacity of 2 m^3 and open to the atmosphere. The water was pumped around the system by a self priming Certikin Aquaspeed 0.75kW (1HP) pump with a maximum capacity of 15$m^3.hr^{-1}$ at 10m head, see figure A-1 Appendix (A). The flow rate of water was controlled by means of a throttling valve downstream of the pump. The pumped water was metered before the point where it was mixed with the gas, to measure the superficial liquid velocity (V_{SL}). This was done with an electromagnetic flow meter (ABB K280/0 AS model, 0.0 - 18m^3/hr range), see Figures 6-1and 6-3.

This initial test pipeline had a total length of 12m; the majority of it was made from 50mm (2") Acrylonitrile Butadiene Styrene (ABS) class E pipe. The test section was a 300mm length of 50mm (2") ID, stainless steel pipe. As shown in Figure 6-1 this was placed in the middle of the return flow line. The stainless steel pipe had an AE sensor attached, see Figure 6-1. Visual observation of the water/air flow regimes during the tests was through a transparent pipe section installed upstream of the stainless steel test section, see Figures 6-1 and 6-2.

The transparent section was made of 50mm (2”) ID Perspex pipe of 1000mm length placed inside a Perspex box of dimensions 150x180x1000mm.The Perspex box was filled with water to reduce light refraction and enhance the quality of the visual observations.

Figure 6-2: Perspex box used to reduce unwanted reflected light

6.1.2 Air supply system

Air was supplied to the test rig by an Ingersoll Rand compressor unit with 10 bar maximum output with an integrated air tank of 500 litre capacity and 12 bar maximum working pressure. The air tank acted as a settling chamber and was connected to air injector by two flow meters in parallel. These flow meters were of two different types and ranges, see Figures 6-1 and 6-3:

1. Thermal mass flow meter, Endress + Hauser, Proline t-mass flanged 65 F 15, for inline use with flows in the range 0 to 2m^3/hr at 9 bar, was connected into the 12.5mm(0.5”)airline, and
2. Vortex flow meter, Endress and Hauser Proline Prowirl 72 F 25 for inline use with flows in the range 3 to 100m^3/hr at 9 bar connected into the 25mm (1”) airline.

The air flow was controlled by means of a brass gate type valve installed upstream of the gas flow meters. The metered air was then injected into the 50mm (2”) water pipe at the designated air velocities to simulate two-phase

flow. All air pipes were fitted with pressure transducers and thermocouples, marked P and T, respectively in Figure 6-1. The gas flow meters had a 4-20mA HART analogue that was connected to the data acquisition system, and had values ranging from 0 to 10V DC. The temperatures and pressures measured in the 12.5mm (0.5”), 25mm (1”) and 50mm (2”) pipes were used to calculate corrected values for superficial velocity entering the 50mm pipe.

The different superficial velocities of liquid and gas (V_{SL} and V_{SG}) were achieved by throttling valves upstream of the flow meters, as shown in Figure 6-1.

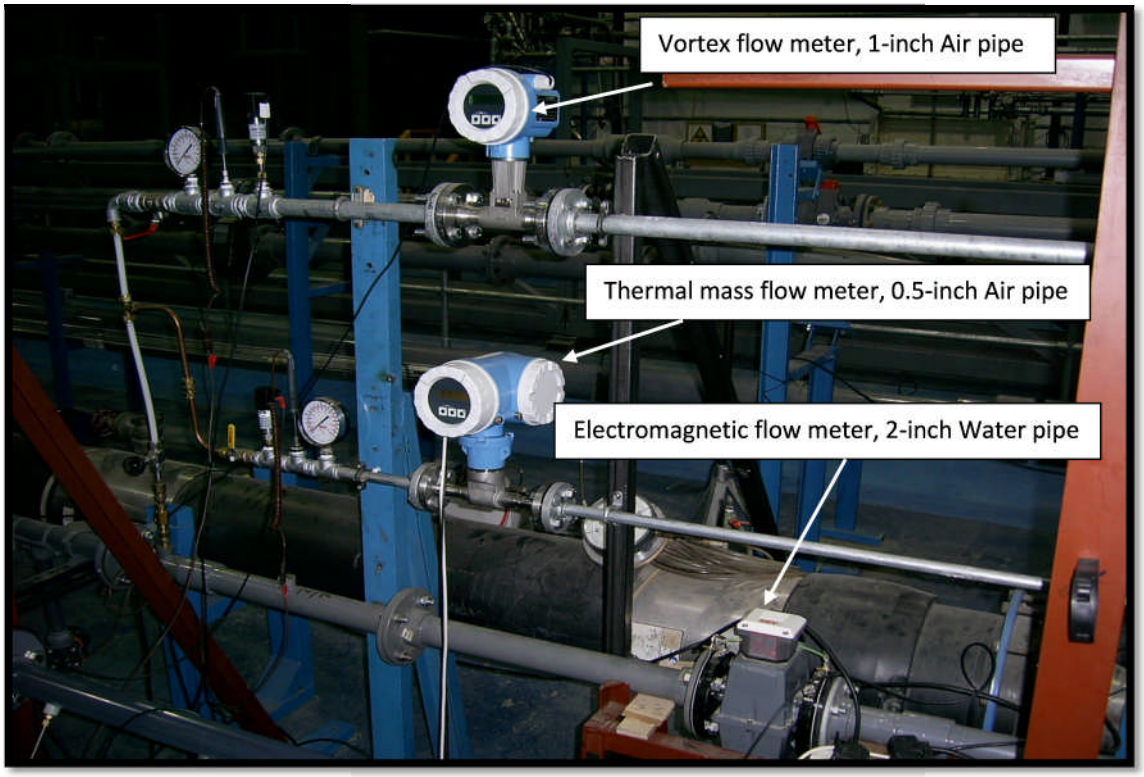

Figure 6-3: Gas and water flow meters

6.1.3 Flow data acquisition system

All measured data from the flow meters, pressure transducers and thermocouples for both water and air supplies were acquired using a 12 channel PC based Data Acquisition System (DAS). The signal was then fed to the PC via a 32 channels parallel port multiplexer (SCB-68) after being converted to an appropriate digital signal. A runtime 6.2 version of Labview 'National Instrument' was used to gather these data in real time and display the results on a computer monitor, after being converted to engineering units for the corresponding instruments, for example volt to bar, in the case of pressure measurements. The PC system runs with a Windows XP operating system and 2.8GHz Pentium processor, with a hard disc capacity of 100 GB.

6.1.4 Experimental procedures

The investigations of this experiment were carried out involving 10 different superficial liquid velocities (V_{SL}) and 24 superficial gas velocities V_{SG}. That is, at each V_{SL}, all the 24 gas velocities V_{SG} were investigated, giving 240 measurements. Digital readings for the flow meters were displayed on a 17-inch LCD monitor, which assisted the adjustment and fine-tuning of V_{SL} and V_{SG}. The liquid superficial velocity (V_{SL}) ranged from $0.3ms^{-1}$ to $1.2ms^{-1}$ in increments of $0.1ms^{-1}$, and the gas superficial velocity (V_{SG}) ranged from $0.1ms^{-1}$ to $4.0ms^{-1}$ using both the 12.5mm (0.5") and 25mm (1") air supply pipelines. The 12.5mm air line was used to supply V_{SG} over a range of 0.0 to $2.0ms^{-1}$ at increments of $0.1ms^{-1}$, and the 25mm line was used to supply V_{SG} from 2.5 to $4.0ms^{-1}$ at increments of $0.5ms^{-1}$.

Data was sampled from the AE sensors for 120 seconds for each and every pair of V_{SL} and V_{SG} values. The time-domain signal was analysed to give its Absolute Energy, Root Mean Square (RMS) and Average Signal Level (ASL).

6.2 Advanced 50mm (2") test facility

This second test rig was designed to produce different flow regimes for water/air flows. A number of test parameters were investigated; AE sensor type (see Section 6.3), liquid and gas velocities, pipe internal surface roughness, liquid viscosity and temperature, pipes that were straight and pipes with elbows. Such detailed measurements were not made on the initial test-rig.

In this experiment a new and different type of sensor was added; conductivity electrode rings (see Figure 6-6). The experimental facilities again consisted of liquid and gas supply systems, Perspex pipes, steel specimen test section, circulating pipes and fittings, see Figure 6-4. The next sections give more detailed descriptions of the experimental apparatus used.

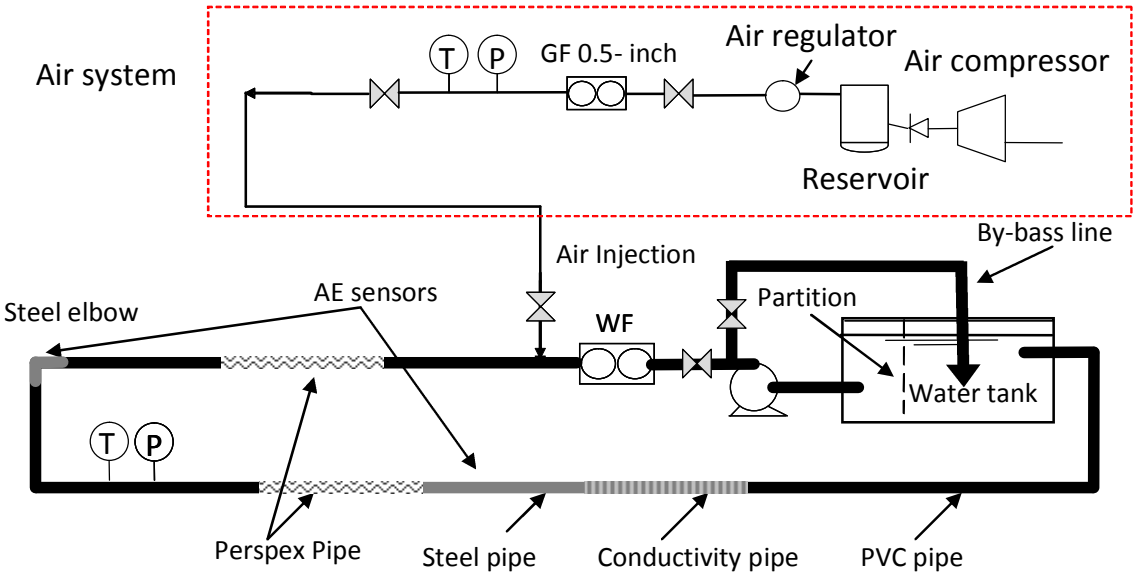

Figure 6-4: Experimental setup for Two-phase GVF measurement

6.2.1 Liquid supply system

The liquid (water) used in this test was stored in 4m^3 fibreglass tank, open to atmosphere with its base resting on the floor. The water was circulated through

a closed loop of 50mm (2”) ID pipe by a Worthington Simpson centrifugal pump with a maximum capacity of $40m^3.hr^{-1}$ and a maximum discharge pressure of 5 bar. The pump was sited on the floor while the suction side of the pump was at 20cm from the bottom of the tank to allow debris and other solids present in the water, to settle on the bottom and not be sucked into the pump. This was assisted by inserting a plate partition with rows of holes cut into it, between suction and return. The bubbles brought by the return pipe naturally rose to the surface of the tank and only clear returned water entered the suction side of the pump.

Because of the high capacity of the centrifugal pump, a by-bass line was inserted to recycle the extra flow to the tank via a valve, see Figure 6-4. The valve was adjusted to ensure that the pump was always running at the smoothest possible working condition, thus generating minimum hydraulic noise. This arrangement was kept unchanged throughout all investigations. The water flow rate was controlled by a throttling valve, and metered using an Electromagnetic flow meter, Khrone Altoflux type, with a maximum supply capacity of $20m^3.hr^{-1}$. The flow meter was placed upstream of the water/air mixing point.

The pipe used was 50 mm (2”) ID ABS (class E) and total length of 22.5 m, see Figure 6-4. The pipeline length was such to allow flow stabilization and to ensure that the regime was fully developed before the flow entered the steel test section. The test sections were made of 50 mm (2”) ID stainless steel pipe, and steel elbow section as shown in Figure 6-4. Included in the pipeline were two transparent Perspex tubes, see Figure 6-4; the first was 1500mm long, placed 2 meter downstream the air injection point to observe the early stages of air/water mixing. The second Perspex pipe was 3 meters long and positioned immediately before the steel pipe test section, so the flow patterns could be observed and to ensure that the regimes were fully developed before the flow reach the test section. There was a single steel elbow at the end of the supply

run, see Figure 6-4 and an AE sensor was attached to it. The other 90^o connection, to the return run, was a plastic elbow, see Figure 6-13.

6.2.2 Air supply system

Air was again supplied by the Ingersoll Rand compressor as described above in Section 6.1.2. However, to avoid high the pressure fluctuations experienced in the initial test rig, an additional manual pressure regulator pre-set at 6 bar, was introduced to gain additional control in fine-tuning the air flow, as shown in the air supply system of Figure 6-4. On leaving the manual pressure regulator the air flow entered the 12.5mm (0.5") pipe with needle type valve which further increased the controllability of the air velocity (V_{SG}). The air flow rate was metered over the range 1-8$m^3.hr^{-1}$ by a Quadrina turbine air flow meter system. The air was then injected into the 50mm (2") water pipe at the desired gas velocity to simulate two-phase flow.

6.2.3 Test sections

The test section was 50mm (2") ID stainless steel pipe of 750mm length and 10mm thick, see figure 6-12(a). Figure 6-13 (a) shows the single 90^o steel elbow of 4mm thickness which was a permanent feature of the test rig. An AE sensors was permanently fixed to the steel elbow, as shown in Figures 6-4 and 6-13(b). The steel test pipe, on the other hand, was connected to the pipeline by flanges to facilitate inter-changeability of the steel pipes.

- Sensor location

To investigate the best position of AE sensors on steel pipes (e.g. top or bottom of the pipe) the interface between the steel test pipe and the pipeline was designed to allow rotation of the steel pipe. Changing the position of the sensor from top to bottom of the pipe can be achieved simply by rotating the test pipe 180^o while the same sensors remained glued to the pipe and with the test flow

still running through the pipe. Applying this technique should prevent the errors that would appear if other sensors were used or the same sensors were removed from the top side and re-glued on the bottom of the pipe; where the consistency of glue, the contact area between the sensor and the surface of the pipe and the homogeneity of the pipe material in the first position cannot be perfectly repeated. Accordingly, the acquired signal would differ regardless of any effect due to sensor position alone. Moreover, these arrangements will allow investigating the sensor signal at different rotational positions with the same flow condition.

- Temperature effect:

The water tank was fitted with two domestic electric heaters, each with input power of 2700W; this arrangement was used to increase the temperature of the circulated water to investigate the effect of water temperature on the AE signature of the flow. Water temperatures investigated ranged from 14^{o}C to 45^{o}C at increment of 1^{o}C. The temperature effect was investigated at a constant superficial liquid velocity, V_{SL}= 1.0ms^{-1} and constant superficial gas velocity, V_{SG} =0.5ms^{-1}. A thermocouple was used to measure the two phase temperature.

- Effect of surface roughness and pipe fittings

Three different stainless steel pipe test sections each of length 750mm, and wall thickness 10mm were used; each pipe was designated with different internal surface roughness grades; Grade-1 (10µm R_a), Grade-2 (3.2µm R_a) and Grade-3 (1.6µm R_a). While three different steel tubes were used the steel elbow remained in place, unchanged, with the same AE sensor attached.

- Thickness effect

In order to investigate the effect of pipe thickness on the strength of the AE signalm four different wall thickness were used: 8mm, 6mm, 4mm and 2mm. The pipe with roughness Grade-1 was milled so that its wall thickness was stepped. On each step a WD type AE sensor was attached, see Figure (6-14).

- Viscosity effect

A chemical substance, Sodium Carboxymethyl Cellulose (CMC), was used to increase the viscosity of the water. CMC powder was added carefully to the water tank in order to simulate liquids with higher viscosities than water (1Cp). Three viscosities (8, 14 and 20Cp) were produced using the CMC powder after a good mix was attained. The viscosity of the resulting solution was measured by rotational BROOKFIELD, DV-I *Prime* viscometer, see Figure 6-5.

Figure 6-5: Rotational BROOKFIELD viscometer

6.2.4 Conductivity electrode rings

The measuring section of the conductivity probe was a 500mm long Perspex pipe of 50mm ID, fitted internally with flush-mounted twin ring electrodes or conductivity probes as seen in Figure 6-6(a). The electrodes consist of two stainless steel rings with a width of (S_p) 3.7mm and spaced at 17mm (=D_e) apart, see Figure 6-6(b). The electrical impedance between the electrodes was measured. Probes such as this have been used by Fore (1993), Fossa et al., (2003) and Al-Lababidi (2006). The conductivity measurements were to be compared to the signals obtained from the AE sensors.

Fossa et al., (2003) stated that, based on both theoretical and experimental investigations, the response of the conductivity probe is affected by the probe geometry and even more by the flow pattern. As a consequence, at the same mean void fraction, the mixture impedance changes with the phase distribution. To overcome this problem, the conductivity probe geometry was chosen to produce a probe response that is relatively insensitive to the changes between the uniformly dispersed (bubble) regime and the stratified regime. Based on preliminary tests, Fossa *et al*. (2003) suggested that the probe geometry aspect ratios (D_e/d) and (S_p/d) should be 0.34~0.4 and 0.071~0.08 respectively. The selection of these electrode aspect ratios resulted in small measuring volumes as compared with holdup spatial fluctuations. Labview software and a National Instruments data acquisition (DAQ) card were used to acquire and store the impedance data continuously onto the computer hard disk

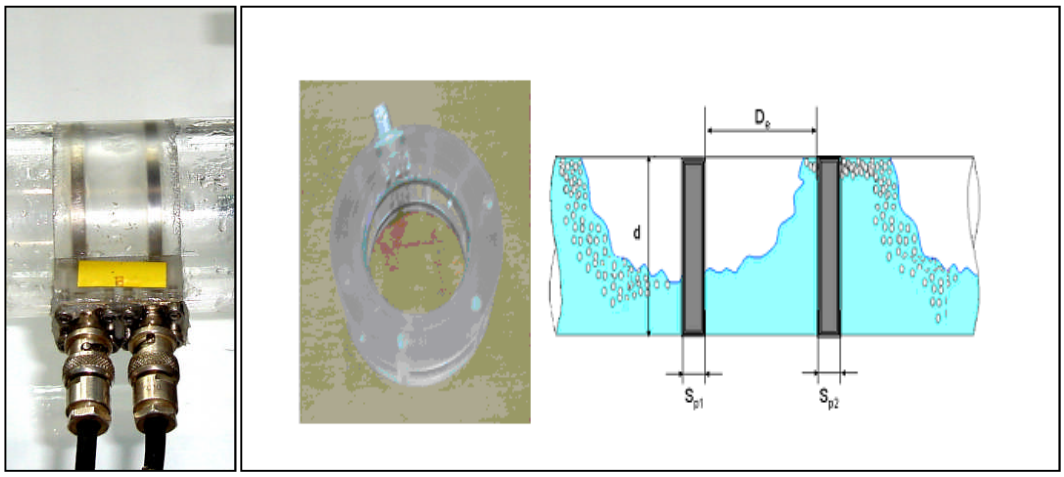

(a) **(b)**

Figure 6-6: Flush mounted stainless steel conductivity ring electrodes

6.2.5 Conductivity rings calibration

As stated above, the aspect ratios of the probe: De/d=0.34 and S_p/d=0.074 were chosen based on the design recommendations of Fossa (1998), and d

was equal to 50mm. Calibration of the probe was performed by connecting the electrode pairs to a Conductivity Electronic Box that supplied a 7kHz A.C. carrier signal. The gas-liquid phase fractions were achieved by injecting known liquid volumes, using syringe, into the horizontally positioned test pipe, see Figure 6-7. The test section was removed from rig and the ends sealed by flanges. It was then carefully levelled and the output voltage between the rings measured. Using a syringe, tap water was carefully added to the test section, always taking care to maintain it level. In each case the voltage was measured until the test section was full of water. The results are presented in Figure 6-8. For each measurement, both the mass of the water (excluding the mass of the apparatus) and the corresponding value in volt was recorded. A series of 38 measurements were made over the liquid fraction range 0~1.

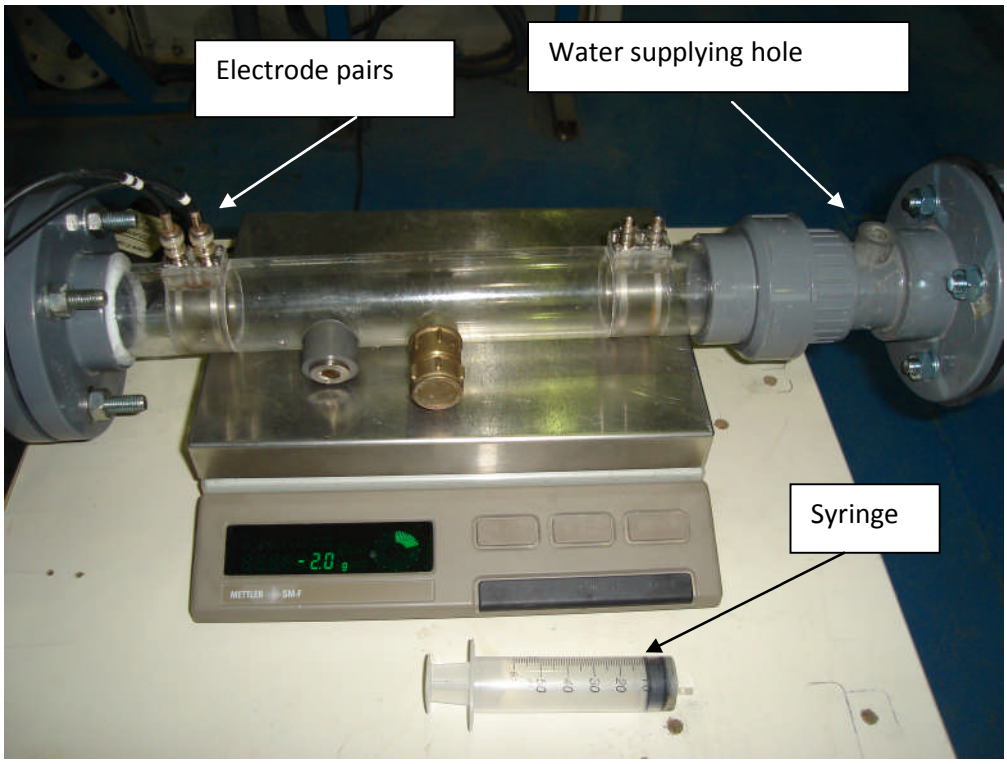

Figure 6-7: Conductivity rings calibration apparatus

The calibration curve for Figure 6-8 which relates water holdup (E_L – where holdup is the ratio of the volume of water to the total volume of the flow at the point of examination) to the normalised probe output voltage (G) with 1 for a full pipe and 0 when the pipe was empty was:

$$E_L = -1.489 \times G^4 + 1.475 \times G^3 + 0.368 \times G^2 + 0.623 \times G \qquad (1)$$

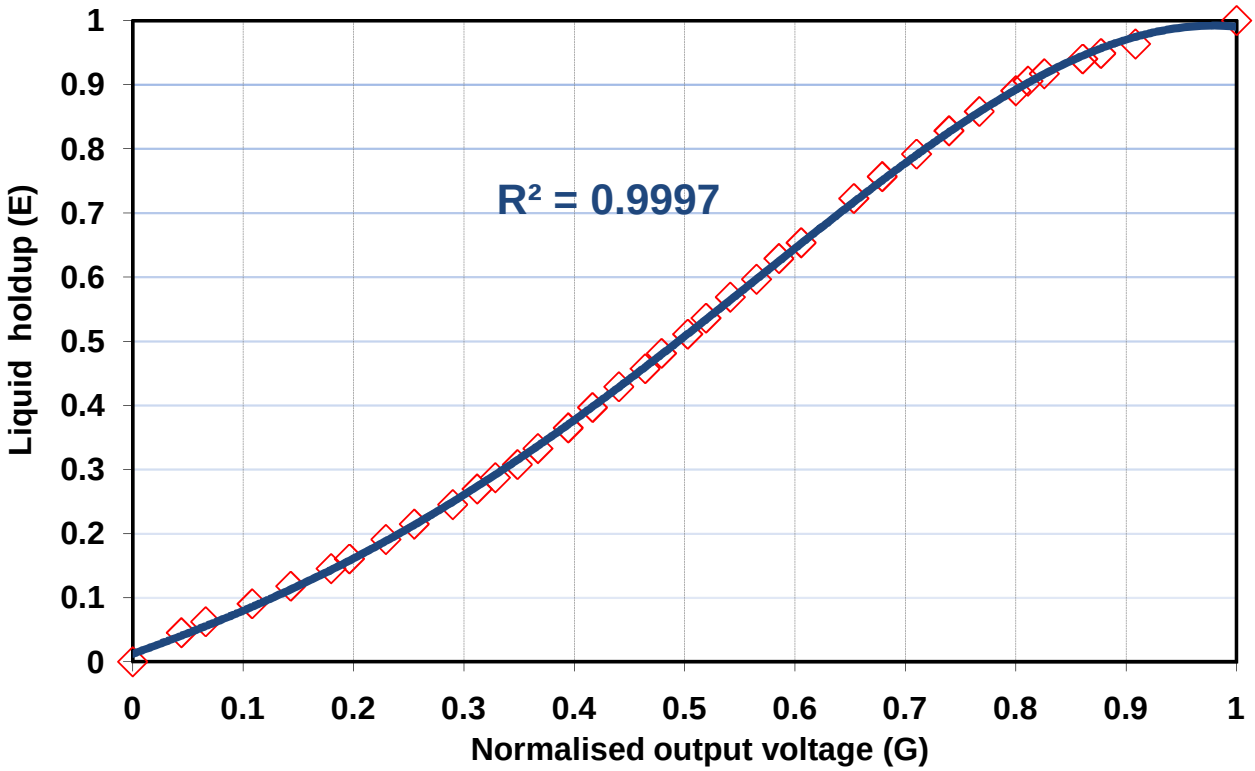

Figure 6-8: Calibration of conductivity ring probe

A sample trace collected from the conductivity probe under slug flow conditions is presented in Figure 6-9.

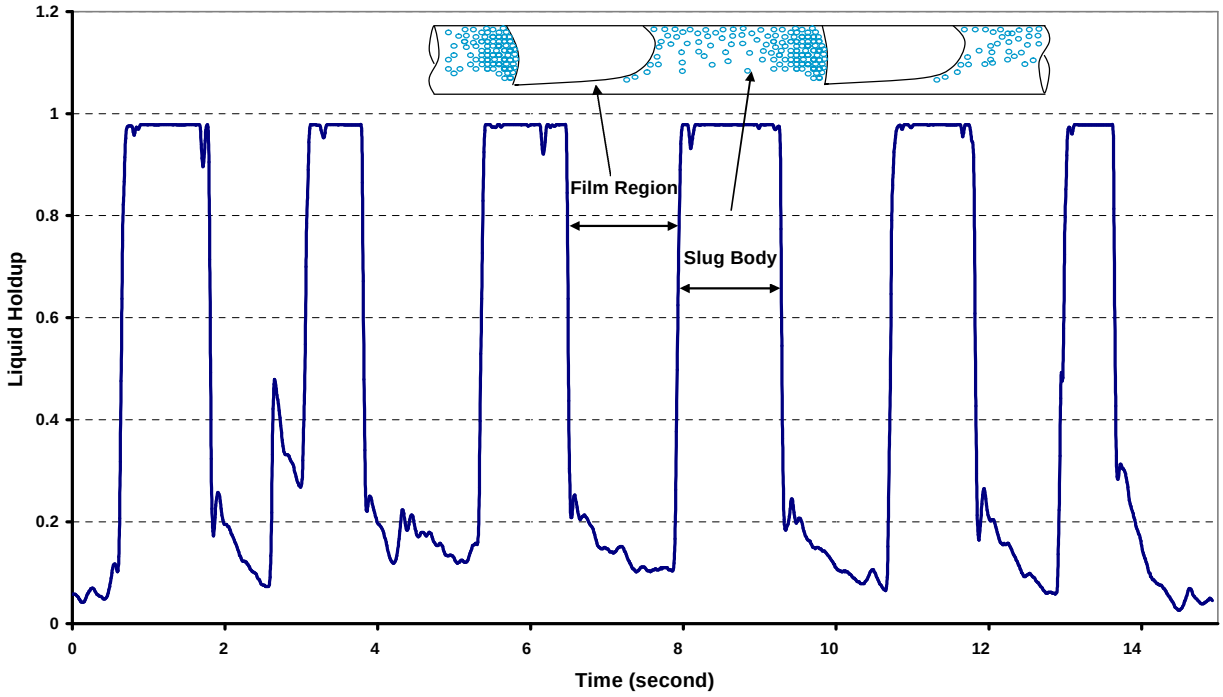

Figure 6-9: Typical Slug trace by conductivity probes

6.2.6 Flow data acquisition system

Data was acquired from the flow instruments using the same data acquisition system as in the preliminary test rig which was upgraded only to accommodate the conductivity rings.

6.2.7 Experimental Procedures

Table 6-1, shows the matrix of the tests carried out, and for which experimental results were obtained in this investigation. The V_{SL} and V_{SG} values were achieved by throttling the valves downstream of the flow meters, the incremental values for V_{SL} and V_{SG} were 0.1 and 0.2 ms^{-1} respectively. The

test range investigated is shown on the Beggs and Brill flow map, and it can be seen slug and bubbly regimes predominate the range investigated, see Figure 6-10.

Table 6-1 Summary of Investigation Matrix

Investigated parameter	Parameter Values	V_{SL} (ms^{-1}) at incr. of 0.1	V_{SG} (ms^{-1}) at incr. of 0.2	No of Tests (663)
Surface roughness (R_a µm), and gas void fraction	10, 3.2 and 1.6	0.3 – 2.0	0.0 – 1.4 at each V_{SL}	432
Pipe fitting (elbow)		0.3-2.0		120*3
Viscosity of liquid (Cp)	8, 14 and 20	0.4 , 0.8 and 1.2		72
Pipe wall thickness (mm)	2, 4, 6, and 8	1.0	0.0-1.4	8
Liquid temperature (C^o) increments of 1^{o}C	14-45	1.0	1.0	31

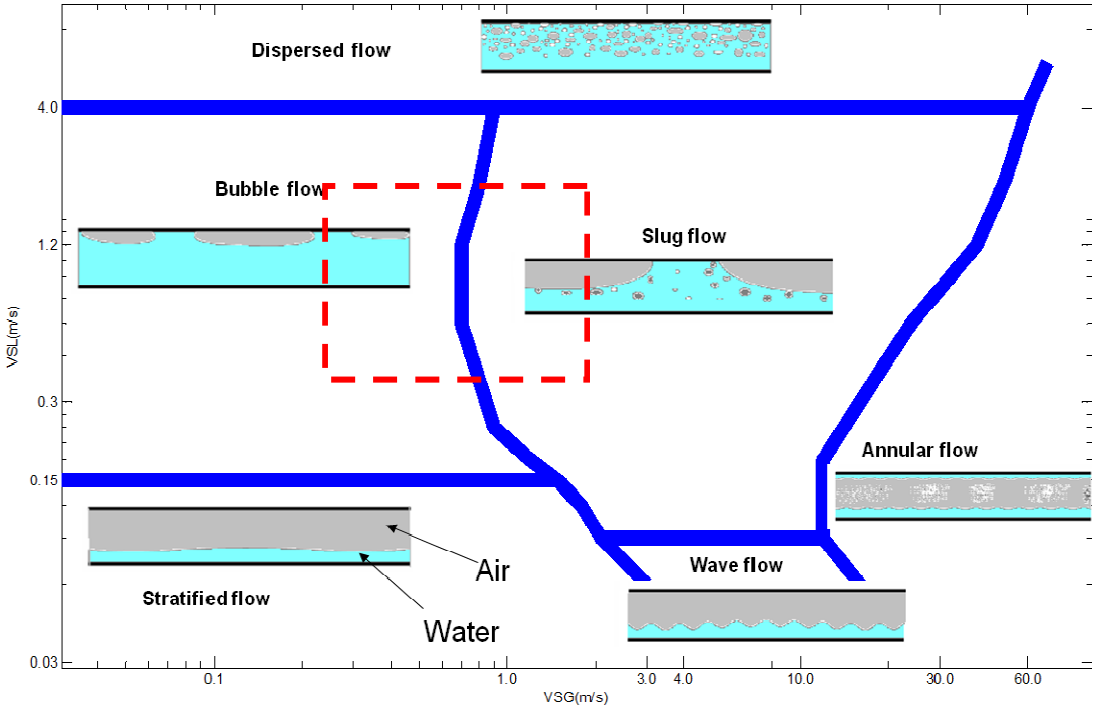

Figure 6-10: Test flow regime map highlighting test region

6.3 AE system

This section describes the AE system used in this research. Two types of AE sensors, both supplied by Physical Acoustics, were used for acquiring the data from all test conditions, but the number of sensors per test depended on the specific investigation.

a) Miniature Pico type AE sensor, 5mm diameter x 4mm high, with a broadband operating frequency range of 200-750kHz.

b) Wide-band WD type AE sensors, 18mm diameter x 17mm high, with a wide operating frequency range of 100 -1000kHz.

The AE sensors were used non-invasively and glued to the outside of the pipes and the elbow test sections by means of EVERBUILD, an Ethylcyanoacrylate based industrial superglue. The superglue acted both as acoustic-coupling and as a bonding agent, see Section 4.5. Pico sensors are characterised by their small size, which enables them to be installed on outside of pipes without the need for flattening the monitored surface. The larger WD sensors require a flat area on the surface as shown in Figure 6-12c. For all the sensors, the contact area between the sensors and the monitored surface was cleaned and polished by using very fine sand paper. Also, as specified by the manufacturer, for both sensor types were case grounded and electrically isolated from the mounting surface in order to reduce electronic noise.

Although the manufacturer's supplied a calibration chart for every sensor, see figures C-1 and C-2 in Appendix (C). Each sensor was checked using the Hsu-Nielsen pencil lead fracture technique prior the start of each investigation. The amplitude of the AE signals were in the average of between 60-70dB which comply with calibration rules as described by Brüel & Kjaer (1981)

It was a common arrangement that the output AE signals from each sensor was pre-amplified by 60dB using 2/4/6 preamplifier type and then connected via coaxial cable directly to the 6 channels of the Physical Acoustics PCI2 data

acquisition card having a maximum sampling rate of 8 MHz. Three PCI2 cards, with 2 AE channels on each card had been installed, each occupies one of the ISA slots within a 2.8GHz Pentium host PC, running AEWin for PCI2 software. The raw AE signal was sampled at 2MHz and time dependant AE parameters such as Absolute energy (atto-Joules), Root Mean Square R.M.S. levels (mV) and Average Signal Level ASL (dB) were sampled at 100Hz over a time constant of 10ms. Furthermore streamed waveforms were captured at every 60 seconds for 1 second length

6.3.1 AE sensors layout

- **Initial investigative 50mm (2") test facility**

Three Pico AE sensors on the straight pipe run were used in the initial investigation. One sensor was mounted on the ABS plastic pipe, and two others were mounted on both bottom and top of the stainless steel pipe as shown in Figures 6-11.

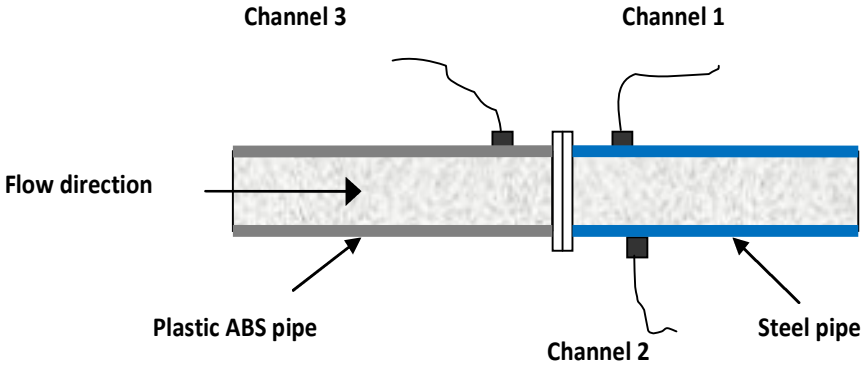

Figure 6-11: AE sensors layout

- **Advanced 50mm (2") test facility**

AE sensors were used on separate occasions to investigate how the AE signal generated from water/air two phase flows is affected by; temperature, internal

surface roughness and pipe fittings, fluid viscosity, pipe thickness, and sensor-pipe orientation.

The core part of this investigation was to correlate measured AE activity to the gas void fraction of air/water flow by monitoring the gas content in the flow. For this investigation, one Pico sensor placed on the steel elbow as shown in Figure 6-13(b), a second Pico sensor was placed on the steel section beside a WD sensor; see Figures 6-12(a) and (b). Similar arrangement was made for investigating the three grades of internal surface roughness of the pipes.

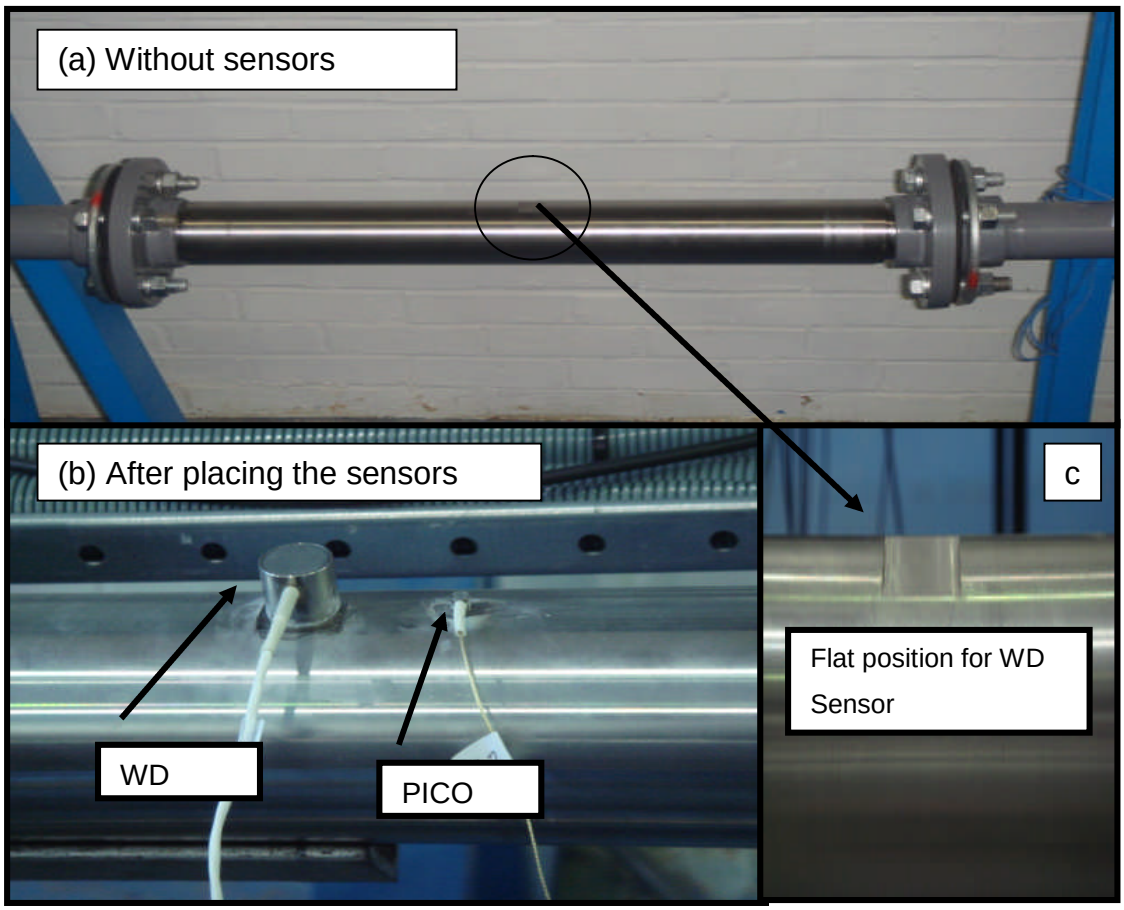

Figure 6-12: Steel pipe test section

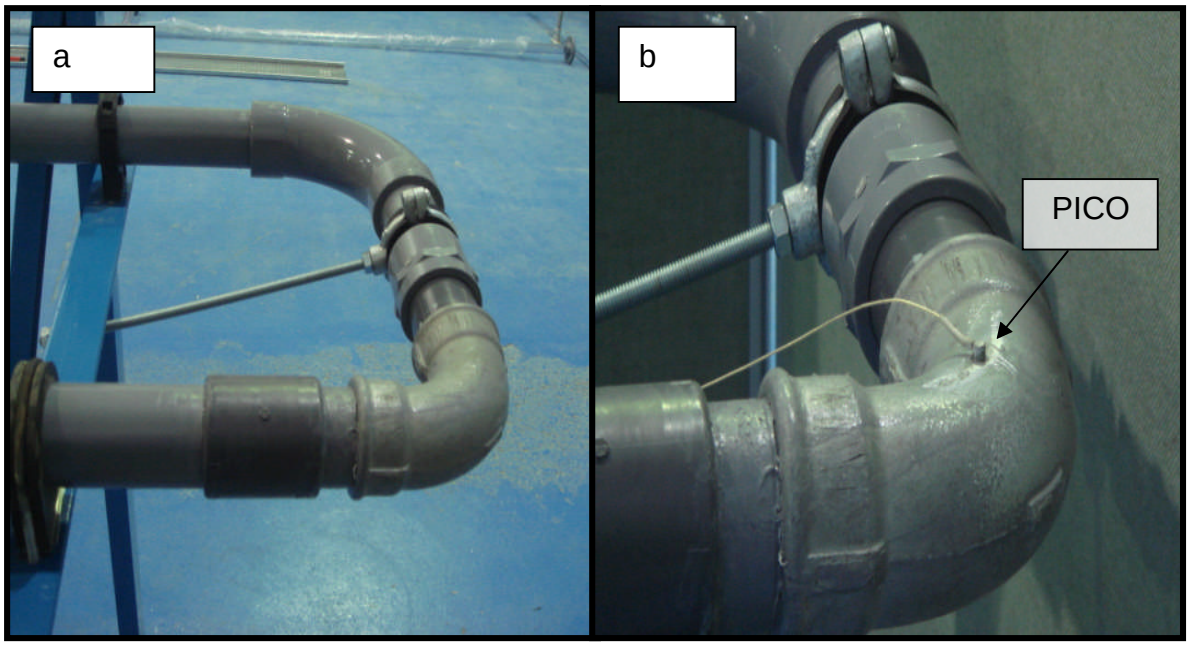

Figure 6-13: Steel elbow test section

The thickness effect was investigated by four WD sensors as shown in Figure 6-14. Four WD sensors were used to investigate the effect of the different pipe thicknesses on the strength of the AE signal. Whereas, the temperature and viscosity effect were investigated by one of the WD sensors that placed on the steel test section.

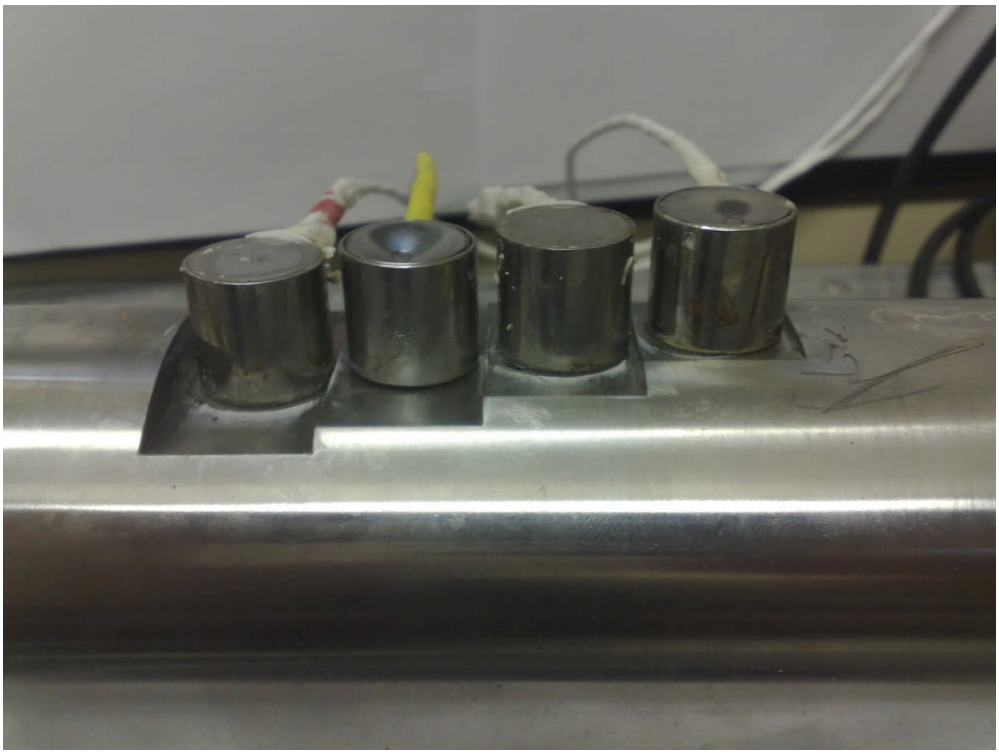

Figure 6-14: Sensor layout for the thickness investigation

Chapter 7: Results, Observations and DIscussions

All results of the experiments undertaken are presented in this chapter.

7.1 Results and observations from initial investigative test

Three Pico AE sensors were used in this investigation, see table 7-1. Typical waveforms of AE signal acquired at a sampling rate of 2MHz from a single phase liquid flow at V_{SL}=0.8 and V_{SG}=0 ms^{-1} (pure liquid) are shown in figure 7-1. Sampling waveforms from two phase flow, at VSL=0.8 and V_{SG}=1.0 ms^{-1} are shown in figure 7-2. The AE signal levels for single liquid flow was approximately 0.01mV for all the three channels, and the nature of the signal associated with this type was of continuous type, see figure 7-1. Whereas the AE signal level for two phase flow were considerably higher, in the order of 0.7, 0.5 and 0.15 mV for Ch1, Ch2 and Ch3 respectively, see figure 7-2. This shows the dramatic increase of the AE levels with the inclusion of a second phase. In addition the nature of AE waveforms for two-phase flow was transient in nature, primarily due to the contribution of the air bubbles. This will be discussed later in this chapter.

Table 7-1: Sensor notation for initial investigative test

Channel number	Sensor position
Ch1	Steel pipe top sensor, Pico type
Ch2	Steel pipe bottom sensor, Pico type
Ch3	Plastic pipe top sensor, Pico type

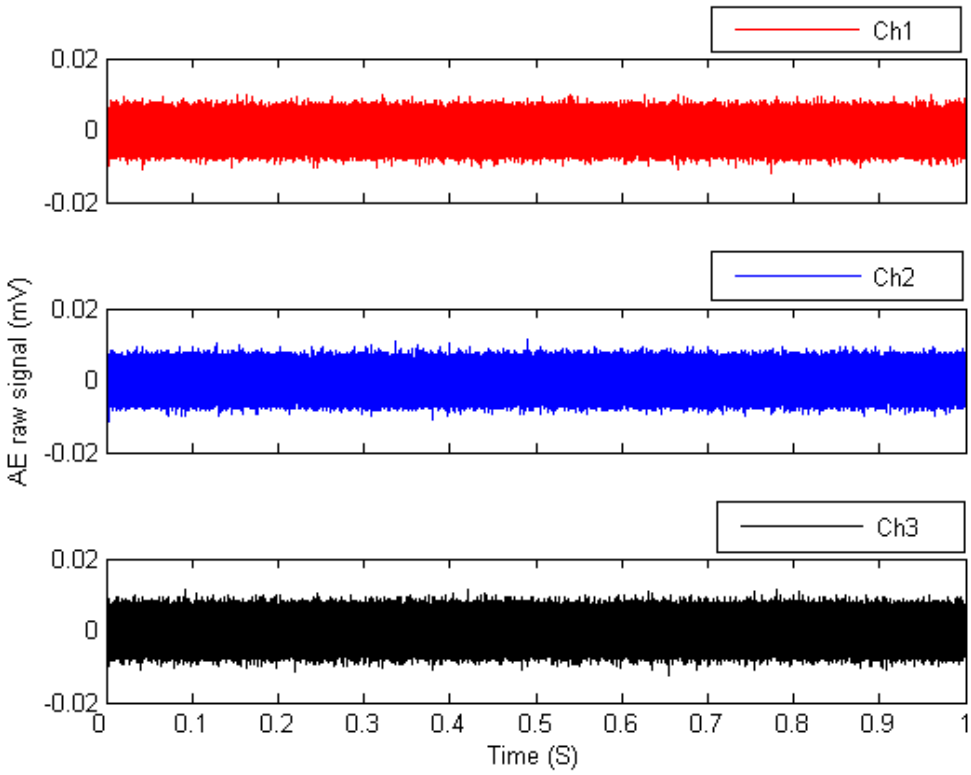

Figure 7-1: AE waveforms, for 1 seconds length at V_{SL}=0.8 and V_{SG}=0 ms^{-1} (pure liquid flow)

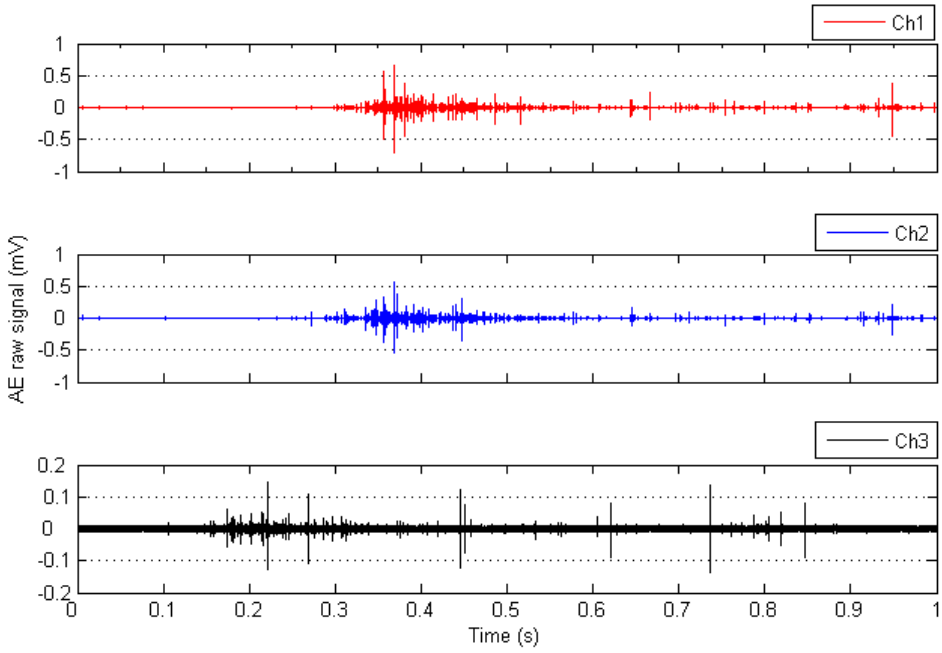

Figure 7-2: AE waveforms for 1 seconds length at V_{SL}=0.8 and V_{SG}=1.0 ms^{-1} (air/liquid flow)

7.1.1 AE parameters

Each test condition was tested for 120 seconds during which AE waveforms were acquired at 2 MHz, as explained in the previous chapter, section 6.1.4. AE parameters such as; absolute energy, RMS and ASL levels were calculated at 100Hz sampling rate and over a time constant of 0.01ms. A typical plot of the absolute energy of the AE levels for a test condition at V_{SL} =1.1ms^{-1} and at V_{SG} =0.8 ms^{-1} is shown in figure 7-3, the time period between 55-60 seconds in this figure (within the dashed frame box) was magnified and shown in figure 7-4. The high amplitude AE events as seen in figure 7-4 are associated with the air/liquid flow activities such as bubble collapse, formation, breakup and coalescence, generated during bubbly or slug flow regimes. Similar plots for RMS and ASL levels are shown in figures D-1 to D-4 in the appendix (D).

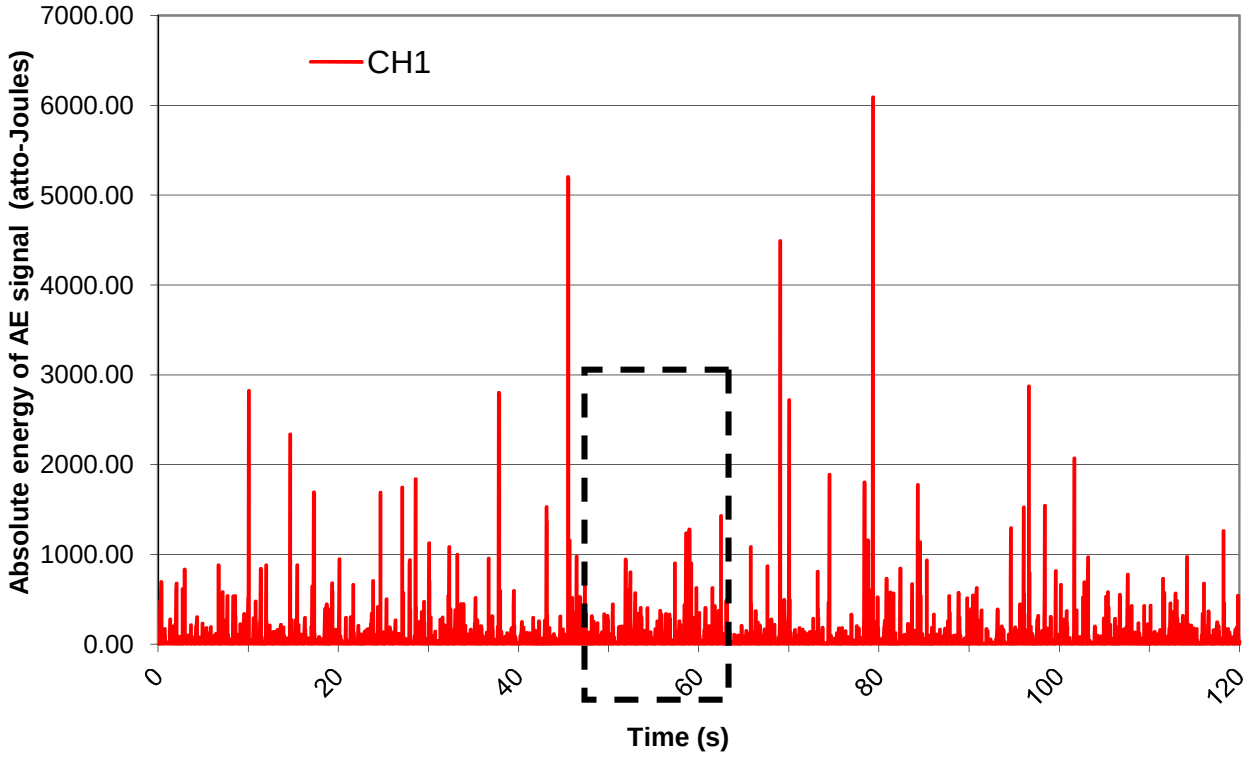

Figure 7-3: Absolute energy of AE levels at V_{SL}=1.1 ms^{-1} and V_{SG} = 0.8 ms^{-1}

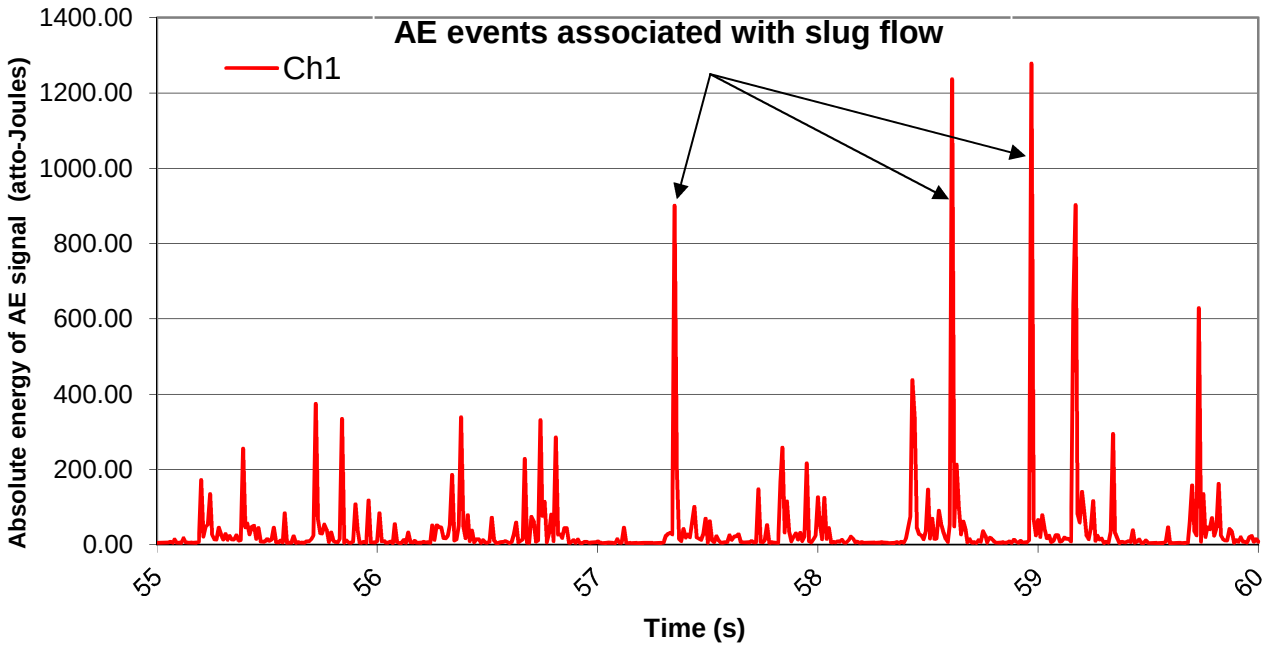

Figure 7-4: Absolute energy of AE levels of time 55-60 seconds of figure 7-3

For each test condition an average value of energy, RMS and ASL was calculated over the test duration (120 seconds), see figure 7-5. A comparison between absolute energy, RMS and ASL levels showed that all parameters exhibited a similar in trend, see figures 7-5 to 7-7. It was noted that absolute energy offered better sensitivity to the flow changes than RMS and ASL values, due to the fact that absolute energy is a measure of the real energy of the signal; it was chosen to be the output parameter identifier for the AE signal throughout this research study.

7.1.2 Statistical parameters

Two statistical parameters; the average (arithmetic mean) and standard deviation values of the AE absolute energy, were calculated for each test. Figures 7-5 and D-5 in appendix (D) showed an example for these parameters calculated at Varying V_{SG} and at V_{SL} =1.1ms^{-1}. Although both parameters were descriptive of the flow changes, however the average values were more

consistent in describing the development of the signal, as such only statistical average parameter of the absolute energy of the AE signal will be considered in investigating the air / water two-phase flow.

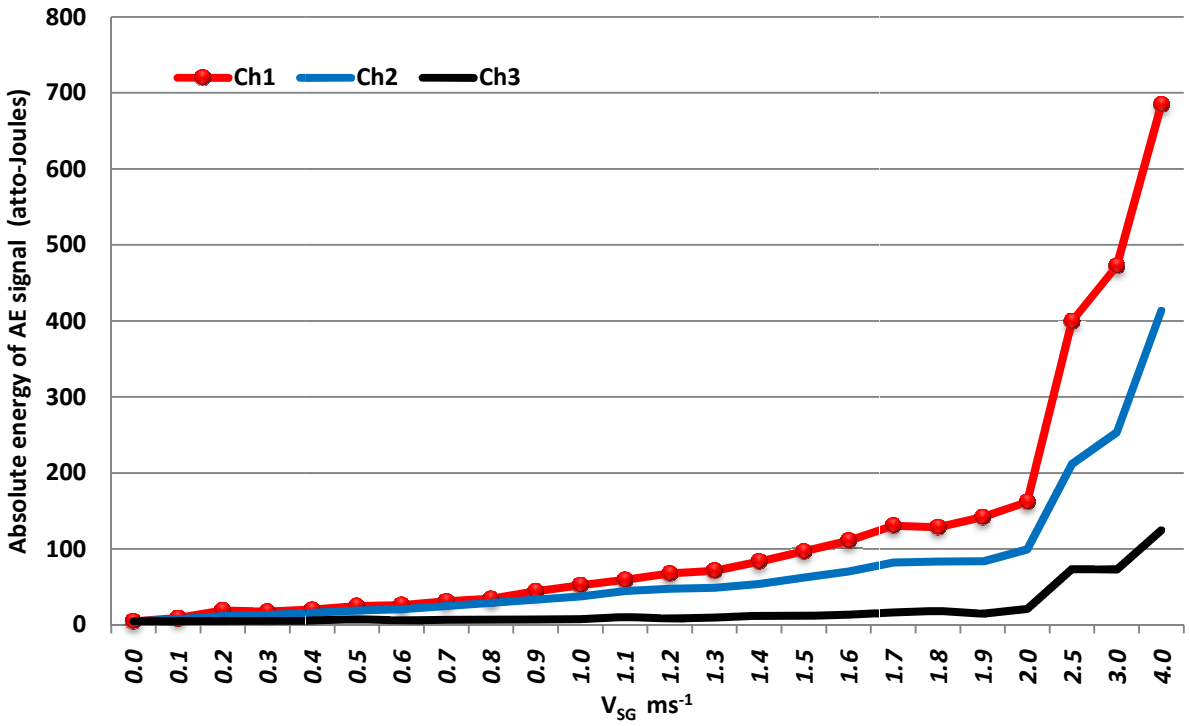

Figure 7-5: Average values for AE absolute energyl for varying V_{SG} and at V_{SL} =0.9ms^{-1}

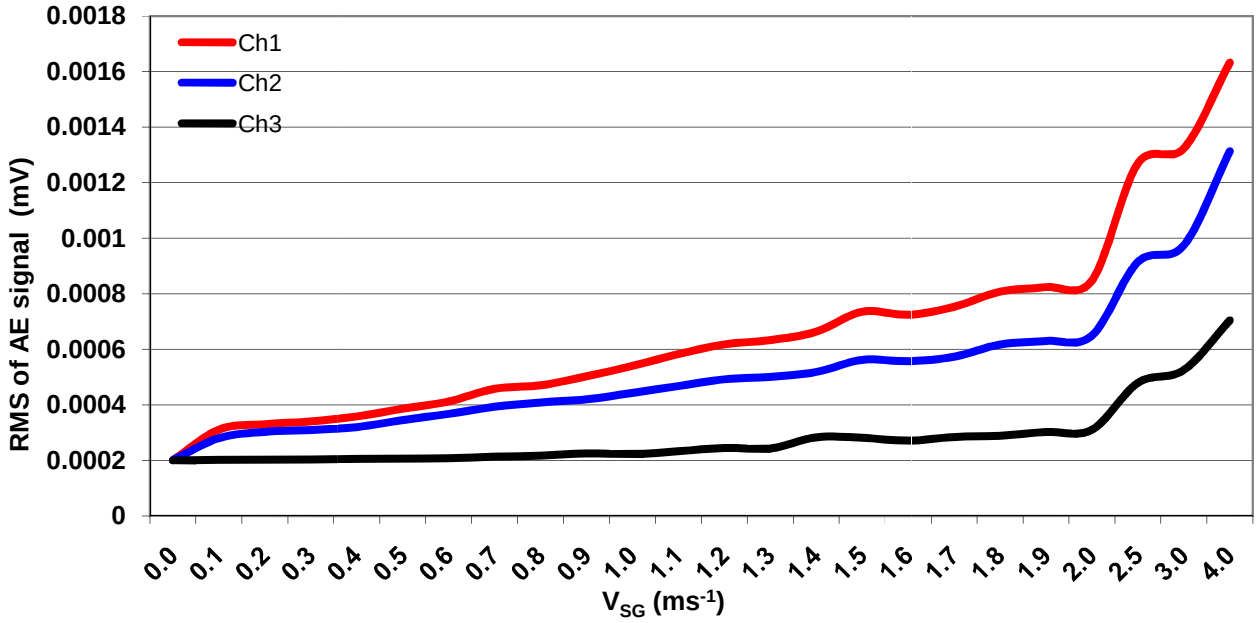

Figure 7-6: Average values for AE RMS for varying V_{SG} and at V_{SL} =0.9ms^{-1}

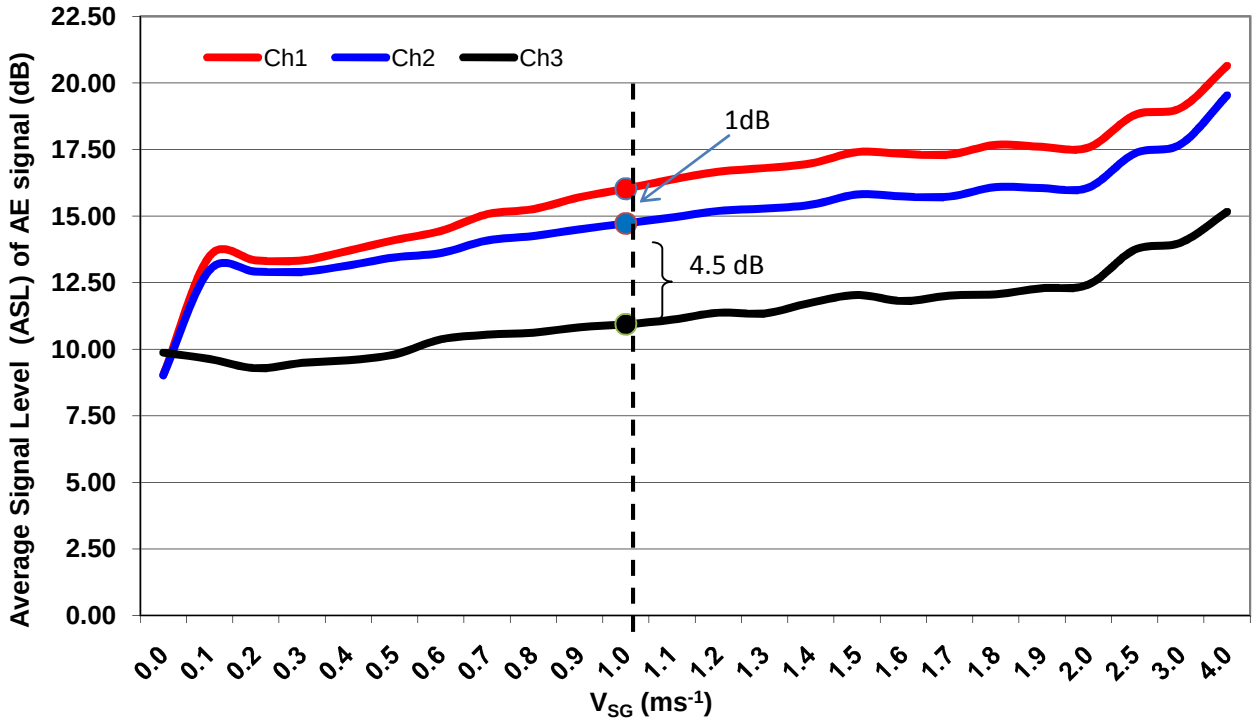

Figure 7-7: Average values for AE ASL for varying V_{SG} and at V_{SL} =0.9ms^{-1}

7.1.3 Sensor orientation and pipe material

The averaged values of absolute energy signal levels were calculated for the three sensors over the test condition. It was observed that AE levels generated from Ch1 sensor were higher than those from Ch2, see figure 7-5. Also, it was observed that whilst AE's were detected with the sensor on the plastic pipe, Ch3, its relative levels in comparison to the steel pipe (Ch1 and Ch2) was lower; as to be expected. Figures 7-5 presents typical results for a given V_{SL} =0.9 ms^{-1}at varying values of V_{SG}., similar observations at V_{SL}=0.5 and 1.1 ms^{-1} were presented on figures D-6 and D-7 in appendix (D). The deference in amplitude between Ch1, Ch2 and Ch3 at V_{SG}=1.0 are shown in figure 7-7; Ch1 was higher than Ch2 and Ch3 by 1 dB, and 4.5 dB respectively.

From Figure 7-5, the increase of the energy level detected by the AE sensor was found to be proportional to the increase of the superficial gas velocities; a

cumulative percentage increase in AE energy levels is presented in figure 7-8, with reference of V_{SG}=0 ms^{-1}**.** The rate of increase was found to be in the order of between 15-20 % across the incremental increases in V_{SG} velocities. All results acquired from Ch1, for varying V_{SL}'s and V_{SG}'s are presented as waterfall plot in figuresD-8 in appendix (D), though an example is presented in figure D-8. It is evident that the increase of energy level was proportional to the increase of the superficial liquid velocities. Interestingly, from Figure 7-9, it shows that AE is relatively more sensitivity to slug flow than bubble flow because of the higher levels of AE energy, for instance at V_{SG}=0.3 and V_{SL} of 0.5 ms^{-1} , AE energy levels were at 5.3 atto-joules in comparison to 180 atto-joules at a V_{SG}= 1.8 and V_{SL} of 1.1 ms^{-1}

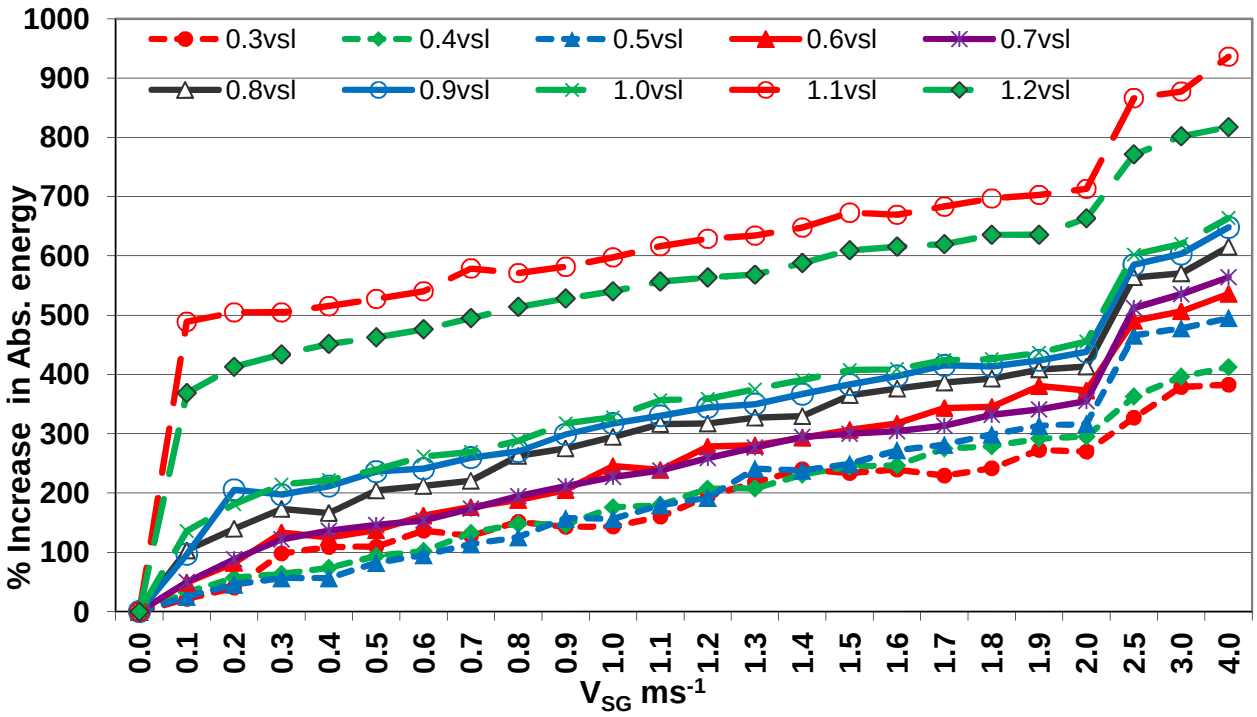

Figure 7-8: Relative percentage increases in averaged AE abs. energy for varying V_{SG} and V_{SL}

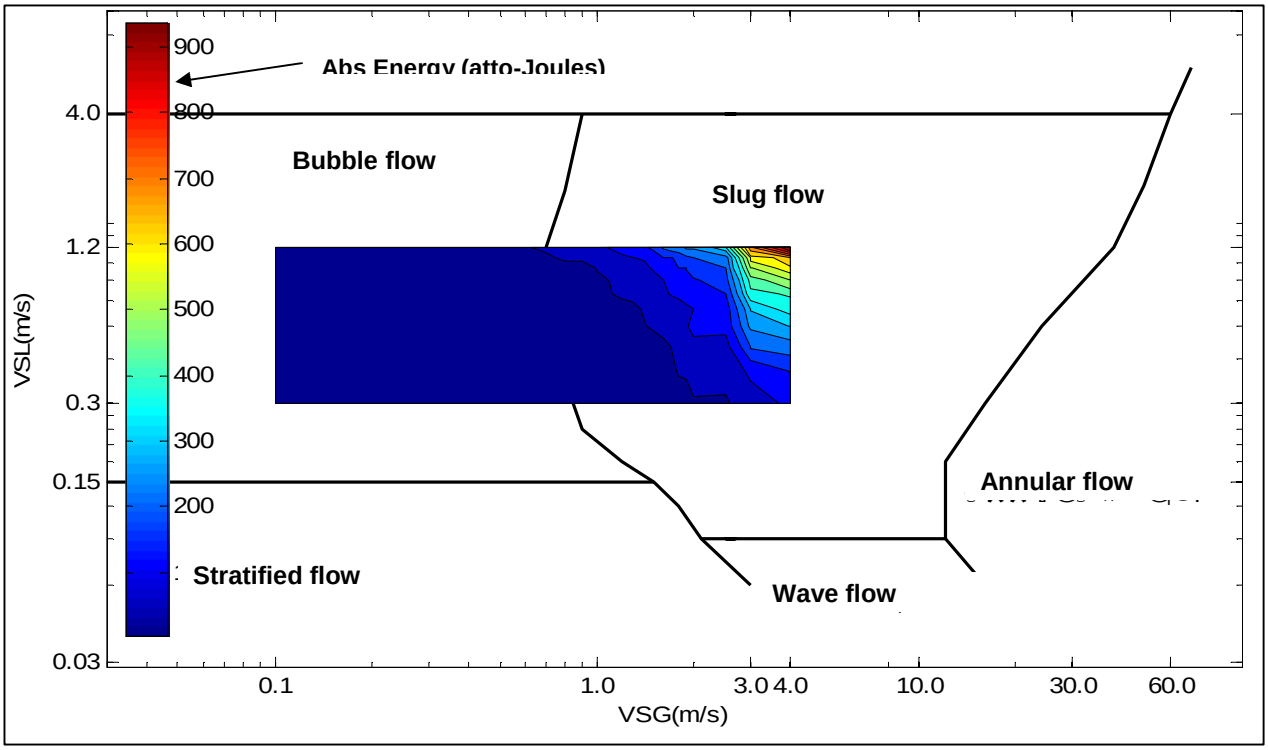

Figure 7-9: Contour plot of AE energy levels for varying flow regimes

The outcome of the current test investigation can be summarised as:

- average value of the absolute energy of the AE level was the preferred parameter to monitor the flow condition,
- top steel sensor (Ch1) provided the strongest signal of AE generated from the flow compared to bottom steel(Ch2) and top plastic (Ch3) sensors, and
- AE levels increased proportionally with V_{SL} and V_{SG}

Having established these results, it was very encouraging to proceed to a more detailed investigation in order to establish a correlation between AE activity and the gas void fraction of gas/liquid flow under different flow regime.

7.2 Results and observations from advanced 50 mm (2”) test facility

This new facility allowed for more control of gas velocity through the use of air pressure regulator and needle air valve in the air supply line, also higher liquid superficial velocity (up to V_{SL}= 2.0 ms^{-1}) was facilitated by using large capacity pump. In addition, conductivity rings were installed and used as reference for gas void fraction (GVF) measurements. As explained in section 6.3.1, and shown in figures 6-12 and 6-13, three sensors were used for investigating the GVF measurement, the sensors were named according to table 7-2

Table 7-2: Sensor notation for the advanced test

Channel number	Sensor position
Ch1	Steel pipe sensor, Pico type
Ch2	Steel pipe sensor, WD type
Ch3	Steel elbow sensor, Pico type

The liquid superficial velocity (V_{SL}) ranged from 0.3 $ms^{-1}$to 2.0 ms^{-1} at increments of 0.1 $ms^{-1,}$ and the gas superficial velocity (V_{SG}) ranged from 0.1 ms^{-1} to 1.4 ms^{-1} at increments of 0.2 ms^{-1}, at each V_{SL} value all range of V_{SG} were investigated.

Results from this test rig complemented the results obtained from the Initial investigative test, absolute energy of AE signal from the three sensors gradually increased with the increase of V_{SG} at all V_{SL} velocities. Compared to the electronic noise level, the three mounted AE sensors; Ch1, Ch2 and Ch3, showed insignificant contribution in the AE absolute energy (10^{-18} Joules) for single-phase water flow at velocity ranges from 0.3 to 2.0 ms^{-1}.

However, the measured values of AE from single-phase water tests were still higher than the electronic noise level of the system, see figure 7-10. For instance, electronic noise levels were at 5.2 atto-Joules for Ch1, whilst a single flow levels were 5.8 atto-Joules.

The Pico elbow mounted sensor (Ch3) exhibited the highest energy level compared to its twin Pico steel pipe's sensor (Ch1) and WD steel pipe's sensor (Ch2), see for example figure 7-11. As expected, the same figure showed that absolute energy levels from the steel pipe test section acquired from the Pico sensor (Ch1) were less than those of the WD sensor (Ch2). This was attributed to the difference in sensors sensitivity, where the WD type is more sensitive than Pico, as depicted in the calibration sheets for both sensors, figures C-1 and C-2 in Appendix (C).

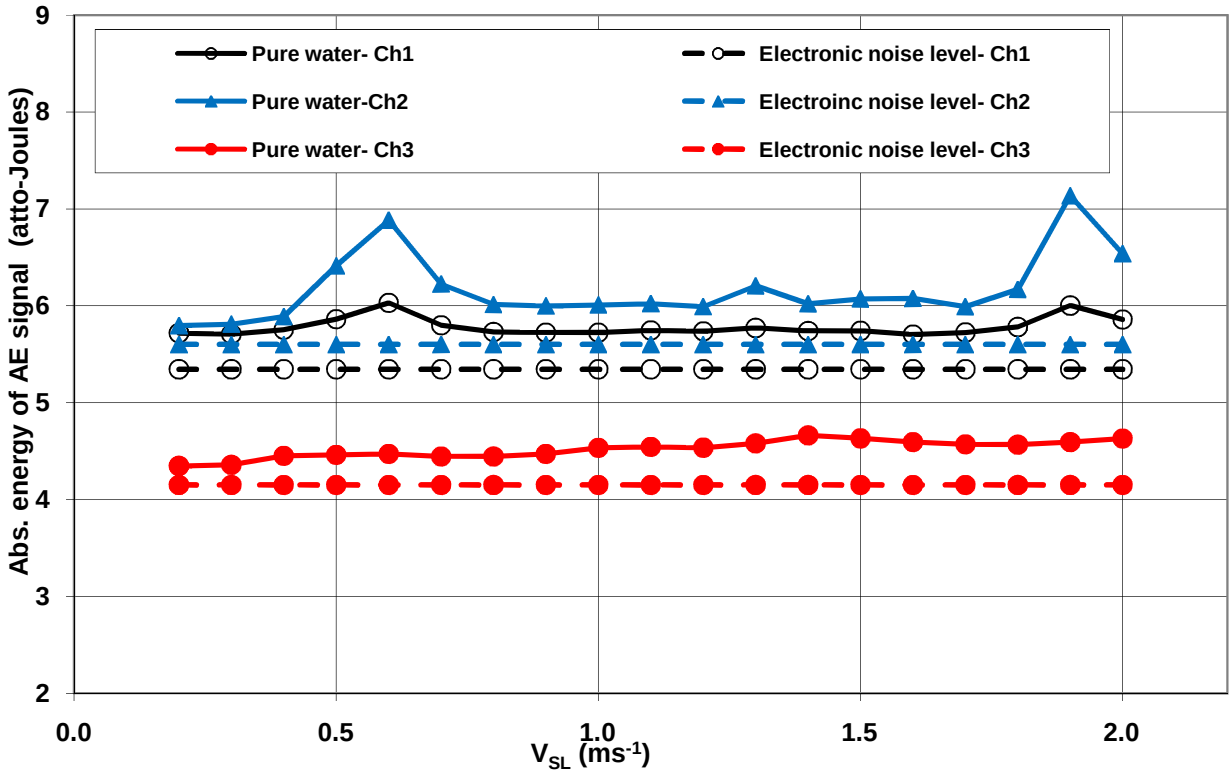

Figure 7-10: The influence of pure liquid and background noise on AE abs. energy levels

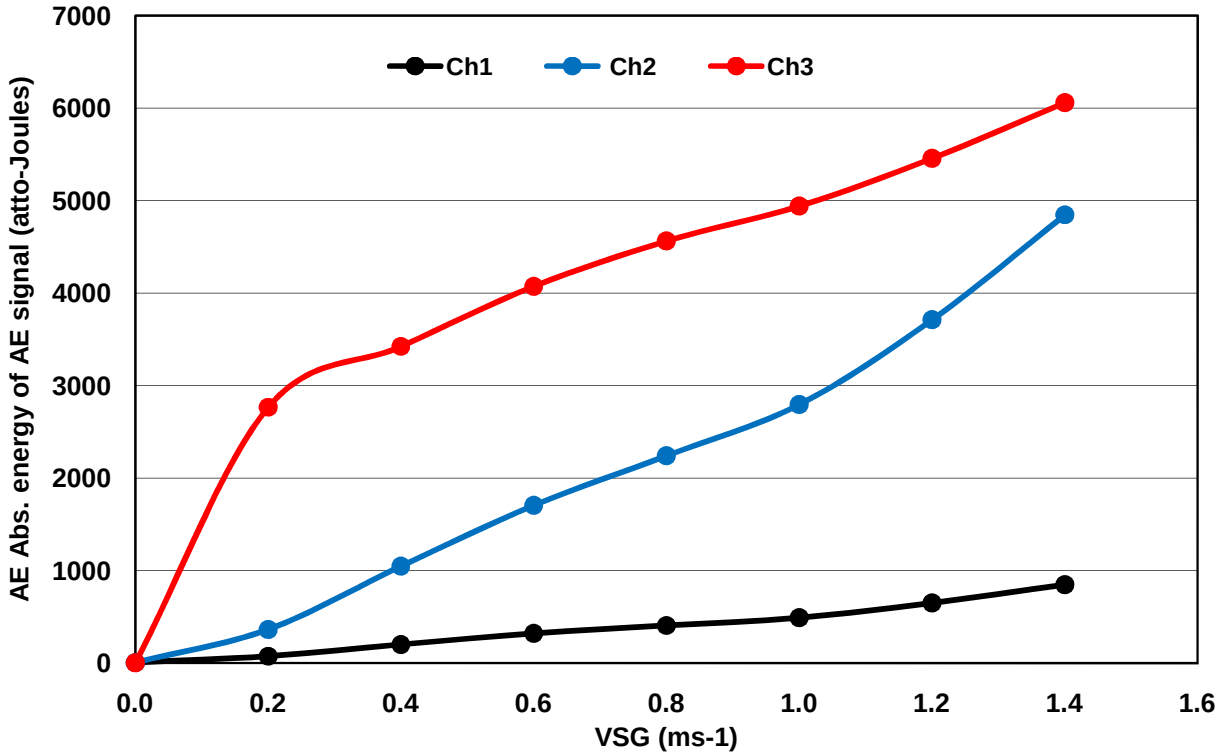

Figure 7-11: AE Absolute Energy level for varying V_{SG} at V_{SL} =2.0 m/s

As explained previously (Conductivity electrode rings sections 6.2.4 and 6.2.5), GVF values were measured for all test programs. Although the conductivity rings were already calibrated, it was thought prudent to compare GVF measured values with theoretical values of GVF at all velocities. The mathematical equation was used to calculate GVF numerically: is defined in equation (7-1)

$$GVF = \frac{V_{SG}}{V_{SG} + V_{SL}} \qquad 7\text{-}1$$

Figure 7-12, presents plots of measured and calculated GVF at the designated velocities. Also figures 7-12 to 7-14, show comparison between measured GVF and absolute energy level of AE signal acquired from Ch1,

Ch2 and Ch3 at varying V_{SG} and V_{SL} =2.0 ms^{-}1. Observations showed that any increase in GVF resulted in an increase in AE absolute energy. A Pearson's correlation factor (r) was used to quantitatively access the degree of correlation between the results presented in figurers 7-12 to 7-14

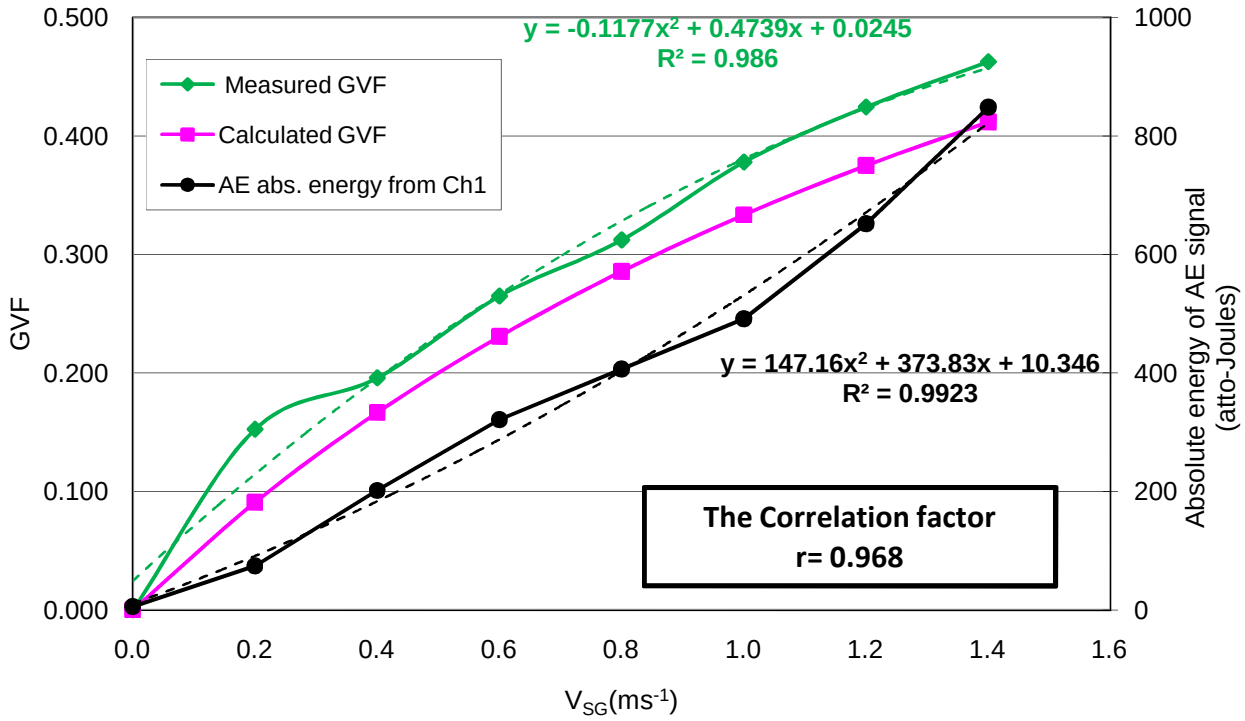

Figure 7-12: GVF and AE abs. energy levels at V_{SL} =2.0 m/s for Ch1.

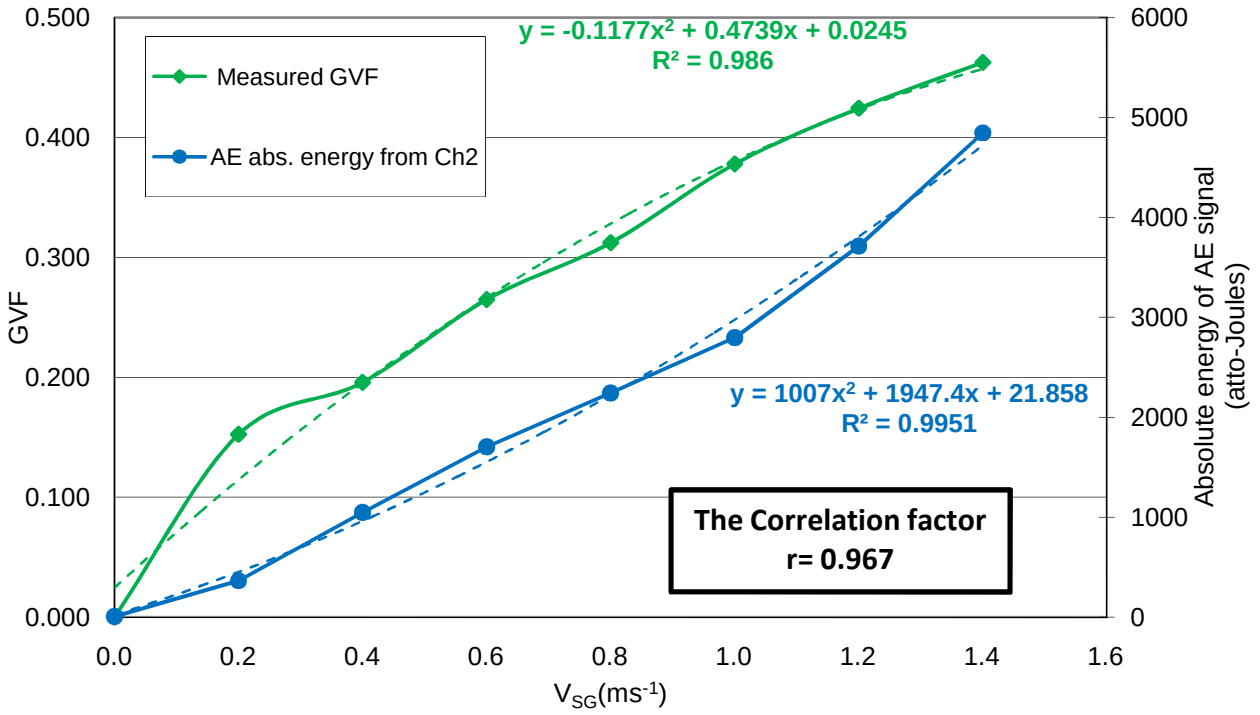

Figure 7-13: GVF and AE abs. energy levels at V_{SL} =2.0 m/s for Ch2.

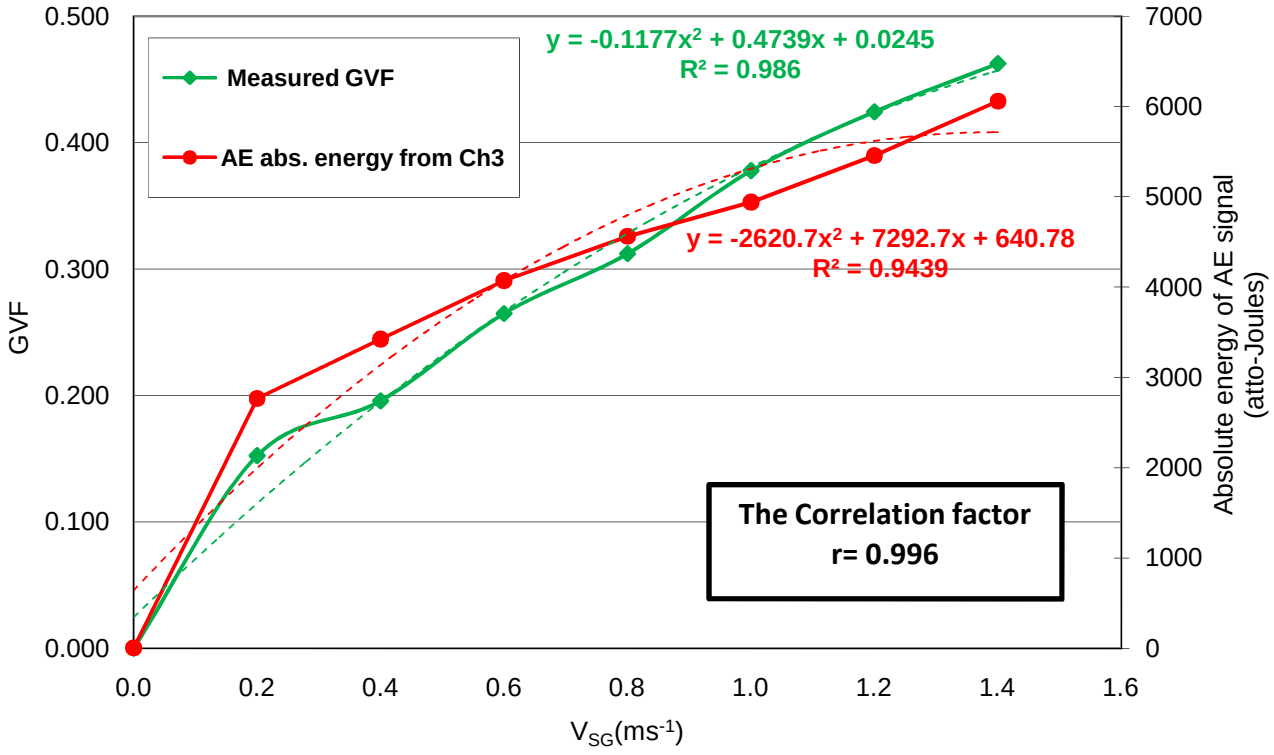

Figure 7-14: GVF and AE ab. energy levels at V_{SL} =2.0 m/s for Ch3**.**

In general, correlation is one of the most common and most useful statistical parameters, and is generally used to quantify the relationship between two or more parameters. Pearson's Correlation factor (r) is a single number that describes the degree of relationship between any two variables. Equation 7-2, was used to calculate factor (r), which ranges between -1.0 and +1.0. If the correlation is positive, we have a positive relationship; if it's negative, the relationship is negative. Figure7-15 shows the correlation relationship types. For a positive relationship, high values on variable (**A**) are associated with high values of variable (**B**) and low values of variable (**A**) are associated with low values on variable (**B**), whereas in a negative relationship; low values of variable (**C**) are associated with high values of variable (**D**) and high values of variable (**C**) are associated with low values of variable (**D**). Also, as the value of (r) approaches +1.0, the correlation between two variables become stronger and vice versa (Cohen, 1988).

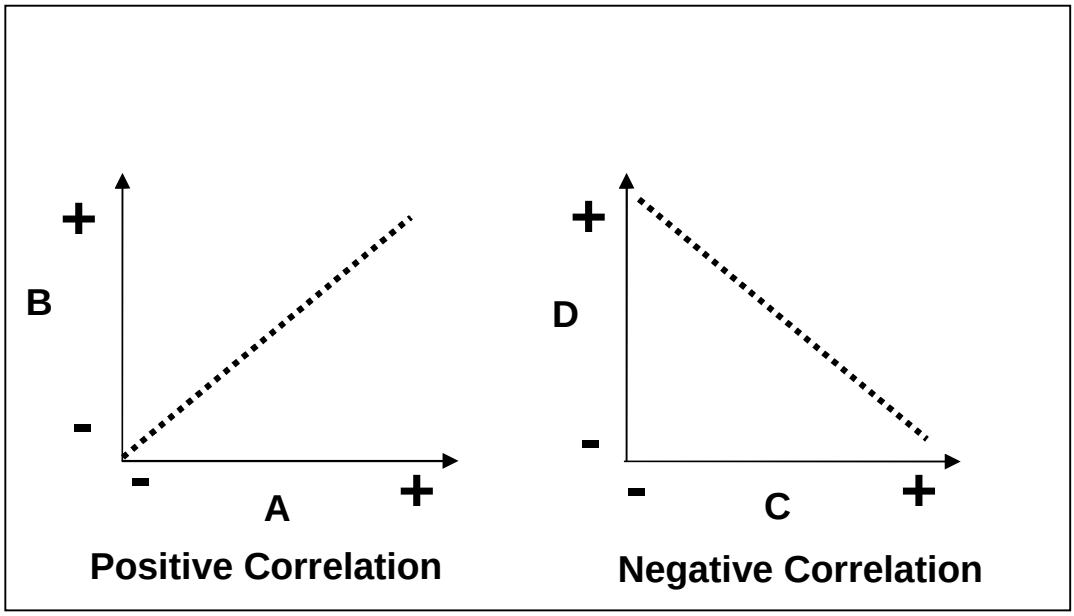

Figure 7-15: Correlation relationship types

$$\mathbf{r} = \frac{\mathbf{N}\sum \mathbf{XY} - (\sum \mathbf{X})(\sum \mathbf{Y})}{\sqrt{[\mathbf{N}\sum \mathbf{X^2} - (\sum \mathbf{X})^2][\mathbf{N}\sum \mathbf{Y^2} - (\sum \mathbf{Y})^2]}} \qquad 7\text{-}2$$

Where:

N = number of pairs of scores, $\sum XY$ = sum of the products of pairs

$\sum X$ = sum of X scores, $\sum Y$ =sum of Y scores

$\sum X^2$ =sum of squared X scores, $\sum Y^2$ =sum of squared Y scores

Therefore, the correlation factor (r) was adopted to measure and describe the nature of relationship between conductivity measured gas void fraction (X values in the equation) curves and absolute energy curve of AE signal (Y values in the equation) at each superficial liquid velocity .Similarly Correlation factors (r) were calculated for all GVF and AE Absolute Energy curves for the whole testing range.

For the evaluation purpose, plots of measured GVF and AE absolute energy of the test campaign and the Pearson's correlation factors (r) are presented in the same plot for each V_{SL}, see figures 7-12 to 7-14. Moreover it was observed that all calculated correlation factors (r) were higher than 0.8 and the vast majority of these values are more than 0.90. Also correlations of the elbow sensor (Ch3) were the highest ranked compared to the other channels (CH1 and Ch2) at any V_{SL}. In addition, and regardless of the sensor position, the correlations factor increased with increased values of V_{SL}. Figure 7-16 shows the trend of the correlation factor for the Pico sensor (Ch1) of the steel pipe.

Observations from all test programs are present in figures 7-17 to 7-19. These show the correlation between V_{SL}, V_{SG} and absolute energy AE levels. These observations will be discussed in section 7.4.

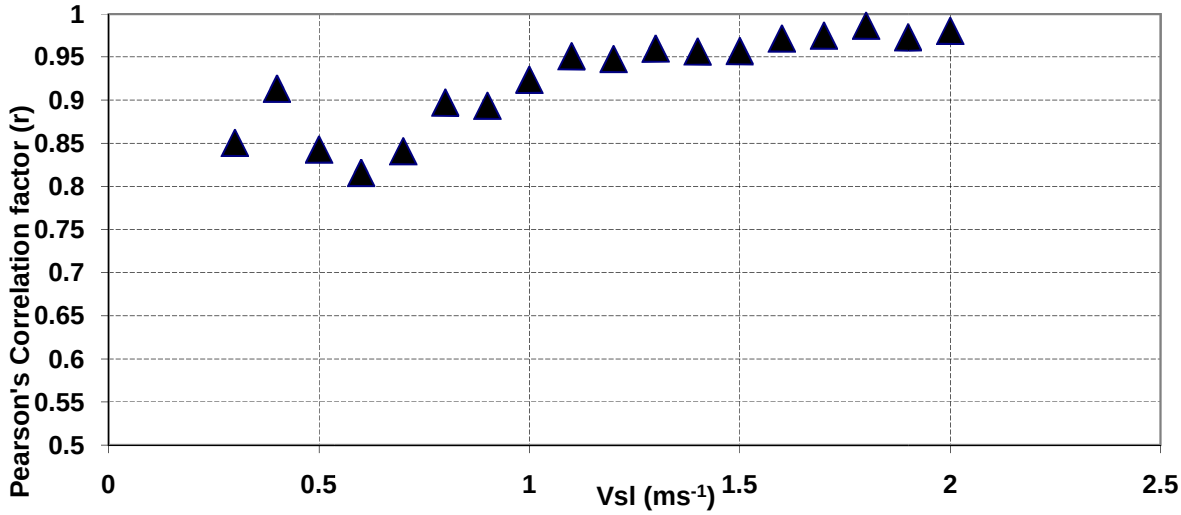

Figure 7-16: The trend of Pearson's correlation factor (r) for Ch1 of the steel pipe

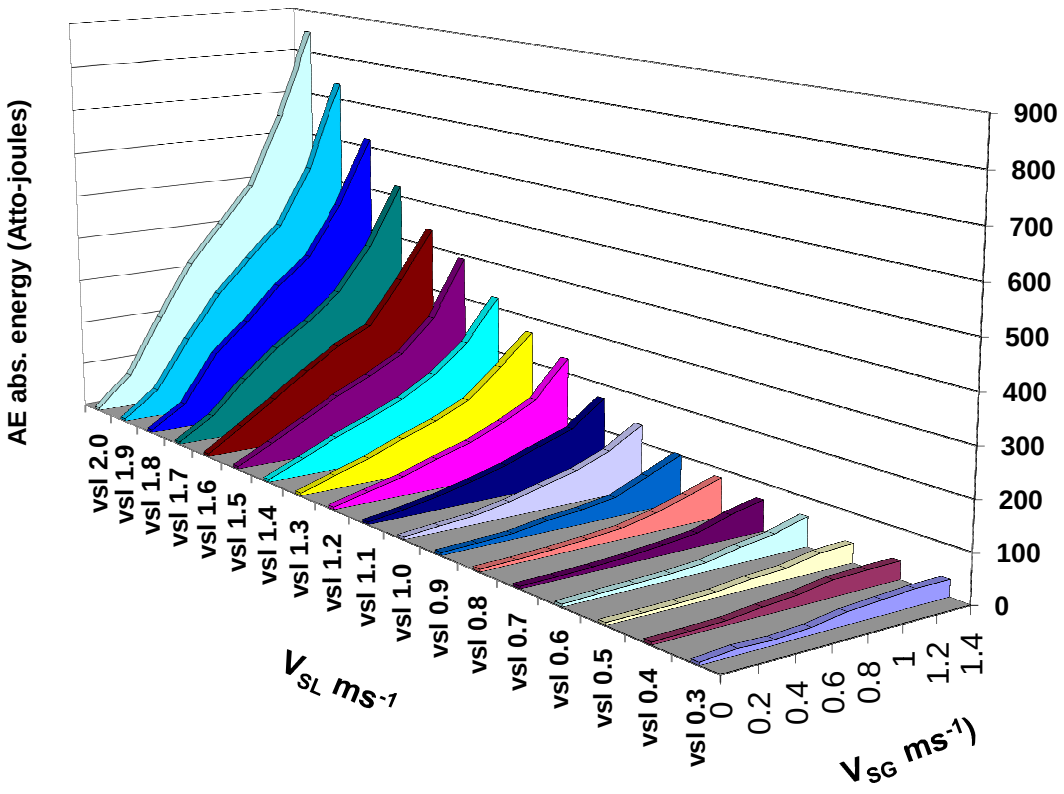

Figure 7-17: Waterfall plot for Ch1 sensor

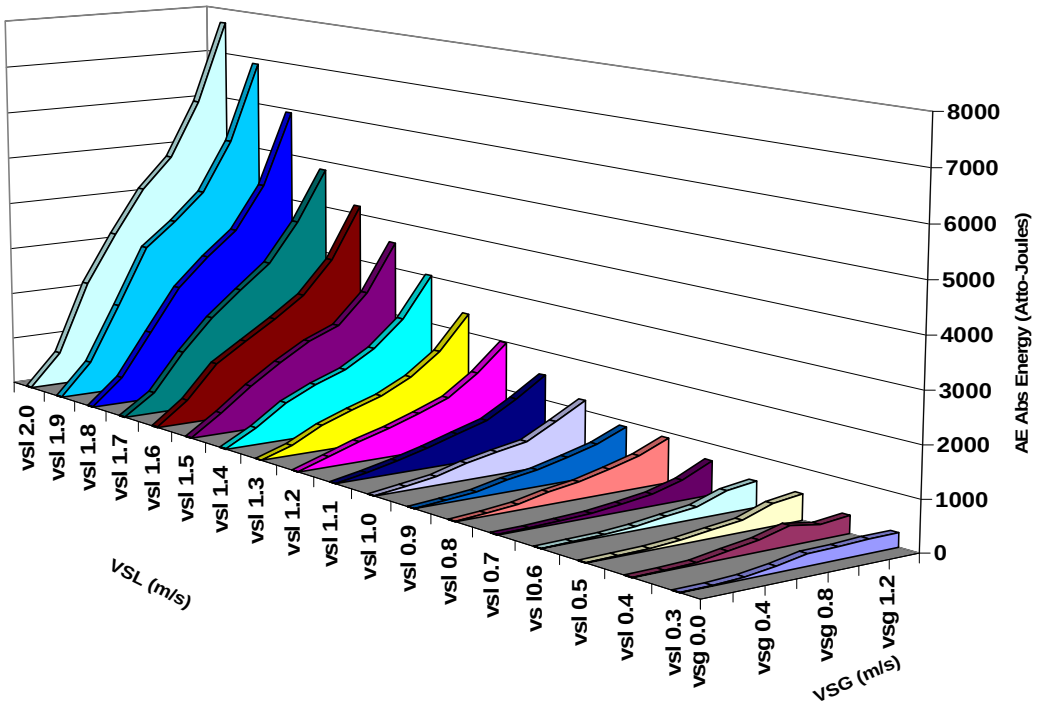

Figure 7-18: Waterfall plot for Ch2 sensor,

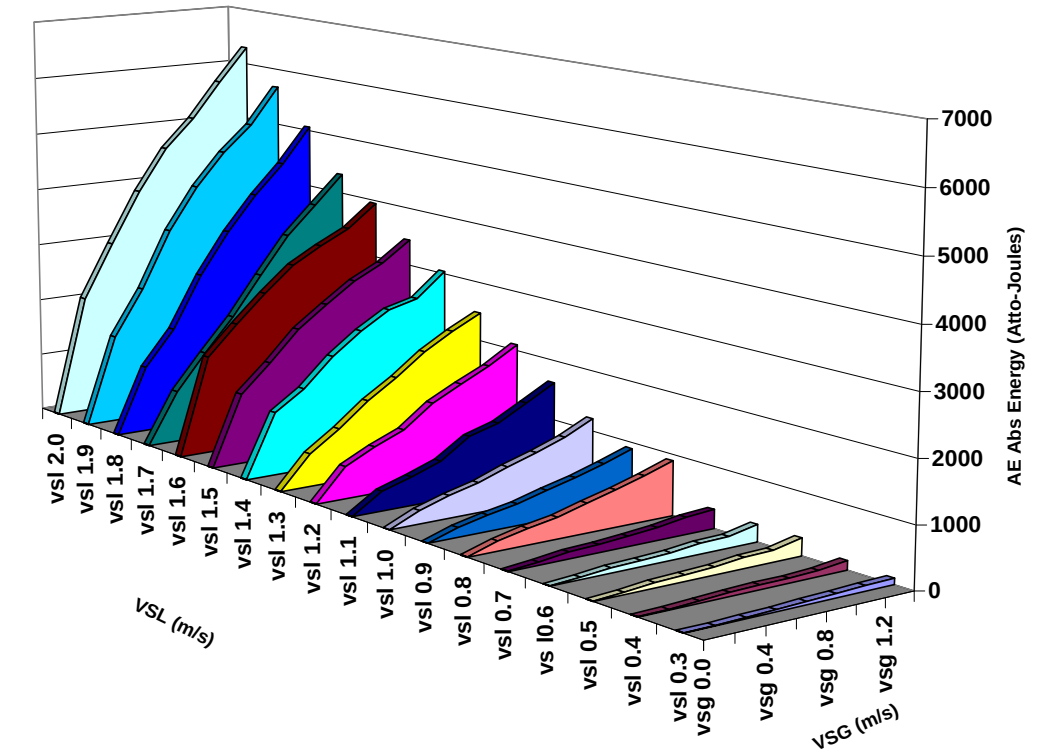

Figure 7-19: Waterfall plot for Ch3 sensor

7.2.1 Temperature Effect:

The investigated range of the temperature (14-45 Celsius degree) showed random and negligible deviation in the absolute AE energy levels, as shown in figure 7-20. This observation would suggest, neglecting any effect on the AE levels as a result of variations in test fluid temperature which could result from pumping and friction heat generation processes accompanied with the transportation of the flow. It was observed that at the fixed test conditions the variation of temperature resulted in random changes of AE energy. Though on average it may be considered that there is a reduction in AE energy with increasing temperature, this was not conclusive.

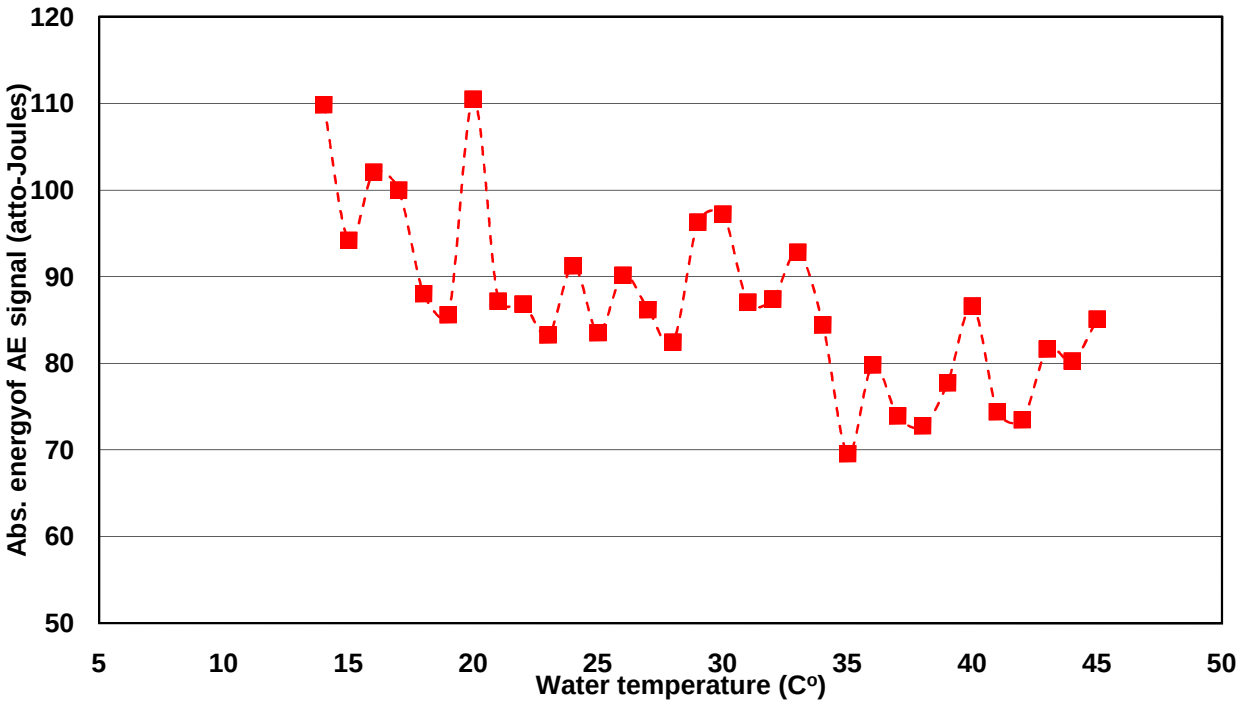

Figure 7-20: The temperature effect on the AE abs. energy signal at V_{SL}=0.8 and V_{SG} =1.0 ms^{-1}

7.2.2 Thickness Effect:

This test highlighted a correlation of increasing AE energy levels with increased wall pipe thickness, see figure 7-21.

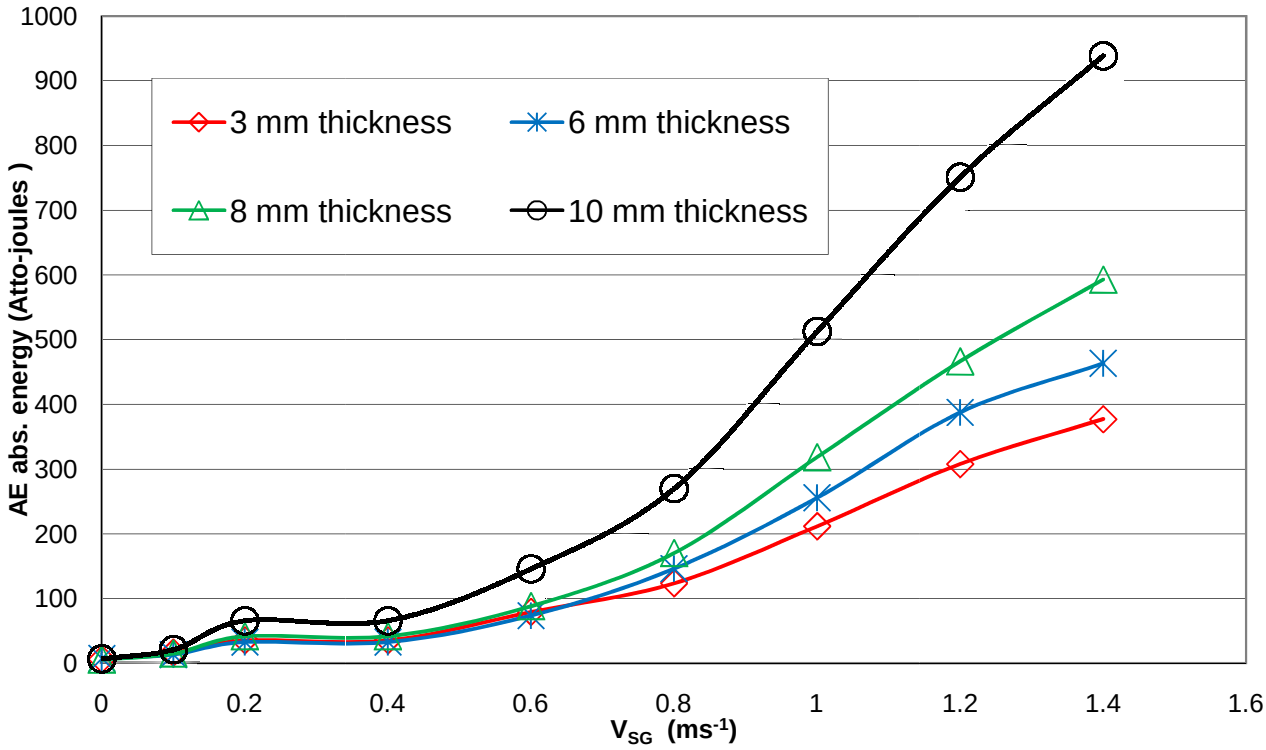

Figure 7-21: The effect of pipe thickness on the AE abs. energy at V_{SL}=1.0 ms^{-1}

7.2.3 Viscosity Effect:

Absolute AE energy levels showed dramatic drop in AE levels as viscosity increased when V_{SG} higher than 0.6 ms^{-1}. Figure 7-22 depicts this observation and compared pure water (1 Cp) in left vertical axis with the other three viscosities grades in right vertical axis. Chapman and Plesset (1971) stated that liquid viscosity has primary contribution to the damping of gas bubble oscillations. This will suppress the two phase activity and consequently reduces AE levels. However, the AE levels of the investigated viscosity grades

increased with the increase of V_{SG} values. Similar results were obtained at V_{SL} = 0.4 and 1.2 ms^{-1}

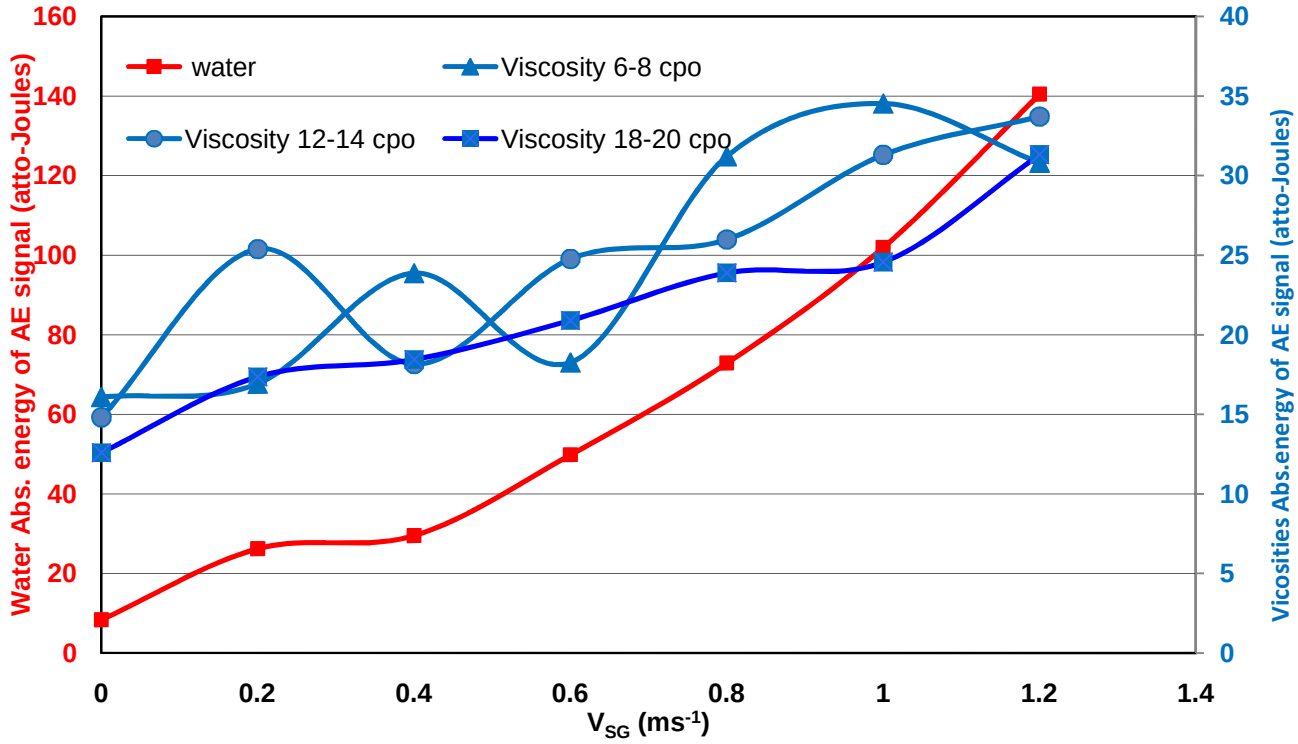

Figure 7-22: The viscosity effect on the AE abs. energy at varying V_{SG} and V_{SL}=0.8 (ms^{-1})

7.2.4 Surface roughness Effect:

The affect of internal pipe surface roughness for all measuring sensors is presented in figures 7-23 and 7-24 at V_{SL} =2.0 ms^{-1}. The affect of internal surface roughness was very obvious; the smoother the internal pipe roughness the less AE Absolute and vice versa. The increase in surface roughness will increase the turbulence of flow, thereby increasing the rate of air bubble

collapse at the internal pipe wall. The increase of the surface roughness from 1.6 to 3.2 (100%) will increase the AE absolute energy measured at Ch1 sensor by an average of 82%. Whereas the increase of the surface roughness from 3.2 to 10 (210%) led to an average increase of 60% in the AE absolute energy for the same sensor. Simillar results obtained at VSL=1.0 ms-1 , see figure D-9 and D-10, in Appendix(D)

Figures 7-25 presents results of AE Absolute Energy levels at V_{SL} =2.0 m/s, from the elbow mounted sensor. The observation suggests that the influence of internal surface roughness downstream of the elbow was insignificant in comparison to the effect on straight pipes.

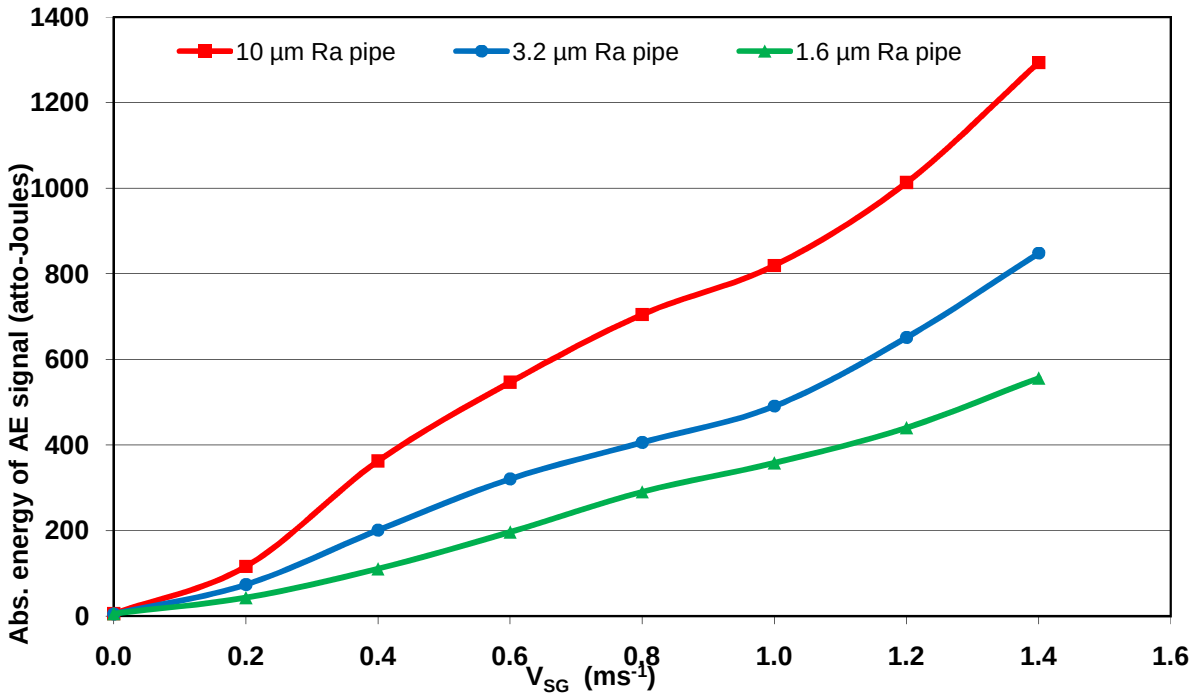

Figure 7-23: AE energy from Ch1 for three surface roughness grades at V_{SL}=2.0 ms^{-1}

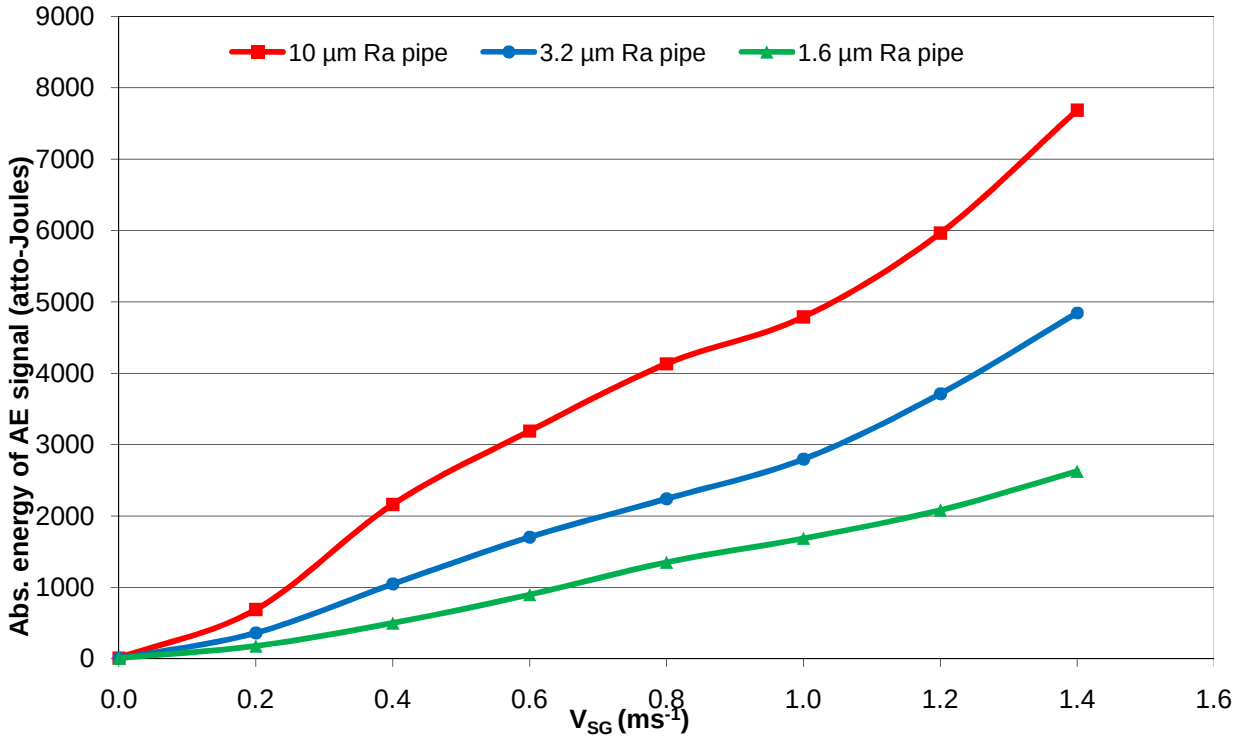

Figure 7-24: AE energy of Ch2 from three surface roughness grades at V_{SL}=2.0 ms^{-1}

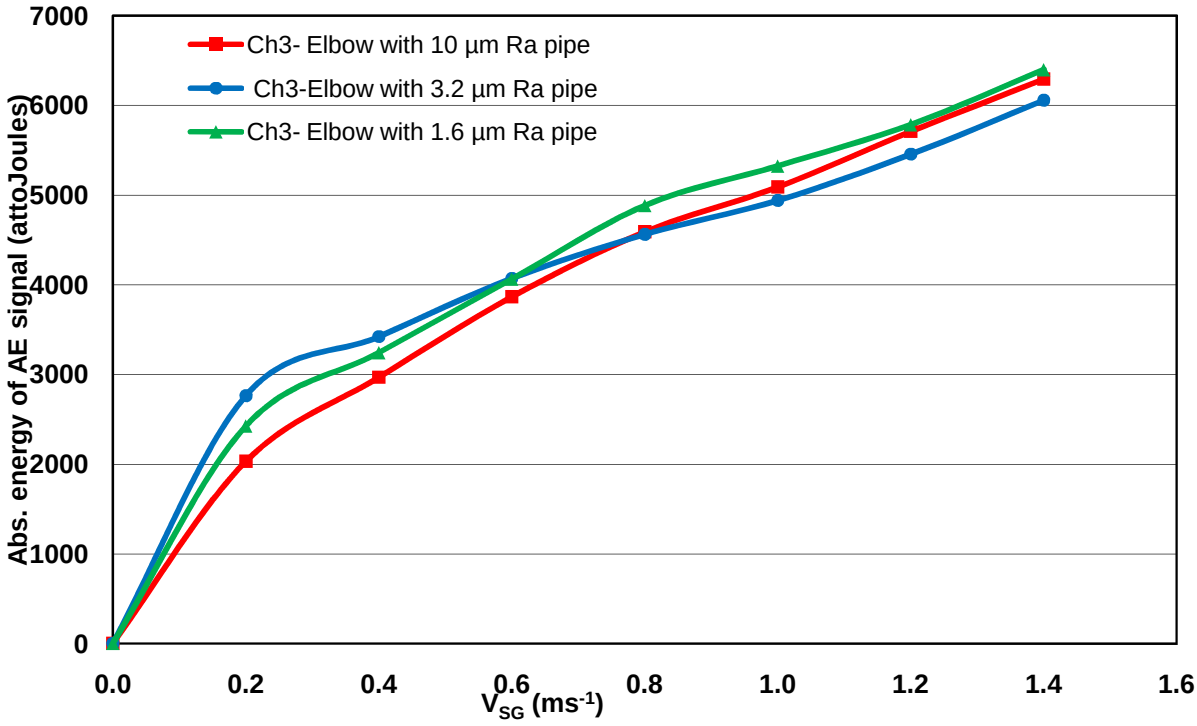

Figure 7-25: AE energy from ch3 for elbow with three pipes at V_{SL}=2.0 ms^{-1}

7.2.5 GVF and AE

Figures 7-26 and 7-27, show the Pearson correlation factor between measured GVF and AE levels of Ch1, for the three grades of surface roughness at V_{SL} =1.0 and 1.5 ms^{-1}. Also, correlation factors (r) corresponding to each surface roughness is presented and it is evident that the variation in internal roughness did not alter the similarity between AE and GVF for the different internal roughness values. This implies that though AE levels are known to be affected by internal roughness, measurements of GVF at a fixed internal surface roughness will still provide a strong correlation with AE. Observations from all surface roughness grades acquired by Ch1 for the majority of the test programmes are shown in figures 7-28 to 7-30.

The increase in V_{SG} values, results in an increase of the gas phase in the flow and consequently increase the bubbles dynamic activities such as; bubbles formation, coalescence, collapse, breaking-up and bubbles oscillation. Furthermore, the increase of V_{SL} values increased the intensity of the turbulence diffusion, which also led to increase in the bubbles activities. As such, any increase in V_{SL} and V_{SG} in gas/liquid flow, will lead to a proportional increase of the absolute energy of AE levels. The waveforms of the gas/liquid flow was of transient type, as a result of the AE events that generated from the bubbles activities, see figure7-2.

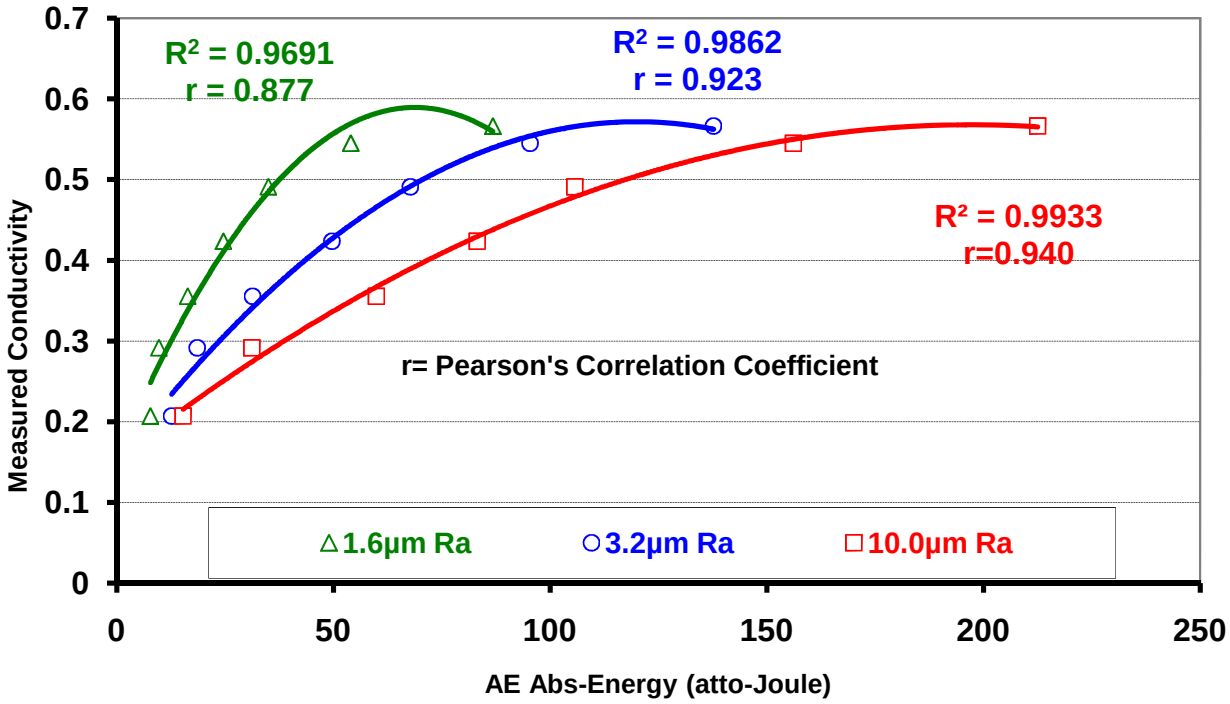

Figure 7-26: Correlation of measured GVF and AE levels at V_{SL} =1.0 ms^{-1}

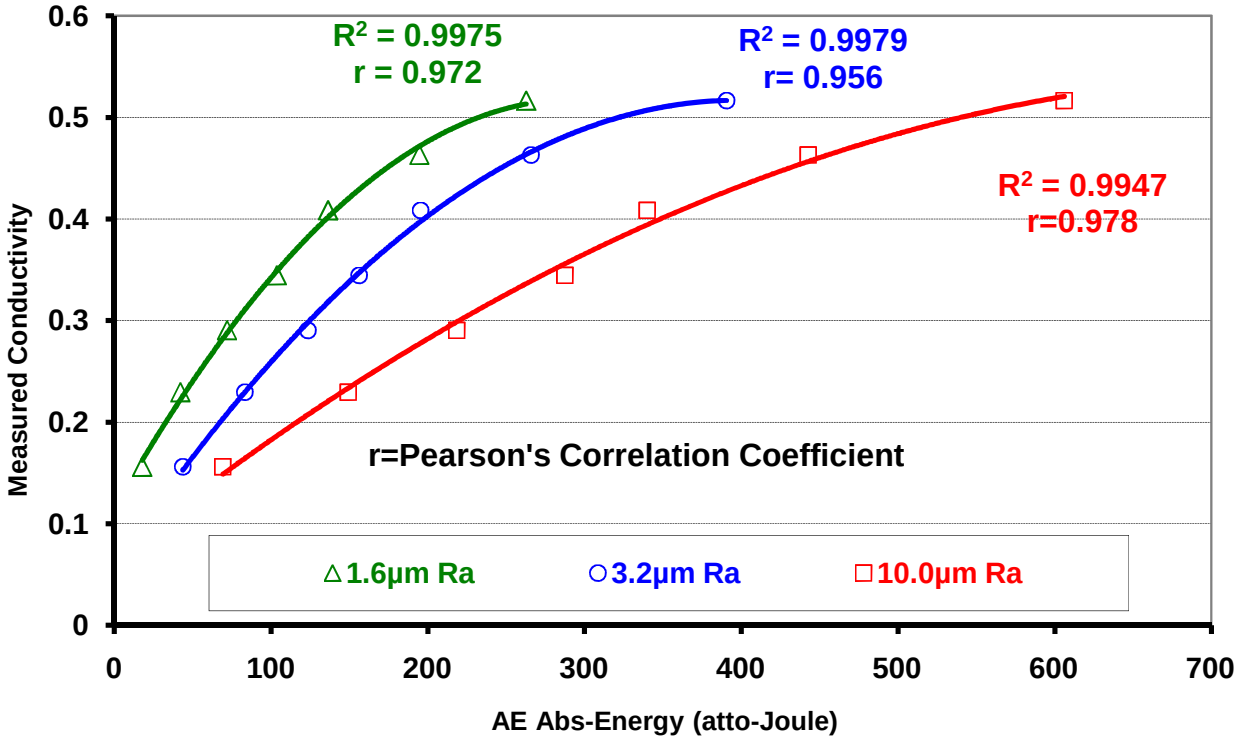

Figure 7-27: Correlation of measured GVF and AE levels at V_{SL} =1.5 ms^{-1}

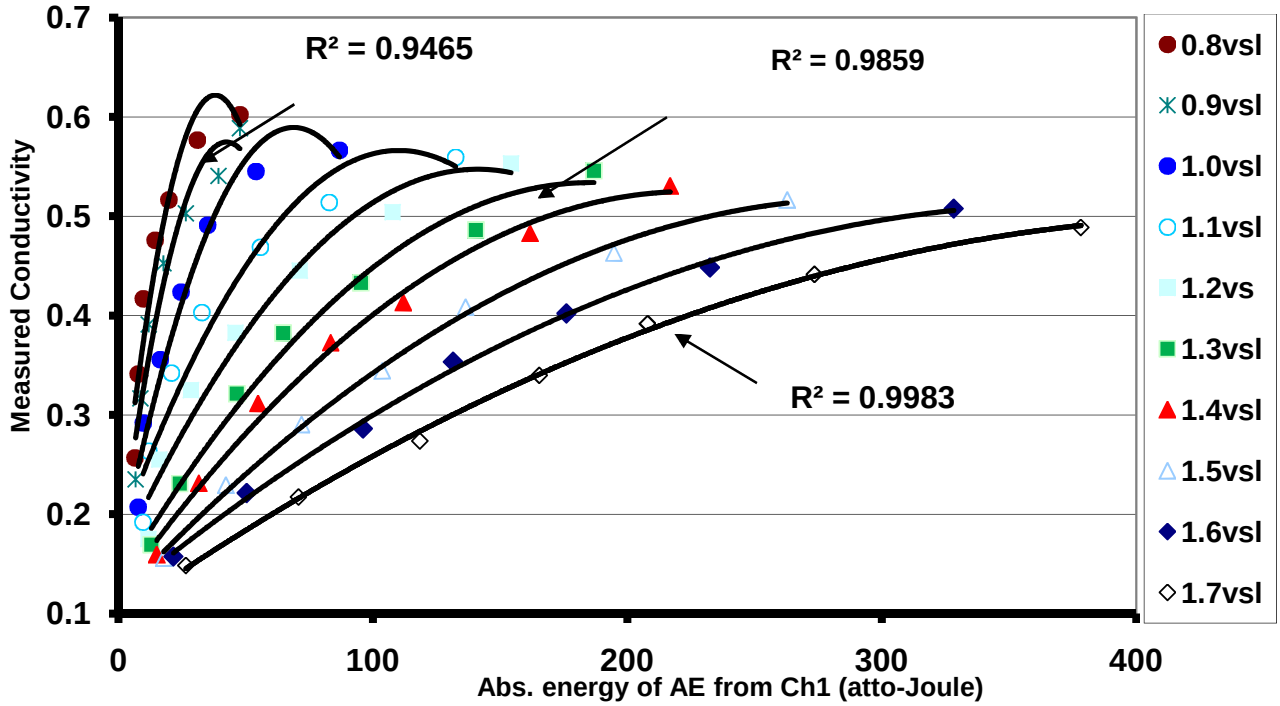

Figure 7-28: Relation between measured GVF and AE of 1.6µm Ra pipe

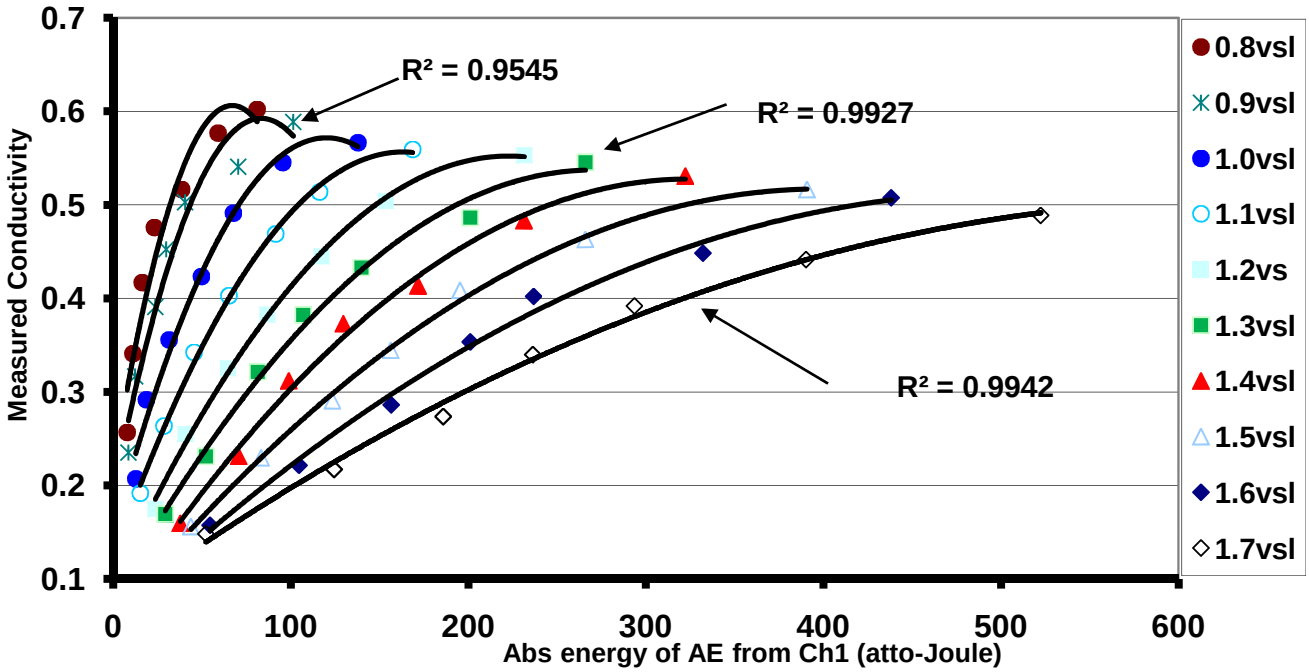

Figure 7-29: Relation between AE and measured GVF of 3.2µm Ra pipe

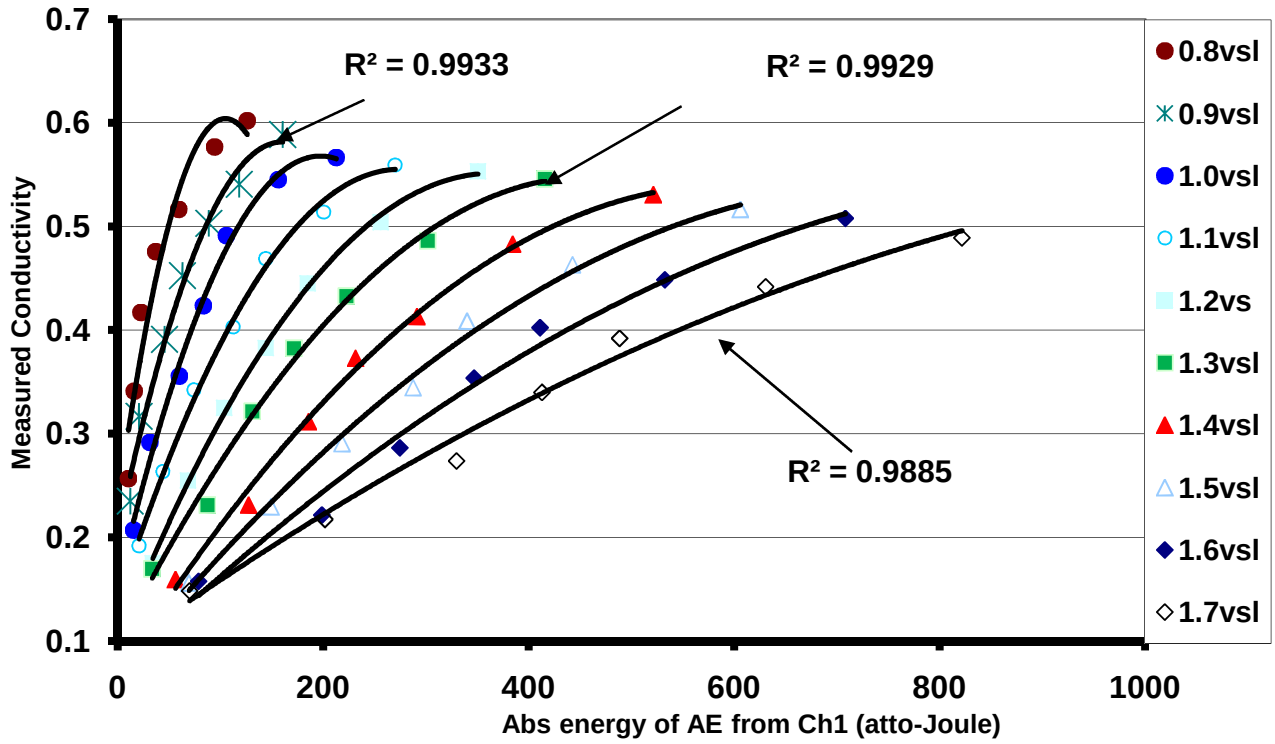

Figure 7-30: Relation between AE and measured GVF of 10.0µm Ra pipe

7.3 Discussion

The AE sensor orientation/position results showed the top steel sensor (Ch1) provided the strongest AE response from the flow, compared to bottom steel (Ch2) and top plastic (Ch3) sensors, see figure 7-5. It was surprising that the AE sensor on the top of the pipe showed more sensitivity than that of the bottom. This is attributed to the presence of bubbles on the top of the pipe due to buoyancy. It was not surprising the sensor on the plastic pipe had the lowest sensitivity due to attenuation across the plastic material.

The influence of single phase (pure liquid) on the AE levels was insignificant due to the lack of AE sources in pure liquid flow, such as the presence of

bubbles or unwanted solid particles. For this reason the type of AE waveform associated with this type of flow was continuous in nature, see figure 7-1. However, this was not the case for two phase flow, where, at any fixed superficial velocity (V_{SL}), the AE waveforms had significant transient element owing to the presence of bubbles within the flow.

The influence of pure liquid flow on generating AE was reinforced experimentally and compared to the electronic noise of the system, as shown in figure 7-10. The contribution of pure liquid was in average of 0.2 atto-Joules above the electronic noise of the system. This was considered insignificant compared to the influence of gas/liquid flow. This is evident that AE energy levels are mainly contribution of the gas/liquid flow.

In fact it was noted under slug flow regimes that the entire movement of the slug through the pipe was seen as increasing and decaying AE levels which could be correlated with the slug head and tail respectively, see figure 7-31. In this instance the waveform is continuous in appearance though it is fundamentally a mixture of several hundred transient AE bursts. The frequency spectrum associated with this slug related AE wave is shown in figure 7-32 with the dominating frequencies within the range of 150 to 450 kHz

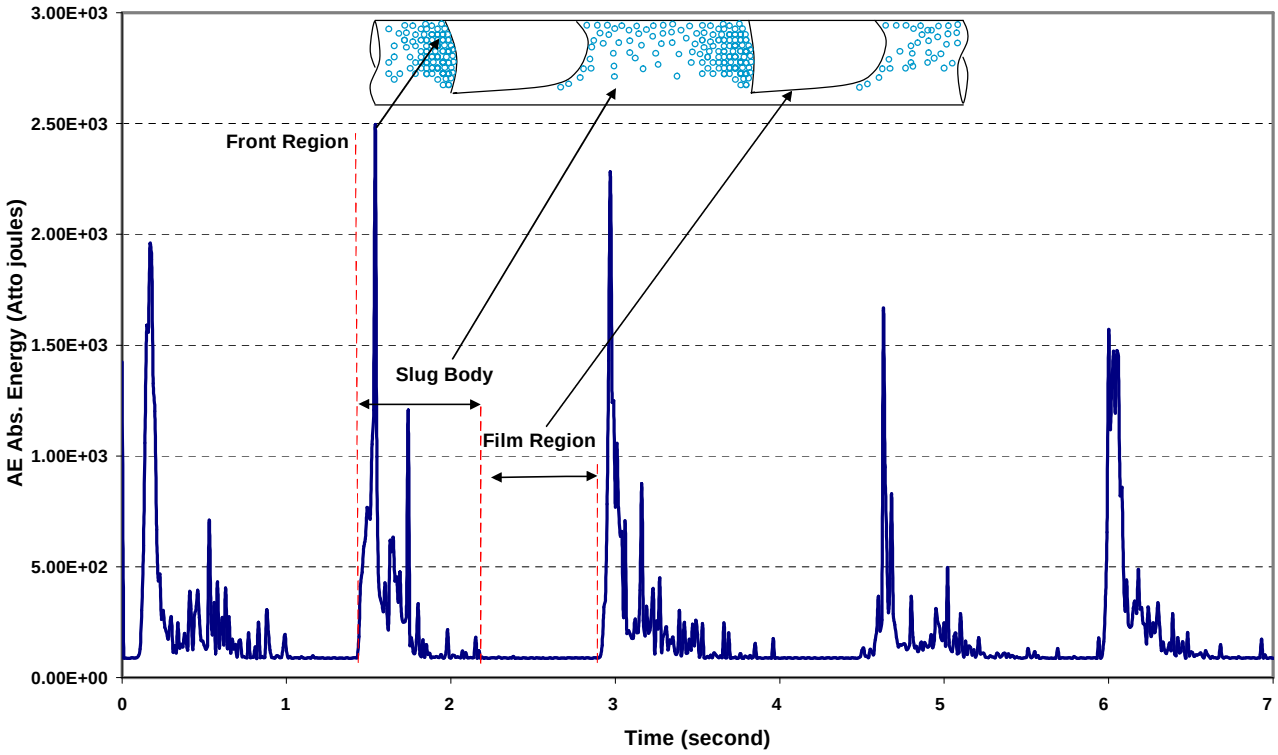

Figure 7-31: Typical AE signal from fully developed slug flow

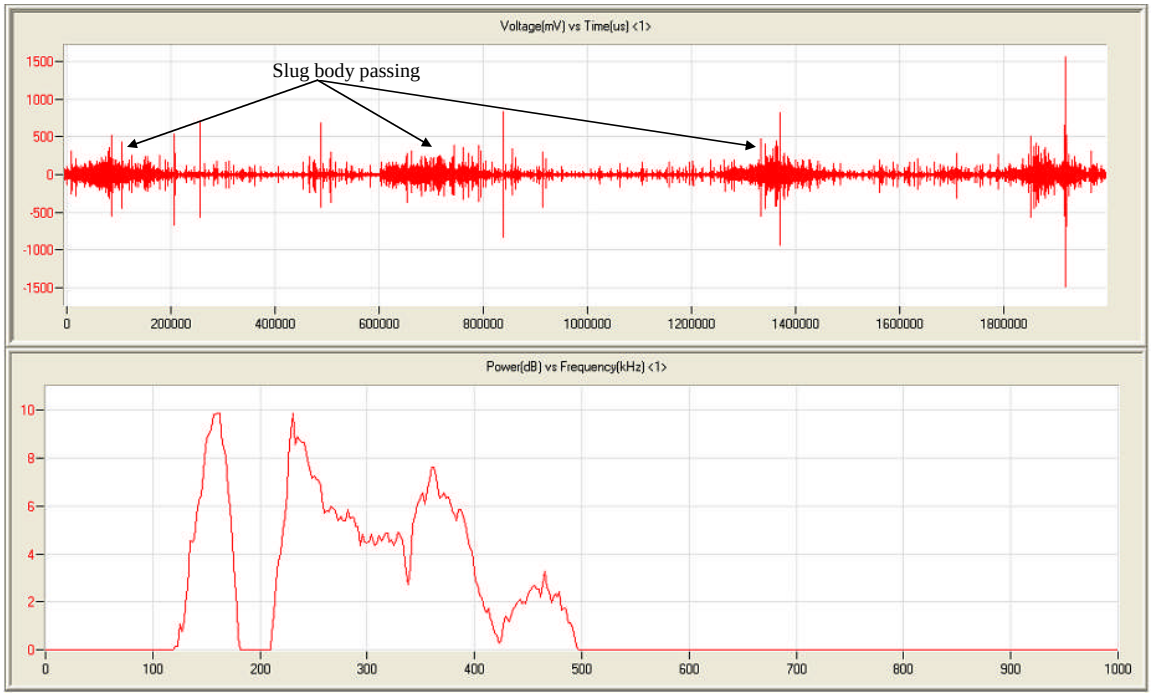

Figure 7-32: AE time waveform and associated frequency spectrum for V_{SL} 1.4 and V_{SG} 1.0

Observations of the influence of the surface roughness on AE measurements on the pipe showed that increasing surface roughness resulted in higher AE level. This was attributed to the increase of turbulent intensity forces on the liquid phase and the increase of bubbles activities rate on the inner pipe wall (collapse, formation, and etc). The turbulent intensity forces increased as a result of increase in the friction coefficient on the liquid phase. The friction between the two-phase flow bubbles and internal pipe surface increased as the surface roughness increased. Thus, resulting in an increase of AE associated with bubble activities. This result suggests the applicability of AE technology of monitoring the condition of internal pipe surface which is subjected to several mechanisms of degradation such as; corrosion, erosion and pipe blockage due to material build up.

Interestingly, whilst viscosity levels affected AE levels, the temperature for a fixed viscosity showed an inconsistent influence with an average of approximately 90 atto-Joules $\pm$ 20 atto-Joules. It is thought that within the temperature range tested, for the specific fluid, the viscosity dependency on temperature did not change significantly enough to be noted as a difference in AE levels, hence the inconsistency in results. Had a more viscous fluid been subjected to a wide temperature variation it is anticipated that the deference on AE would be more evident, as seen on the viscosity results presented in figure 7-22. From this it is observed that an increase in viscosity caused a decrease in AE levels under identical flow condition. This is attributed to damping effect as suggested by Chapman and Plesset (1971); the liquid viscosity has primary contribution to the damping of gas bubble oscillations. This will suppress the two-phase activity and consequently reduce AE levels. A large difference in AE energy generated with water in comparison to increased viscosity fluids was noted, and it was also noted that AE energy generated from three viscosity grades showed increases as V_{SG} values increased, which suggests the applicability of AE technology for monitoring changes in viscosity under two-phase flow conditions.

Also it was observed that Pico elbow's mounted sensor (Ch3) exhibited the highest energy level compared to the Pico sensor (Ch1) and WD sensor (Ch2), as shown in figure 7-11. This was attributed mainly to the increase in turbulent intensity of the flow as it passed through the elbow, due to the increase of flow restrictions introduced by the sudden change of the flow direction, in other words, increase in bubble activities compared to straight pipes.

The absolute energy levels of AE from the steel pipe test section acquired from the Pico sensor (Ch1)were less than those of the WD sensor(Ch2), this was credited to the difference in sensors sensitivity, where WD types are more sensitive than Pico, as illustrated in the calibration sheets for both sensors, figures C-1and C-2 in Appendix (C).

7.4 Acoustic Gas Void Fraction Correlation in Slug Body

The objectives of this section are firstly to develop a new correlation to predict the gas void fraction in two-phase air\water slug flow as a function of the absolute AE energy and slug velocity, and , secondly to validate such a correlation. The use of the proposed AE technology would offer significantly reduced installation time as it can be fitted directly onto a steel pipe without any requirements for modifying the existing pipe infrastructure; in addition, the cost of the AE technology is considerably less than existing systems. These advantages have offered the impetus in developing the AE technology for this application.

Adamson (1990) stated that the surface free energy per unit interfacial area is equal to the interfacial surface tension between a liquid phase and a gas phase. Assuming gas bubbles are all spherical with a diameter, d_{bubble}, the total surface free energy of the discrete gas bubbles ($E_{surface}$) in the liquid slug body was proposed by Brauner and Ullmann (2004) as:

$$E_{surface} = \frac{6\sigma}{d_{bubble}} A\,(1 - H_{LSB})\,L_{LSB} \qquad 7\text{-}3$$

where σ is the interfacial surface tension, A is the internal cross-sectional area of the pipe, L_{LSB} is the length of the liquid slug body, and H_{LSB} is the liquid hold-up in the slug body.

From Barnea *et al*.(1982) a critical bubble diameter, d_{bubble}, is given as:

$$d_{bubble} = 2\left[\frac{0.4\sigma}{(\rho_L - \rho_G)\,g}\right]^{1/2} \qquad 7\text{-}4$$

where, ρ_L and ρ_G are the liquid and gas densities respectively, and g is the gravitational force.

The slug length L_{LSB} was calculated as a function of pipe diameter D (Taitel and Dukler,1976) as:

$$L_{LSB} = 32D \qquad 7\text{-}5$$

Values employed in estimating $E_{surface}$ included:

Slug length =1.6m and Bubble diameter = 0.003451m

Zhang *et al*. (2003) assumed that the surface free energy of the discrete gas bubbles, based on the maximum amount of gas the liquid slug can hold, is proportional to the turbulent kinetic energy in the liquid slug body. This assumption is used in this paper to relate AE to surface free energy. The gas void fraction measured using the conductivity sensor is used to calculate the surface free energy in air/water slug flow conditions as per equation 7-3 and is plotted in figure 7-33. As expected, the relationship between the surface free energy and gas void fraction is linear for the given slug length, bubble diameter and interfacial surface tension. The surface free energy is proportional to the amount of the gas bubbles being held in the slug body.

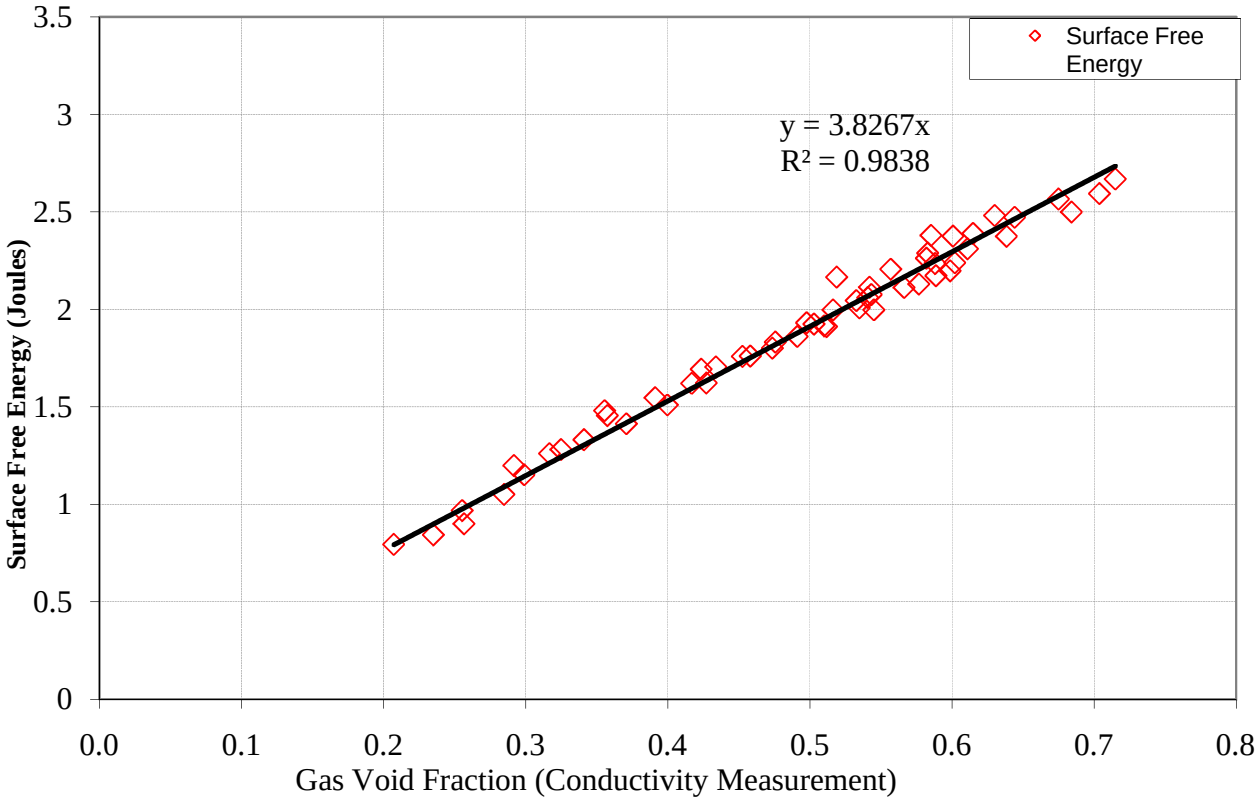

Figure 7-33: Surface free energy and measured gas void fraction in the slug body

At a fixed superficial water velocity, for example V_{SL}=0.8 ms^{-1}, increasing the superficial gas velocity resulted in an increase of the measured absolute AE energy, see figure 7-34. This was observed for all V_{SL} levels investigated. This was not surprising and showed that an increase in bubble content, and its associated bubble dynamics, resulted in an increase of AE generated. It was interesting to note that an increase in V_{SL} for a fixed V_{SG} resulted in a relative decrease in surface free energy whilst a simultaneous increase in AE energy was observed; figure 7-35 describes the relationship between AE energy measured from the AE sensor and the surface free energy calculated from

equation 7-3. This suggests that there are two mechanisms responsible for the generation of AE.

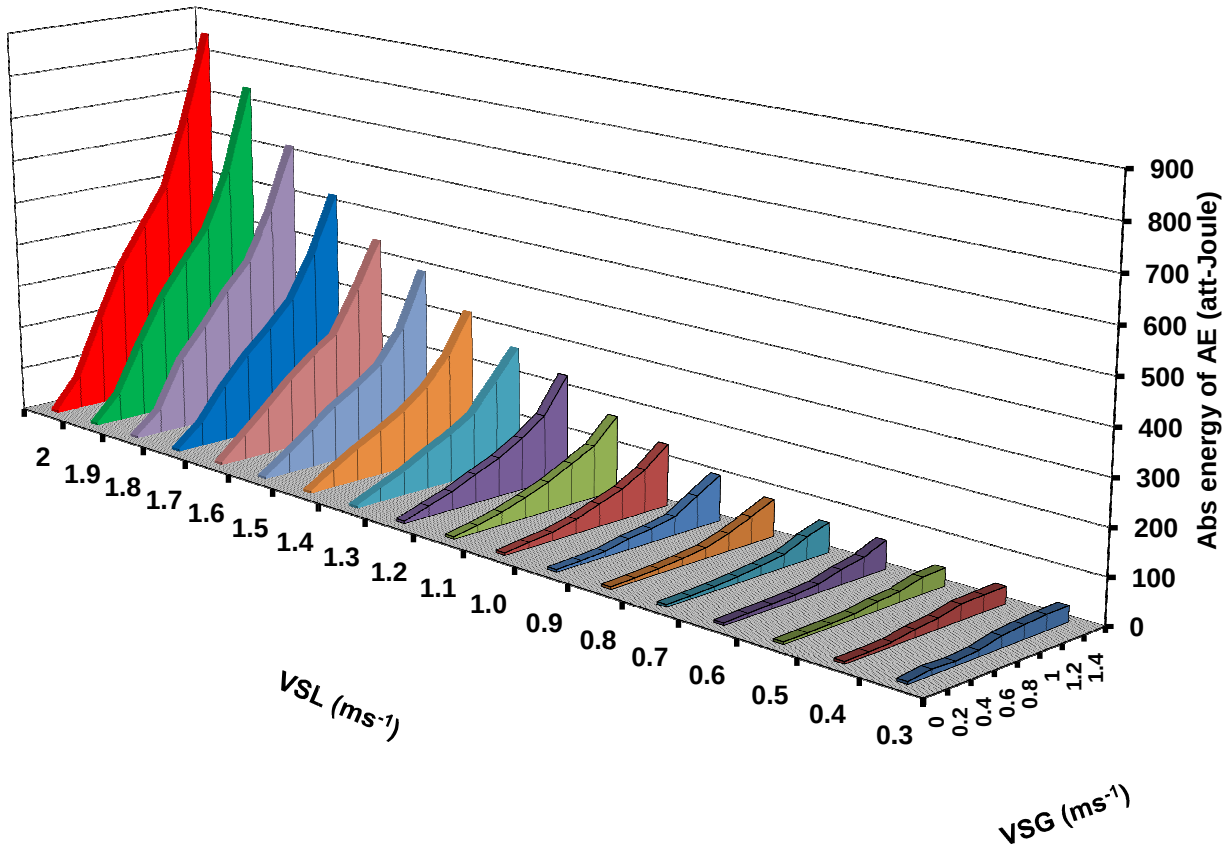

Figure 7-34: Contribution of the liquid and air velocities on the increase of the measured AE abs. energy

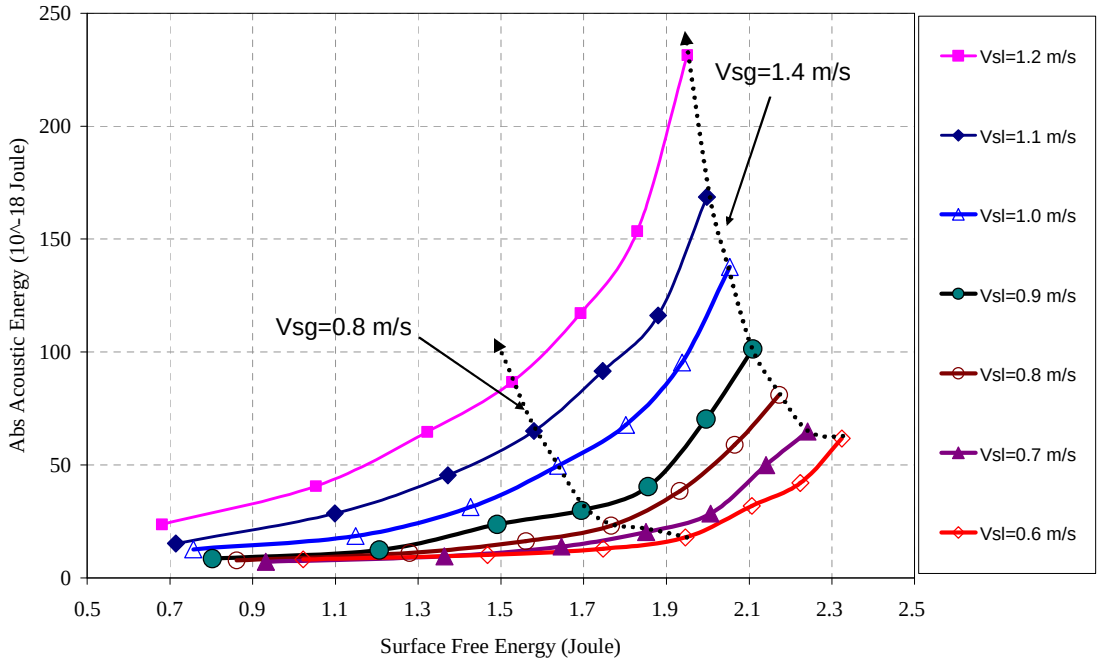

Figure 7-35: Contribution of the turbulence kinetic energy on AE energy levels

When the water superficial velocity increases the intensity of the turbulence diffusion increases, and as a result, the associated absolute AE energy increases as illustrated in figure 7-35. Similarly, an increase in water superficial velocity reduces the GVF for a defined superficial air velocity; this GVF is directly correlated to the free surface energy. Therefore, the author believes that there are two processes influencing the generation of AE; the free surface energy which is a measure of the bubble content in the liquid (air velocity) and the influence of turbulent diffusion (turbulent kinetic energy) due to high superficial liquid velocities. Figure 7-34 illustrates and confirms the above mentioned processes between liquid and air velocities, and the associated absolute AE energy.

Figure 7-36 presents the measured gas void fraction taken by the conductivity sensor and the associated absolute AE energy suggesting a non-linear relationship. Figure 7-35, provided the basis for establishing a relationship between the GVF as a function of the AE energy. A multiple exponential regression resulted in the following relationship:

$$\varepsilon = a\, AE^{b}\, V_{mix}^{\ c}\, V_{SG}^{\ d} \qquad 7\text{-}6$$

where ε is the gas void fraction in slug body, a = 0.768, b = 0.003, c = -0.690.and d = 0.744. Figure 7-37 shows the obtained gas void fraction in the liquid slug body from the developed correlation (7-6) as function of absolute AE energy and slug velocities.

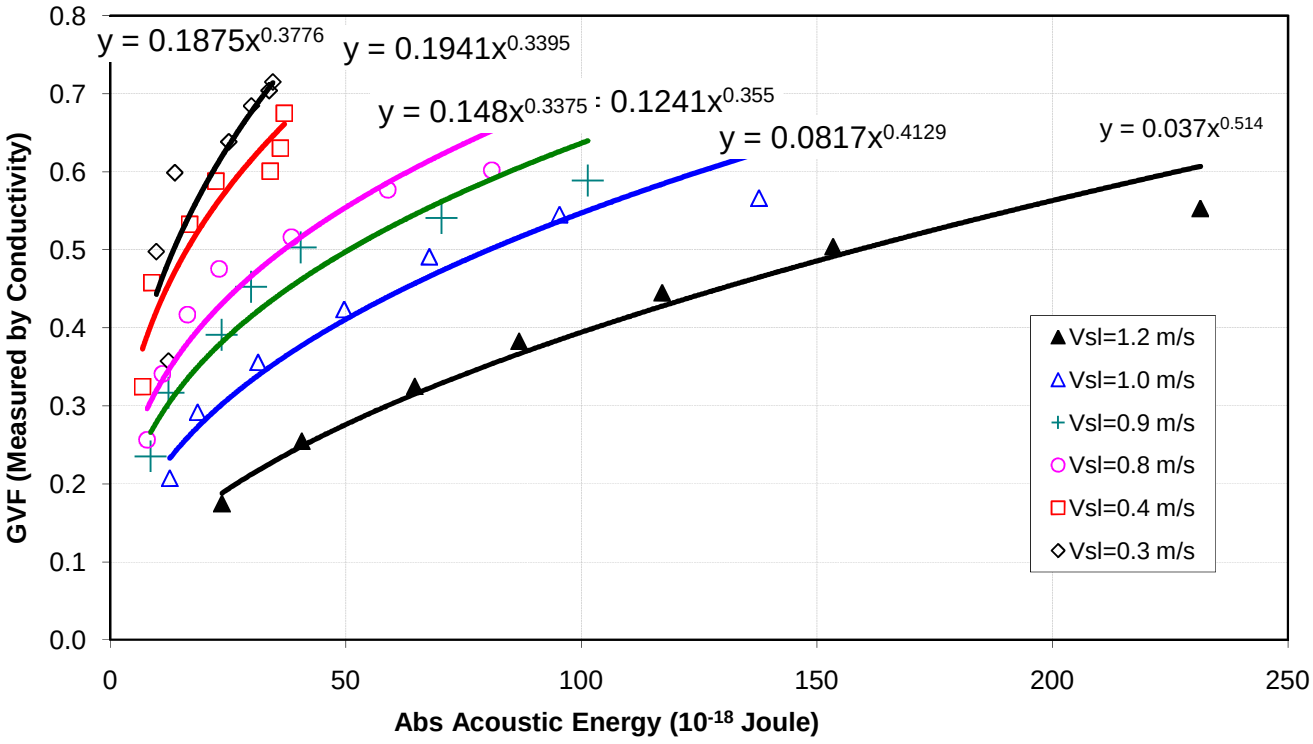

Figure 7-36: AE abs. energy and measured gas void fraction

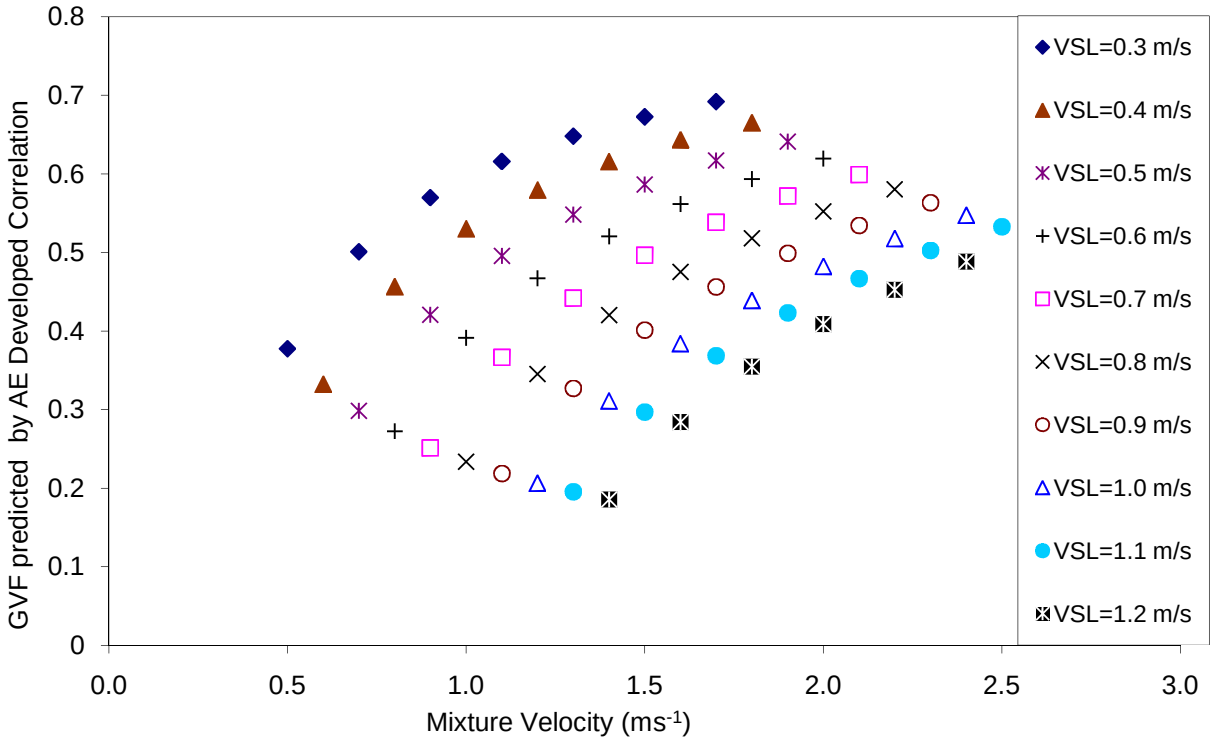

Figure 7-37: Gas Void Fraction predicted from the proposed AE model, equation 7-6

To determine the relative accuracy of new proposed correlation, three familiar statistical measures of reliability were computed: 1) percentage error (PE); 2) the average percent error (APE); 3) the standard deviation (SD). Equations for these measures are:

$$PE = \frac{(\text{Estimated} - \text{Measured})}{\text{Measured}} \times 100 \qquad 7\text{-}7$$

$$APE = \frac{\sum_{i=1}^{n} PE}{n} \qquad 7\text{-}8$$

$$SD = \sqrt{\frac{n\sum_{i=1}^{n}(PE_i)^2 - \left[\sum_{i=1}^{n} PE_i\right]^2}{n^2}} \qquad 7\text{-}9$$

The predictions of the proposed correlation, equation 7-6, and correlations by several researchers (Gregory *et al.,* 1978; Hughmark, 1962; Beggs and Brill,

1972 and Nicklin et al., 1962) are presented in Table 7-3. The statistical parameters for the proposed correlation are smaller than those listed in Table 7-3, demonstrating good performance over all correlations.

Table 7-3: Summary of statistical results for correlations

	APE	SD
This study	***-0.49***	***3.48***
Gregory *et al* (1978)	12.95	10.80
Hughmark (1962)	13.90	10.89
Beggs and Brill (1972)	5.73	8.84
Nicklin *et al* (1962)	13.29	14.77

Figure 7-38 shows the comparison between the predicted correlations and measured gas void fraction based on measurements taken from the conductivity sensor. All of predicated values agree within ±15 % with the measured data. Also shown in figure 7-38 is the large spread of the predicted gas void fraction values at low superficial gas velocity, but this spread of data narrows at higher superficial gas velocities. One of the main advantages of the proposed correlation is that the AE signals improved with the higher gas fraction thus increase the accuracy of the prediction even at higher gas fractions. As a result, the proposed correlation can be successfully applied to two-phase air/liquid flow systems, which have a very high percentage of gas void fraction.

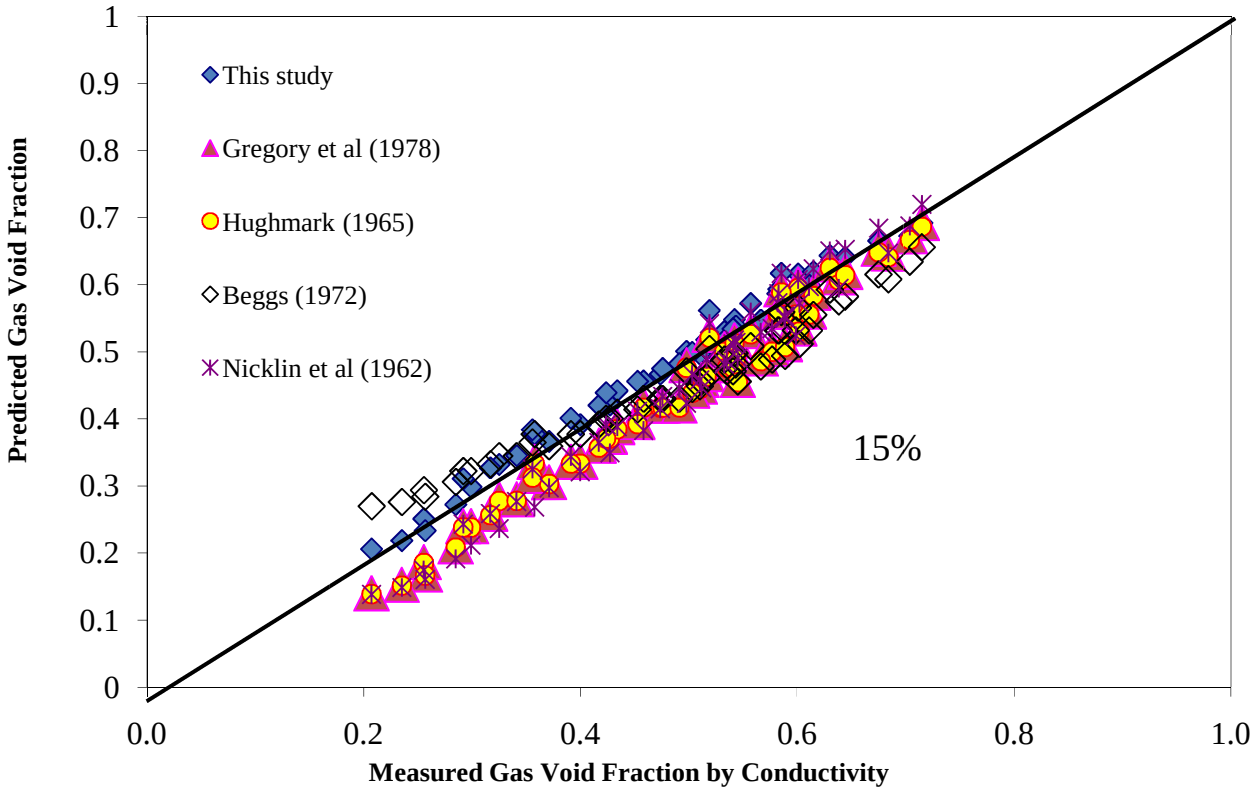

Figure 7-38: Comparison of measured and predicted gas void fraction data; proposed correlation

Chapter 8: Conclusions and Recommendations for Future Work

8.1 Conclusion

This work presents preliminary investigations on the application of AE technology for measuring GVF in two-phase air/water under different flow regimes particularly slug flow conditions. It is evident that the main source of Acoustic Emission is directly correlated with the dynamics of bubbles; its formation, coalescence and destruction. Whilst the movement of bubbles in a fluid is known to be associated with oscillations at frequencies of a few kilohertz, it is thought such movement does not generate energy at the frequencies associated with Acoustic Emissions (AE). As defined earlier, the emissions measured in this investigation cover the frequency range of 100kHz to 1,000KHz. The formation and destruction of bubbles is known to be associated with transient pressure pulses which will excite a broad frequency range which will be detectable in the AE frequency range.

The increase of the superficial gas velocities resulted in an increase in AE due to the increase in bubble content and its associated bubble dynamics. In addition, an increase in the superficial liquid velocity, result in an increase in the intensity of the turbulence diffusion, also generated increased AE energy. It has been demonstrated that two mechanisms are responsible for the generation of AE, the free surface energy which is a measure of the bubble content in the liquid (air velocity) and the influence of turbulent diffusion (turbulent kinetic energy) due to high superficial liquid velocities.

Interestingly, it was noted that the smoother the internal surface roughness of the pipe the lower the AE energy levels for fixed superficial liquid and gas velocities. This was attributed to the increased turbulence at the interface between the fluid and the pipe wall. In addition, it was also noted that the AE sensor placed on the top of the pipe (top-dead-centre) was more sensitive to AE

sources than at any other circumferential position on the pipe. This was attributed to the fact that bubbles in the fluid would float to the top of the pipe due to buoyancy under the flow regimes investigated. As such the dynamics of collapse, coalescence and creation, will be experienced at the top of the pipe and therefore the AE sensor at this location will be inevitably be more sensitive to these AE sources

Lastly GVF levels were correlated with AE at varying internal pipe roughness values. The correlations showed high Pearson correlation levels across all superficial liquid and gas velocities tested. The correlations were validated against other published and showed agreement within ±15 % with the measured data.

In summary the following are concluded:

1. The gradual increase in the level of the energy of the AE sensor was caused by an increase of the superficial gas and liquid velocities.
2. The smoother the internal surface roughness of the pipe resulted in reduced turbulence and consequently relatively lower AE levels.
3. AE activity was more sensitive at the top of the pipe than at the bottom and that due to buoyancy of gas bubbles.
4. GVF and AE generated from two-phase flow were correlated for different internal pipe surface roughness conditions
5. Observations of correlations between AE and liquid viscosity suggest the possible applicability for AE for monitoring changes in fluid viscosity in-situ.

Finally, the introduction of a new passive and non-invasive GVF measuring technique utilising AE technology has been proposed for two-phase air-water flows; providing both a quantitative and qualitative values.

8.2 Recommendations for future work

It has been demonstrated that the time domain analysis of AE signal generated from two-phase gas/water flow is a promising tool in monitoring the flow condition. Although the output identifier parameter adopted in this work was the absolute energy levels of the AE signal, the other parameters such as average signal levels (ASL) and root mean square (RMS) of the AE can also be used to monitor the flow conditions. The successfully developed correlation between the gas void fraction (GVF) and AE generated from the flow need to be more generalised by considering several other parameters such as;

- Pipe diameter: Several pipe diameters have to be investigated, and the effect of the pipe diameter needs to be included in the correlation.

- Fluid viscosity: Tests to be carried out by using different viscosity fluids. It is recommended that the use of viscosity enhancers such as Sodium Carboxymethyl Cellulose (CMC) should be avoided as they not only change the viscosity but also alters the other physical properties such as surface tension and density. It is therefore recommended that oil fluids with several grades of viscosities should be used for further investigation.

- Surface tension: Investigate the influence of surface tension on the generated AE values from the flow using several grades of liquids with different surface tensions.

- Pipeline inclination: The current research study covered two-phase flow in the horizontal pipelines. Further work should be performed to include the effect of pipeline inclination using inclined and vertical pipelines, which will add significant knowledge to this research.

- Pipe wall thickness: Results obtained from wall thickness tests were inconclusive. More investigation on the effect of the pipe wall thickness by adopting different approach that includes the flow direction is recommended.

- Due to the fundamental influence of the bubble content on the generated AE energy, more work has to be done in the frequency domain, in order to investigate the contribution and possibly discriminate the influence of each of the bubble activities such as formation, coalescence and destruction.

REFERENCES

- Abdul-Majeed, G.H. (2000) Liquid slug hold-up in horizontal and slightly inclined two-phase slug flow. *J. Petr. Sci. Eng.* 27 (2000), pp. 27–32.

- Abouelwafa, M.S.A., and Kendall, E.J.M. (1980). The measurement of Component Rations In Multiphase Systems Using Gamma Ray Attenuation. J. of Phys.E:Sci. Instrum. Vol 13, pp 341-5.

- Adamson, A. W., 1990, *Physical Chemistry of Surfaces*, 5th ed., Wiley, New York.

- Albion, K., Briens, L., Briens, C., and Berruti, F., (2007) Flow regime determination in horizontal pneumatic transport of fine powders using non-intrusive acoustic probes, Powder Technology, Volume 172, Issue 3, 23 March 2007, Pages 157-166, ISSN 0032-5910

- Alfayez, L. and Mba, D. (2005), Detection of incipient cavitation and determination of the best efficiency point for centrifugal pumps using acoustic emission, Proceedings of the Institution of Mechanical Engineers, Part E: Journal of Process Mechanical Engineering, vol. 219, no. 4, pp. 327-344.

- Alfayez, L., Mba, D. and Dyson, G. (2005), The application of acoustic emission for detecting incipient cavitation and the best efficiency point of a 60 kW centrifugal pump: Case study, NDT and E International, vol. 38, no. 5, pp. 354-358.

- Alhashmi, S. A., (2005), Detection and Diagnosis of Cavitation in Centrifugal Pumps, PhD, University of Manchester, UK

- Al-lababidi, S., (2006). Multiphase Flow Measurement in the Slug Regime Using Ultrasonic Measurements Techniques and Slug Closure Model, Ph.D. Thesis, University of Cranfield, UK

- Al-lababidi, S., and Sanderson, M.L.,(2004) Transit Time Ultrasonic Modelling in Gas/Liquid Intermittent Flow Using Slug Existence Conditions and Void Fraction Analysis". In: Proceedings of the 12th International Conference on Flow Measurement, FLOMEKO'04, Guilin, China, Sep12-17 2004**.**

- Al-Maskari, A. S. A., (1984), Detection of cavitation in a centrifugal pump using acoustic emission, M.Sc. edn, Cranfield Institute of Technology. School of Mechanical Engineering., UK.

- Al-Masry W., Ali E. and Aqeel Y., (2005) Determination of bubble characteristics in bubble columns using statistical analysis of acoustics sound measurements, Chemical Engineering Research and Design 83 pp1196–1207.

- Al-Sheikh et al.,(1970). Al-Sheikh J.N., Saunders D.E. and Brodkey R.S., Prediction of flow patterns in horizontal two-phase type flow. Can. J. Chem. Eng. **48** (1970), pp. 21–29.

- Andreussi, P., Donfrancesco, Di. and Messia, M. (1988) . An Impedance Method for the Measurement of Liquid Holdup in Two-Phase Flow. International Journal of Multiphase Flow, 14(6), 777–787.

- Baker, O., (1954). Design of pipelines for the simultaneous flow of oil and gas. Oil and Gas Journal. (23), pp185–195.

- Barnea, D. and Taitel, Y. (1993). A model for slug length distribution in gas-liquid slug flow. *International Journal of Multiphase Flow*, 19(5), 829–838.

- Barnea, D., Shoham, O., and Taitel, Y., (1982), “Flow Pattern Transition for Vertical Downward Two Phase Flow,” Chem. Eng. Sci., 37, pp. 741–744.

- Beggs, H. D., and Brill, J. P., 1973, ‘‘A Study of Two-Phase Flow in Inclined Pipes,’’ Trans. AIME, 255, p. 607.

- Bendjaballah, N., Dhaouadi, H., Poncin, S., Midoux, N., Hornut, J. M., and Wild, G. (1999). Hydrodynamics and flow regimes in external loop airlift reactors. Chemical Engineering Science, 54, 5211–5221.

- Bendjaballah-Lalaoui, N. (2000). Hydrodynamique globale et locale dans un réacteur à gazosiphon à recirculation externe. Thèse de doctorat, Institut National Polytechnique de Lorraine, Nancy, France.sited on Boyer, Anne-Marie Duquenne, Gabriel Wild, Measuring techniques in gas-liquid and gas-liquid-solid reactors, Chemical Engineering Science, Volume 57, Issue 16, August 2002, Pages 3185-3215, ISSN 0009-2509

- Benjamin, T.B, (1954), Cavitation in liquids, Ph.D. thesis, University of Cambridge, U.K.

- Betteridge, D., Joshlin, M. T. and Lilley, T., (1981), Acoustic emissions from chemical reactions, Analytical Chemistry, 53, 1064-1073.

- Boczar, T. Lorenc, M., (2004) Determining the Repeatability of Acoustic Emission Generated by the Hsu-Nielsen Calibrating Source, Molecular and Quantum Acoustics vol.. 25, pp177-191

- Bonizzi M, Issa RI, (2003) A model for simulating gas bubble entrainment in two-phase horizontal slug flow, INT J MULTIPHAS FLOW, , Vol:29, Pages:1685-1717, ISSN:0301-9322

- Bouras, S. Zerizer, I. Gheldane, F. Bouazza, M.T. Bouzabata, B., (2008) Study of the resistance to crack propagation in alumina by acoustic emission, Ceramics International, Volume 34, Issue 8, December 2008, Pages 1857-1865, ISSN 0272-8842

- Boyd, J.W.R. and Varley J. (2001), The uses of passive measurement of acoustic emissions from chemical engineering processes, Chemical Engineering Science, Volume 56, Issue 5, pp1749-1767, ISSN 0009-2509.

- Boyer, Anne-Marie Duquenne, Gabriel Wild, Measuring techniques in gas-liquid and gas-liquid-solid reactors, Chemical Engineering Science, Volume 57, Issue 16, August 2002, Pages 3185-3215, ISSN 0009-2509.

- Bragg Sir W. H., (1921), The World of Sound .London, Bell, pp 69-74.

- Brauner, N., and Ullmann, A., (2004), “Modelling of Gas Entrainment From Taylor Bubbles. Part B: A Stationary Bubble,” Int. J. Multiphase Flow, 30, pp. 273–290.

- Brennen, C. E., (1995) Cavitation Bubble Dynamics, Oxford University Press, ISBN: 0-19-509409-3

- Broring S., Fischer J., Korte T., Sollinger S. and Lubbert A.,(1991) Flow structure of the dispersed gasphase in real multiphase chemical reactors investigated by a new ultrasound-Doppler technique. Canadian Journal of Chemical Engineering **69** (1991), pp. 1247–1256.

- Brüel & Kjaer,(1981) Technical Review, No 2, 38-40, 1981.ISSN:0007-2621

- Buttle, D.J. and Scruby, C.B. (1990) Characterisation of particle impact by quantitative acoustic emission. Wear, 137, pp63-90.

- Callaghan, P. T. (1991). Principles of nuclear magnetic resonance microscopy. New York: Oxford University Press. ISBN 0198539444

- Carvalho, R.D.M., Bergles, A.E., 1991. The use of hot-wire anemometry for local void fraction measurements in pool boiling. In: Proceedings of the 11th ABCM Mechanical Engineering Conference (XI COBEM), vol. 1, pp. 279–282.

- Chabot, J., Farag, H., & De Lasa, H. (1998). Fluid dynamics of bubble columns at elevated temperature modelling and investigation with refractive fiber optic sensor. The Chemical Engineering Journal, 70, 105–113.

- Chapman, R.B. and Plesset, M.S. (1971). Thermal effects in the free oscillation of gas bubbles. ASME J. Basic Eng., 93, 373—376.

- Cheng, W., Murai, Y., Sasaki, T. and Yamamoto, F. (2005). Bubble velocity measurement with a recursive cross correlation PIV technique. Journal of Flow Measurement and Instrumentation, 16 (1), 35-46.

- Cho, H., Arai, Y., Takemoto, M., (2004) Development of stabilized and high sensitive optical fiber acoustic emission system and its application. Progress in AE XII:43-48, JSNDI

- Clayton T. Crowe, (2005). Multiphase Flow Handbook, Taylor and Francis, ISBN-10: 0849312809

- Cohen, J. (1988). *Statistical power analysis for the behavioral sciences* (2nd ed.) ISBN: 978-0805802832

- Corneliussen, S., Couput, J., Dahl, E., Dykesteen, E., Frøysa, K. E., Malde, E., Moestue, H., Moksnes, P. O., Scheers, L. and Tunheim, H. (2005). Handbook of Multiphase Flow. Norwegian Society for Oil and Gas Measurement (NFOGM) and The Norwegian Society of Chartered Technical and Scientific Professionals (Tekna), Norway, Revision 2, March 2005.

- Costigan, G. and Whalley, P. B. (1997). Slug Flow Regime Identification From Dynamic Void Fraction Measurement in Vertical Air-Water Flows. International Journal of Multiphase Flow, 23(2), 263-282.

- Cravarolo L. and Hassid A.(1965), Liquid volume fraction in two phase adiabatic systems, Energia Nucleare, 14, (11), 569-576.

- Crowther, T. G., Wade, A. P., Wentzell, P. D., and Gopal, R. (1991) Characterization of acoustic emission from an electrolysis cell. Analytica Chimica Acta, 254, 223-234.

- Darling, J. and Johnston, D. N., 1991, "The Use of Acoustic Emission for Condition Monitoring in High-pressure Hydraulic Pumps," in EUROTECH Direct 91, IMechE, Birmingham, UK, 2-4 July, Paper C414/011, 137-143.

- Deeprose, N. W. King, P. J. McNulty, I.S. Pearsall,(1974) Cavitation Noise, Flow Noise and Erosion, Proc. Conf. on Cavitation, Inst. Mech. Engrs., Fluid Machinery Group, Herriot-Watt Univ., Edinburgh., 373-381, Sept. 1974.

- Delhaye and G. Cognet (Eds.), Measuring techniques in gas–liquid two-phase flows (pp. 199–228). Berlin, Heidelberg, New York, Tokyo: Springer.

- Delhaye, J.M., 1969. Hot film anemometry in two-phase flow. In: Proceedings of the 11th National ASME/AIChE Heat Transfer Conference: Two-Phase Flow Instruments, pp. 58–69.

- Delheaye J.M. (1972), Local measurements in two phase flow, Fluid Dyn. Meas. Ind. & Medical Environment, l9l-200, Ed. Cockrell D.J., Leicester Univ. Press.

- Derakhshan, O., Houghton, J.R., Jones, R.K. and March, P.A., (1991), Cavitation monitoring of hydroturbines with RMS acoustic emission measurement, Symposium on Acoustic Emission: Current Pratice and Future Directions, Mar 20-23 1989Publ by ASTM, Philadelphia, PA, USA, Charlotte, NC, USA, pp. 305.
- Dong, F., Xu, Y. B., Xu, L. J., Hua, L. and Qiao, X. T. (2005). Application of dual-plane ERT system and cross-correlation technique to measure gas-liquid in vertical upward pipe. Journal of Flow Measurement and Instrumentation, 16(2-3), 191-197.

- Drouillard, T.F. (1996) A history of acoustic emission. Journal of AE 14(1), pp1-34.

- Duclos, J. B. Reuben R. L., and Steel J. A.,(2004) Study of Particle Impacts in Fluid Flow using Acoustic Emission, COMADEM 2004 International Congress & Exhibition On Machine Tool Performance Monitoring, Heriot-Watt University, UK, pp 566-575, ISBN 0 – 954 1307 – 1 – 5

- Dukler A.E., Wicks III M., and Cleveland R.G. (1964). Frictional pressure drop in two-phase flow: (a) a comparison of existing correlations for pressure loss and holdup, (b) an approach through similarity analysis.AIChE J. 10, pp. 38–51

- Fan, Z., Lusseyran, F. and Hanratty, T. J. (1993a). Initiation of slugs in horizontal gas-liquid flows. *Journal of American Institute of Chemical Engineering* . 39, 1741-1753.

- Ferschneider, G. (1983). ´Ecoulements Diphasiques Gas-Liquid á Poches et á Bouchon en Conduits. Cited in: Hale, C. P. (2000). *Slug Formation, Growth and Decay in Gas-Liquid Flow*, *chapter 3, p211.*PhD Thesis, Imperial College, London, UK, 2000.

- Foerster F and Scheil E (1936) Akustische Untersuchung der Bildung von Marten-sitnadeln (Acoustic Study of the Formation of Martensile Needels). Zeitschrift fur Metallkunde 28(9), pp245-247.

- Folkestad, T., and Mylvaganam, K. S. (1990) Acoustic measurements detect sand in North Sea flow lines. Oil and Gas, pp 33-39.

- Fossa, M. (1998). Design and Performance of a Conductance Probe for Measuring the Liquid Fraction in Two-Phase Gas-Liquid Flows. Journal of Flow Measurement and Instrumentation, 9, 103-109.

- Fournier, T., and Jeandey, C. (1993). Optimization of an experimental setup for void fraction determination by the X-ray attenuation technique. In J.M.

- Fowler, T. J., (1992) Chemical industry applications of acoustic emission. Materials Evaluation, 875-882.

- Franz G. J., (1959), Splashes as Sources of Sound in Liquids, J. Acoust. Soc. Am. 31, 1080.

- Froystein, T. (1997). Flow imaging by gamma-ray Tomography: Data processing and reconstruction techniques. Frontiers in Industrial Process Tomography II, Delft, April 8–12, 1997.

- George, D. L., Torczynski, J. R., Shollenberger, K. A. O'Hern, T. J. Ceccio, S. L., (2000). Validation of electrical-impedance tomography for measurements of material distribution in two-phase flows, International Journal of Multiphase Flow, Volume 26, Issue 4, 1 April 2000, Pages 549-581, ISSN 0301-9322,

- Govier G.W. and Aziz K.(1972), The Flow of Complex Mixtures in Pipes, Van Nostrand Reinhold, New York, N.Y (1972), p. 503

- Graham, B; Wallis, G. B. and Dobson, J. E. (1973). The onset of slugging in horizontal stratified air-water flow. *International Journal of Multiphase Flow*, 1(1), 173-193.

- Grant B. D., (1997) Sound generation and air entrainment by breaking waves in the surf zone, J. Acoust. Soc. Am. 102, 267.

- Gregory, G. A. and L. Mattar, "An In-Situ Volume Fraction Sensor for Two-Phase Flows of Non-Electrolytes", pp. 48-52, Apr.-Jun. (1973)
- Gregory, G. A., Nicholson, M., and Aziz, K., (1978), “Correlation of the Liquid Volume Fraction in the Slug for Horizontal Gas Liquid Slug Flow,” Int. J. Multiphase Flow, 4(1), pp. 33–39.

- Gregory, G.A. and Scott, D. S. (1969). Correlation of liquid slug velocity and frequency in horizontal cocurrent gas-liquid slug flow. *Journal of AIChE,* 15, 933-935.

- Gregory, G.A., Nicholson, M. and Aziz, K. (1978). Correlation of the liquid volume fraction in the slug for horizontal gas liquid slug flow. International Journal of Multiphase Flow,4(1), 33–39.

- Hale, C. P. (2000). *Slug Formation, Growth and Decay in Gas-Liquid Flow*, PhD Thesis, Imperial College, London, UK, 2000.

- Hewitt G.F. (1972), The role of experiments in two-phase systems with particular reference to measurement techniques, Progress in Heat and Mass Transfer **Vol. 6**, Pergamon Press, New York.

- Hewitt, G. F., Harrison, P. S., Parry, S. J. and Shires, G. L. (1995). Development and Testing of the 'Mixmeter' Multiphase Flowmeter. In: Proceedings of the 13th North Sea Flow Measurement Workshop, Lillehammer, Norway, October 24-26 1995.

- Hewitt, G.F. (1982), "Liquid-Gas System," In G. Hetsroni (Editor), Handbook of Multiphase Systems, chap. 2, pp. 2–1 – 2–136, McGraw-Hill Book Company, New York.

- Hinze, J.O. (1955) Fundamentals of the hydrodynamic mechanism of splitting in dispersion processes. AIChE Journal, 1 (3), p289-295.

- Hogsett, S., and Ishii, M., (1997) Local two-phase 4ow measurements using sensor techniques, Nuclear Engineering and Design, 175, 15–24.

- Holroyd T. J.,(2000), The Acoustic Emission & Ultrasonic Monitoring Handbook", First Edition, Machine & Systems Condition Monitoring Series, Coxmoor Publishing Company's. ISBN: 1 901892 018

- Hughmark, G. A.,(1962), Holdup in Gas-Liquid Flows, Chem. Eng. Prog.,58,pp 62-65

- Hutton, P.H., (1969) Detecting acoustic emission in the presence of hydraulic noise, Non-Destructive Testing, Volume 2, Issue 2, May 1969, Pages 111-115, ISSN 0029-1021.

- Imai S., Burger G. J., Lammerink T. S. J., and Fluitman J. H. J., (1997), Output characteristics of a thin-film piezoelectric AE sensor for magnetic head-disk interaction, Japan Soc. Mech. Eng. Int. J., Series C, vol. 40, no. 1, pp. 33–41.

- Ismail, I. Gamio, J. C. Zhang, Z. and Yang W.,(2004) Review of multi-phase meters for oil industry, in Proc. 4th Int. Symp. Meas. Tech. Multiphase Flows, Hangzhou, China, Sep. 10–12, 2004, vol. 1, pp. 596–601.

- Jama A. A., (2004). Wet Gas Flow Metering With Pattern Recognition Techniques, Ph.D. Thesis, University of Cranfield, UK.

- Jamaludin, N., Mba, D. and Bannister, R.H. (2001) "Condition monitoring of slow-speed rolling element bearings using stress waves", Proceedings of the Institution of Mechanical Engineers. Part E. Journal of Process Mechanical Engineering, 215: pp.245-271.

- Jantunen, E., Miettinen, J. and Ollola, A. (1993) "Maintenance and downtime costs of centrifugal pumps in Finnish Industry" in Proceedings of the The 13th International Pump Technical Conference, Pumps for a Safer Future, London, UK, pp.9-20.

- Jiaa, C.L. and Dornfeld, D.A. (1990) "Experimental studies of sliding friction and wear via acoustic emission signal analysis", Wear, 139: pp.403-424.

- Jones, O.C. and Delhaye, J.M., (1976) Transient and statistical measurement techniques for two-phase flows: a critical review, Int. J. Multiphase Flow **3** (1976), pp. 89–116.

- Kaiser J., (1950) A study of acoustic phenomena in tensile tests. Dr.-Ing. dissertation, Technical University of Munich.

- Kidin, N., Librivich, V, Roberts, J. and Vuillermoz, M. (1984) Progress in Astronautics and Aeronautics. Vol 95 pp343-355.
- Kim, J., Ahn, Y., and Kim, M.H., (2009). Measurement of void fraction and bubble speed of slug flow with three-ring conductance probes. Flow Meas. Instrum. 20(3), p.103-109

- Kordyban, E. S. and Ranov, T. (1970). Mechanism of Slug Formation in Horizontal Two-Phase Flow. *Journal of Basic Engineering.* 92, 857-864.

- Kumar S.B., Moslemian D. and Dudukovic M.P., A gamma-ray tomographic scanner for imaging voidage distribution in two-phase flow systems. Flow Measurement Instrumentation **6** (1995), pp. 61–73.

- Lamb, H. (1945) Hydrodynamics, Dover Publications, New York, 6th ed

- Lee, M.R., Lee, J.H., (2006) A study on characteristics of leak signals of pipeline using acoustic emission technique, Journal of Solid State Phenomena (110): 79-87.

- Leighton T. G., Phelps, A. D., Ramble, D. G., and Sharpe D. A. (1996), Comparison of the abilities of eight acoustic techniques to detect and

size a single bubble, Ultrasonics, Volume 34, Issue 6, August 1996, Pages 661-667

- Leighton, T. G. (1994). The acoustic bubble, London: Academic Press.

- Leighton, T.G, White, P.R. and Schneider, M.F.,(1998) The detection and dimension of bubble entrainment and comminution, Journal of the Acoustical Society of America, 103(4), 1825-1835, 1998.

- Lingard, S., Yu, C.W. and Yau, C.F. (1993) Sliding wear studies using acoustic emission, Wear of Materials: Proceedings of the 9th International Conference, Volumes 162-164: pp.597-604, Part 1, 13 April 1993, , ISSN 0043-1648.

- Lockett, M. J. , Safekourdi, A. A. (1977)., “Light Transmission Through Bubble Swarms”, AIChE Journal ,vol. 23, No. 3 ,pp. 395-398 .

- Lockhart R.W. and Martinelli R.C.,(1949) Proposed correlation of data for isothermal two-phase, two-component flow in pipes. Chem. Engng Prog. **45** (1949), pp. 39–48.

- Lubetkin, S. D. (1989), Measurement of bubble nucleation rates by an acoustic method. Journal of Applied Electrochemistry, 19(5), 668-675.
- Lynch G.F. and Segel S.1., (1977). Direct measurement of the void fraction of a two phase fluid by nuclear magnetic resonance, Int. J. Heat Mass Transfer, 20, 7-14.

- Mahalingham R., Limaye R. S., And Brink J.A., (1976), Velocity measurements in two-phase bubble-flow regime with Laser-Dopler Anemometry", AIChE J., 22, (6), ll52-1155, 1976.

- Malnes, D. (1979). Slip relations and momentum equations in two-phase flow. Cited in: Bendiksen, K. H., Malnes, D. and Nydal, O.J. (1996). On the modelling of slug flow. *Journal of Chemical Engineering Communications,* 141, 71-102.

- Malnes, D., 1982. Slug flow in vertical, horizontal and inclined pipes. V. Inst. for Energy Tech., Kjeller, Norway Report IFE/KR/E-83/002

- Manasseh R., Yoshida S. and Rudman M., (1998) Bubble Formation Processes and Bubble Acoustic Signals, Third Int. Conf. on Multiphase Flow, ICMF'98, Lyon, France.

- Manasseh, R., (2004) Passive acoustic analysis of complex bubbly flows, 16th International Congress of Chemical and Process Engineering, CHISA 2004, 22-26 August 2004, Prague - Czech Republic,Paper No.1272

- Manasseh, R., Lafontaine, R. F., Davy, J., Sheperd, I., and Zhu, Y.-G. (2001) Passive acoustic bubble sizing in sparged systems. Experiments in Fluids, Volume 30, Issue 6, pp. 672-682 (2001).

- Manasseh, R., Riboux., G. and Risso, F. (2007) Sound generation on bubble coalescence following detachment. International Journal of Multiphase Flows, 34 pp 938–949.

- Mandhane, J.M., Gregory, G.A., and Aziz, K. 1974. Aflow Pattern Map for Gas-Liquid Flow in Horizontal Pipes. International Journal of Multiphase Flow 1(1974), p 537-553.
- Mathews, J. R., (1983), Acoustic emission, Gordon and Breach Science Publishers Inc., NewYork. ISSN 0730-7152.

- Mba, D., Rao, Raj B. K. N.,(2006) Development of Acoustic Emission Technology for Condition Monitoring and Diagnosis of Rotating Machines: Bearings, Pumps, Gearboxes, Engines, and Rotating Structures. The Shock and Vibration Digest 2006 38: 3-16.

- McAllister E.W. (2009), Pipeline Rules of Thumb Handbook - Quick and Accurate Solutions to Your Everyday Pipeline Engineering Problems (7th Edition), Gulf Professional Publishing, ISBN: 1856175006.

- McNulty, P.J. (1985), PUMP HYDRAULIC NOISE: ITS USES AND CURES, Marine Engineers Review, , pp. 22-23.

- Merilo, M., Dechene, R. L. and Cichowlas, W.M. (1977). Void Fraction Measurement with a Rotating Electric Field Conductance Gauge. ASME Journal of Heat Transfer 99, 330-332.

- Meyer E. and Tamre K., Akust. Z. 4, 1945 (1939); available in English as Taylor Model Basin Translation 109.sited on, Strasberg M., (1956), Gas Bubbles as Sources of Sound in Liquids. The Journal of the Acoustic Society of America, 28(1) .

- Miller, R. K**.** (1987),(Ed.) Acoustic emission testing. ASNT Nondestructive Testing Handbook, 1987, Vol. 5 (American Society of Nondestructive Testing), ISBN: 0-931403-02-2.

- Minnaert, M., (1933) On musical air-bubbles and the sounds of running water. Philosophical Magazine, 16, 235-248.

- Mishima, K. and Ishii, M. (1980). Theoretical prediction of onset of horizontal slug flow. *Journal of Fluids Engineering, Transactions of the ASME .* 102, 441-445.

- Morozov, S. A., Kovtun, S. N., Budarin, A. A., Dvornikov, P. A., Shvetsov, D. M., Kudryaev, A. A., Belousov, P. A., (2007), Main sources of background acoustic noise of the main circulation loop in VVER-1000 reactors, Atomic Energy, Vol. 103, No. 3, 2007 , pp. 681 – 688.
- Neill, G.D., Brown, E.R. Reuben, R.L., Sandford, P.M., and Steel, J.A. (1998), "Detection of Recirculation in pumps using acoustic emission", COMADEM 1998. Monash University, Australia. 643-649.

- Neill, G.D., Reuben, R.L., Sandford, P.M., Brown, E.R. and Steel, J.A. (1997), "Detection of incipient cavitation in pumps using acoustic emission", Proceedings of the Institution of Mechanical Engineers, Part E: Journal of Process Mechanical Engineering, vol. 211 E4,pp. 267-277.

- Nevstrueva E.I. and Tyutyaev V.V. (1975), Interrelationship among two-phase pressure drop, steam void fraction and flow patterns, Int. Sem. Future Energy Prodn. Heat Transfer Problems, Dubrorvnik, Yugoslavia, 225-232 Aug 25-30, 1975.

- Nicklin, D. J., (1962), “Two-Phase Bubble Flow,” Chem. Eng. Sci., 17, pp. 693–702.

- Nishinoiri S, Enoki M (2004) Development of in-situ monitoring system for sintering of ceramics using laser AE technique. Progress in AE XII: 69-76, JSNDI

- Noma H., Ushijima, E. Ooishi, Y., (2006), Development of High-Temperature Acoustic Emission Sensor Using Aluminium Nitrade Thin Film,Journal of Advanced Materials Research ,Acoustic Emission Tesing,(Volumes 13 - 14),pp 111-116

- Nydal, O.J., Pintus, S. and Andreussi, P. (1992). Statistical characterisation of slug flow in horizontal pipes. *International Journal of Multiphase Flow*, 18(3), 439-453.

- Nyfors E, (2000). " Industrial Microwave Sensors-A Review", Subsurface Sensing Technologies and Applications, Vol. 1, No. 1,23-43

- Oguz, H. N. and Prosperetti, A. (1990) Bubble entrainment by the impact of drops on liquid surfaces. Journal of Fluid Mech. **219**, pp 143-179,

- Olsen, A.B. (1993) Framo Subsea Multiphase Flow Meter System Proc. Sem. Multiphase Meters and their Subsea Application, London, England.
- Paglianti, A., Andreussi, P.and Nydal, O. J. (1993). The Effect of Fluid Propoerties and Geometry on Void Distribution in Slug Flow. In: *Proceedings of the 6th International Conference on Multiphase Production,Cannes*, France, June 16-18, 1993.

- Pan, L., (1996) High Pressure Three-phase (gas-liquid-liquid) flow. PhD Thesis. Imperial College,London.

- Pandit, A.B., Varley, J., Thorpe, R.B. and Davidson, J.F. (1992), Measurement of Bubble Size Distribution: An Acoustic Technique. Chemical Engineering Science, Vol. 47, No. 5, pp1079-1089.

- Pike E.R., Jackson O. A., Bourke P.J. and Page D.I.,(1967) Measurement of turbulent velocities from the Doppler shift in scattered laser light, AERE-R5648' 1967'

- Pumphrey, H. C. and Crum, L.A., (1989) Sources of ambient noise in the ocean and experimental investigation, Technical Report NCPA LC.011989, University of Mississippi.

- Reis, E. d. and Goldstein Jr. L., (2005) A non-intrusive probe for profile and velocity measurement in horizontal slug flows. Journal of Flow Measurement and Instrumentation, 16 (4), 229-239.

- Richardson E.G., (1948), The Impact of a Solid on a Liquid Surface, Proceedings of the Physical Society, 61, 352.

- Roberts, T. M., Talebzadeh, M.,(2003) Acoustic emission monitoring of fatigue crack propagation, Journal of Constructional Steel Research, Volume 59, Issue 6, June 2003, Pages 695-712, ISSN 0143-974X.

- Ruffer, H.M., Bröring S. and Schugerl K., (1995) Fluid dynamic characterization of airlift tower loop bioreactors with and without motionless mixtures, Bioprocess Engineering 12 (1995), pp. 119–130.

- Rzesotarska, J., Rejmund, F., and Ranachowski, P., (1998) Acoustic emission measurement of foam evolution in H_2 O-C_2 H_5 OH-air systems with content of detergent triton X-100, Ultrasonics, 36, 953-958.

- Schiebe, F. R., 1969, The influence of gas nuclei size distribution on transient cavitation near inception. Project No. 107, St. Anthony Falls Hydraulic Laboratory, University of Minnesota.
- Schmitz D. and Mewes D. (2000), Tomographic imaging of transient multiphase flow in bubble columns. Chemical Engineering Journal **77** (2000), pp. 99–104.

- Schofield, B.H. (1961) Acoustic emission under applied stress. Report ARL-150, Lessels and Associates, Boston.

- Serizawa A., Kataoka I., And Michiyoshi I., (1975), Turbulence structure of air-water bubbly flow. measuring techniques, International Journal of Multiphase Flow, Volume 2, Issue 3, December 1975, Pages 221-233.

- Sharma N.D. and Sachdeva M.M.,(1976), An air lift pump performance study, AICHE J. **32**(1976), pp. 61–64.

- Shearer, C.J. and Nedderman, R.M.: "Pressure Gradient and Liquid Film Thickness in Co-Current Upwards Flow of Gas/Liquid Mixtures: Application of Film-Cooler Design," Chem. Eng. Sci. (July 1965)20. 671-683.

- Sikorska J.Z. and Hodkiewicz M. 2005 Comparison of Acoustic, Vibration and Dynamic Pressure Measurement for Detecting Change in Flow Conditions on a Centrifugal pump. Proceedings of the 18th International Congress on Condition Monitoring and Diagnostic Engineering Management (COMADEM), Cranfield, UK.

- Sikorska J.Z., (2006) The application of Acoustic Emission monitoring to the detection of flow conditions of centrifugal pumps, PhD thesis, University of western of Australia

- Stiffler R. and. Henneke E.G, (1983), The application of polyvinylidene fluoride as an acoustic emission transducer for fibrous composite materials. Mater. Evaluat. 41, 8 pp. 956–960.

- Strasberg M., (1956), Gas Bubbles as Sources of Sound in Liquids. The Journal of the Acoustic Society of America, 28(1).

- Taitel, Y. and Dukler, A. E. (1976). A model for predicting flow regime transitions in horizontal and near horizontal gas-flow. *Journal of American Institute of Chemical Engineering*. 22(1), 47-55.

- Terrill, E.J. Melville W.K.,(2000) A Broadband Acoustic Technique for Measuring Bubble Size Distributions: Laboratory and Shallow Water

Measurements, Journal of Atmospheric and Oceanic Technology 2000 17:2, 220-239.

- Thorn, R., Johansen, G. A., and Hammer, E. A. (1997). Recent developments in three phase flow measurement. Measurement Science and Technology, 8(7), 691–701.

- Tily, P. J., Porada, S., Scruby, C. B., and Lidington, S., (1987). Monitoring of mixing processes using acoustic emission, fluid mixing III, Bradford, September 8-10, Symposium Series no. 108, pp. 75-94.

- Tsujimoto, H., Yokoyama, T., Hang, C.C. and Sekiguchi, I. (2000) Monitoring particle fluidisation in a fluidised bed granulator with an acoustic emission sensor. Powder Technology, Volume 113, Number 1, 20 November 2000 , pp. 88-96(9)

- Tuss, B., Perry, D. and Shoup, G. (1996). Field tests of the high gas volume fraction multiphase meter. In: Proceedings of the SPE Annual Technical Conference and Exhibition. Denver, USA, October 6-9, 1996, SPE Paper 36594.

- Utiger, M., StNuber, F., Duquenne, A. M., Delmas, H., and Guy, C. (1999). Local measurements for the study of external loop airlift hydrodynamics. Canadian Journal of Chemical Engineering, 77, 375–382.

- Van Ooijen, J. A. C., van Tooren, E., and Reedijk, J. (1978). Acoustic emission during the preparation of dichloro (pyrazine) zinc(II). Journal of the American Chemical Society, 100(17), 5569-5570.

- Vergniolle, S., G. Brandeis, and J.C. Mareschal (1996), Strombolian explosions: 2. Eruption dynamics determined from acoustic measurements, J. Geophys. Res., 101(B9), 20,449–20,466.

- Walter J.F. and Blanch H.W. (1986) Bubble break-up in gas–liquid bioreactors: break-up in turbulent flows, Chemical Engineering Journal **32** pB7-B17.

- Warsito M., Ohkawa N., Kawata S. and Uchida S., (1999) Cross-sectional distributions of gas and solid holdups in slurry bubble column investigated by ultrasonic computed tomography. Chemical Engineering Science **54** 21 (1999), pp. 4711–4728.

- Withers, P.M. (1996) Ultrasonic, acoustic and optical techniques for the non-invasive detection of fouling in food processing equipment, Trends in Food Science & Technology, Volume 7, Issue 9, Pp293-298, ISSN 0924-2244.

- Woldesemayat, MA. Ghajar, AJ. (2007) Comparison of Void Fraction Correlations for Different Flow Patterns in Horizontal and Upward Inclined Pipes. *International Journal of Multiphase Flow,* vol. 33, no. 4, pp. 347–370, 2007

- Xie, C.G. (2005) Review of multiphase flow measurement in the oil–gas industry, in Proc. Int. Workshop Process Tomography, Beijing, China,Apr. 15–23,2005.

- Xie, C.G., Stott, A. L., Plaskowski, A., and Beck.,M. S.(1990),Design of Capacitance Electrodes for Concentration Measurement of Two-Phase Flow. Meas. Science & Technology 1, p.65-78, 1990.

- Yang, W. Q. and Beck, M. S. (1997). An intelligent cross correlation for pipelines flow velocity measurement. Journal of Flow Measurement and Instrumentation, 8(2), 77-84.

- Zhang, H. -Q., Wang, Q., Sarica, C., and Brill, J. P., (2003), “Unified Model for Gas-Liquid Pipe Flow Via Slug Dynamics—Part 2: Model Validation,” ASME J. Energy Resour. Technol., 125, pp. 266–273.

- Zhang, H.J., YUE W.T. and HUANG, Z.Y. (2005). Investigation of Oil-Air Two-Phase Mass Flow rate Measurement using Venturi and Void Fraction Sensor. Journal of Zhejiang University SCIENCE,6A(6),601-606.

APPENDICES

Appendix A PUBLICATIONS

• Journal Papers

1. Al-lababidi, S., Addali, A., Yeung, H., Mba, D. and Khan. F. (2009), Gas void fraction measurement in two-phase gas/liquid slug flow using Acoustic Emission technology, ASME: Journal of Vibration and Acoustics. 131, 064501 (2009).

2. Addali, A., Al-lababidi, S., Yeung, H., Mba, D. and Khan. F. (2010), Acoustic Emission and gas phase measurements in two-phase flow, Proceedings of the Institution of Mechanical Engineers, Part E, Journal of Process Mechanical Engineering, Accepted for publication and In-press.2010

3. Al-Balushi, R., Addali, A., Charnley, B. and Mba, D. (2009), Energy Index technique for detection of acoustic emissions associated with incipient bearing failures, Journal of Applied Acoustics, Accepted for publication and In-press.2010

• Conference Papers

1. Addali, A., Al-Lababidi, S., Yeung, H. and Mba, D. (2009), Measurement of Gas content in two-phase flow with Acoustic Emission, In the 4th World Congress on Engineering Asset Management (WCEAM 2009) Athens , Greece, 28 - 30 September 2009.

2. Addali A., Mba, D., Al-Lababidi, S. and Yeung, H., Observation of Acoustic Emission in two-phase Flow. 21st International **(**Comadem 2008), Prague, Czech Republic, 11 – 13 JUNE 2008.

3. Addali, A., Al-Lababidi, S. and Mba, D., An attempt to correlate Gas Void Fraction with Acoustic Emission generated from two-phase air/water flow in the Fifth International Conference on Condition Monitoring and Machinery Failure Prevention Technologies (CM 2008 and MFPT 2008). The Edinburgh Conference Centre, Heriot-Watt University, Edinburgh, UK, 15-18 July 2008.

4. Addali, A., Al-Lababidi, S. and Mba, D., Application of Acoustic Emission to monitoring two phase flow in Second World Congress on Engineering Asset Management and the Fourth International Conference on Condition Monitoring. Harrogate, UK, 11-14 June 2007, pp. 10-16. ISBN: 978-1-901892-22-2.

Appendix B

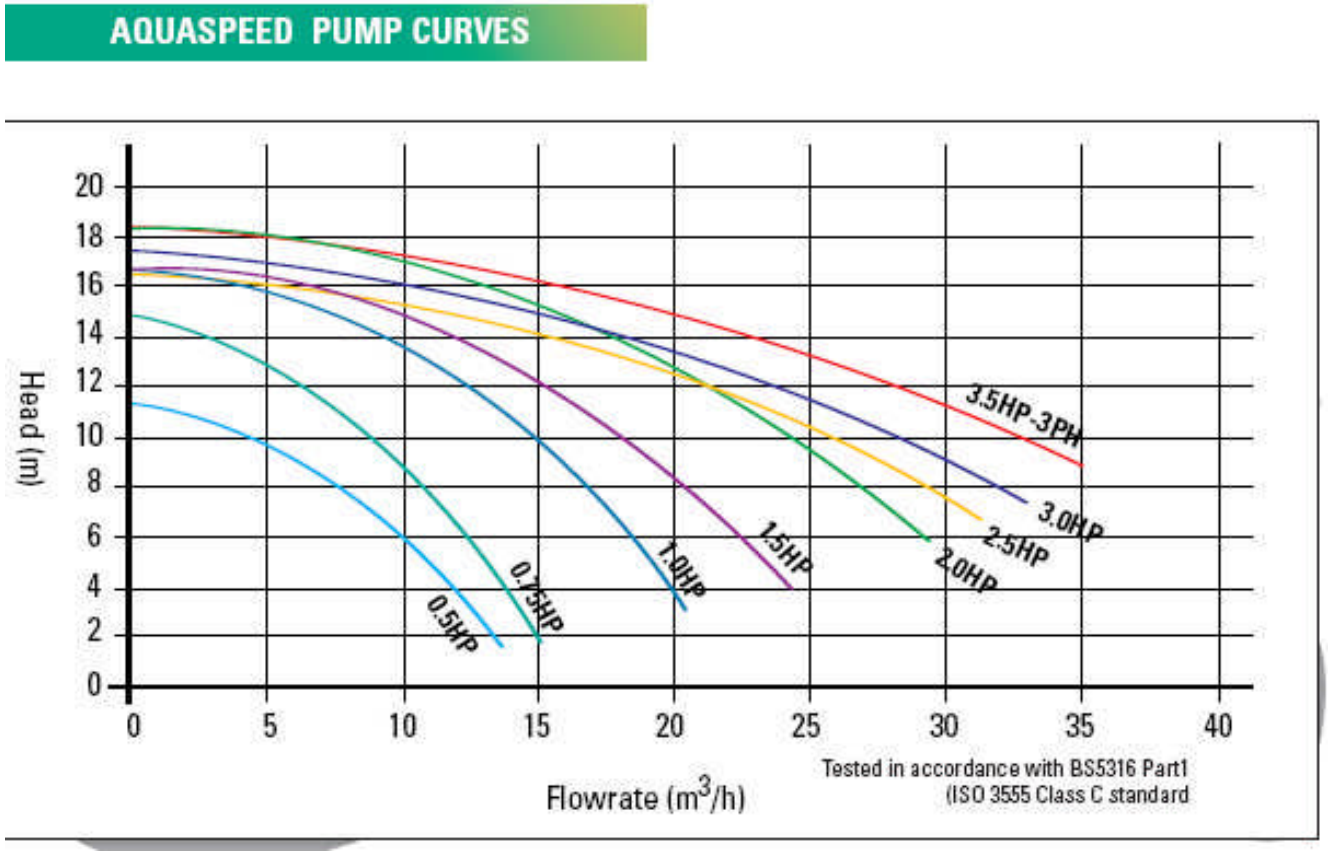

Figure A-1: Pump curve of Certikin Aquaspeed 0.75kW (1HP)

Appendix C

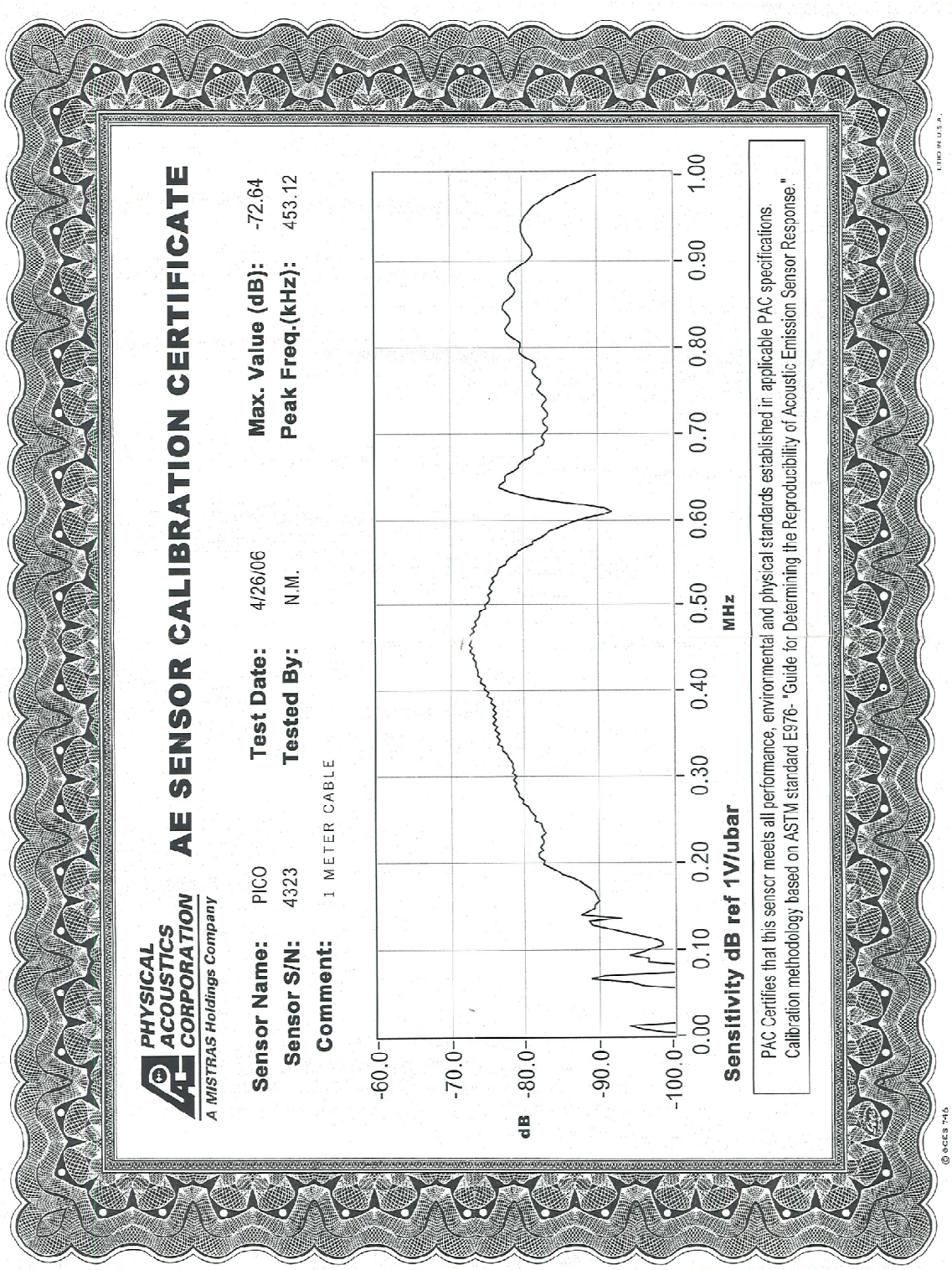

Figure C-1: Calibration Certificate for PICO type sensor

Figure C-2: Calibration Certificate for WD type sensor

Appendix D

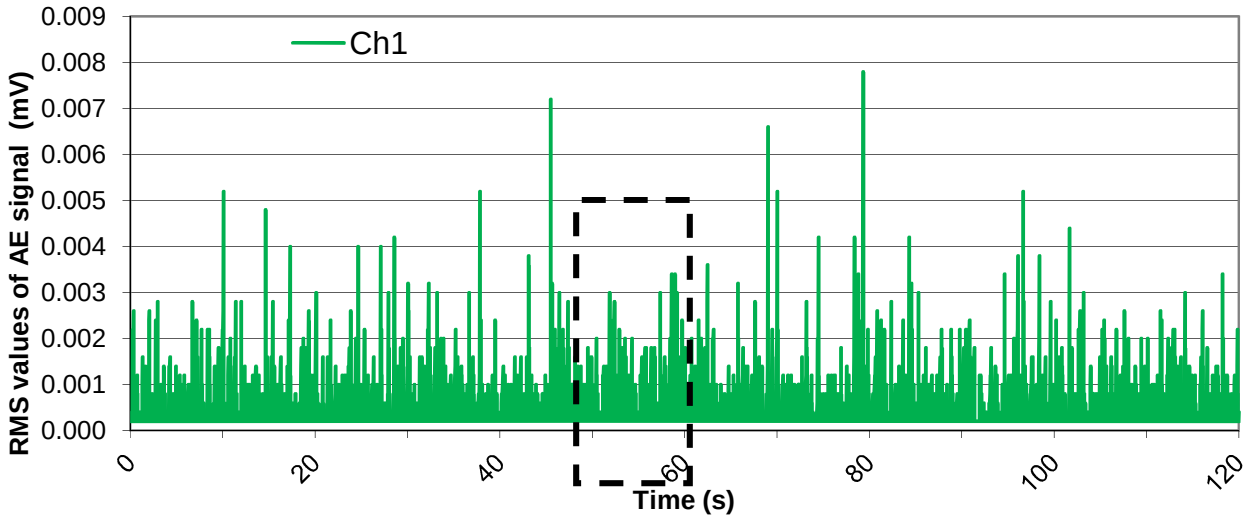

Figure D-1: RMS of AE levels at V_{SL}=1.1 ms^{-1} and V_{SG} = 0.8 ms^{-1}

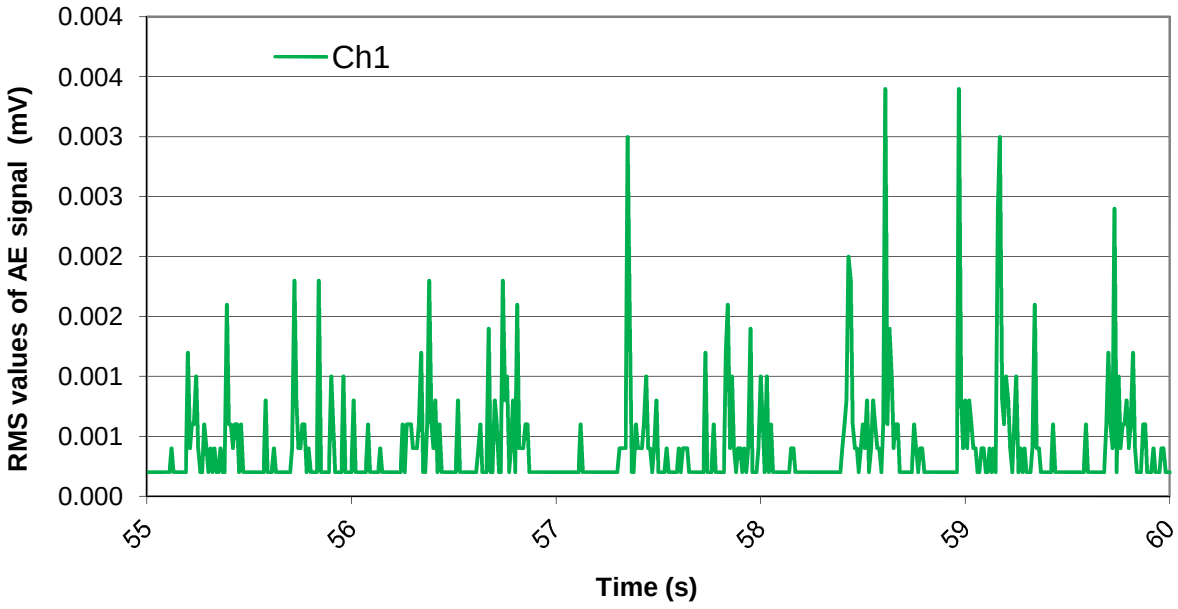

FigureD-2: RMS of AE levels of time 55-60 seconds of figure D-1

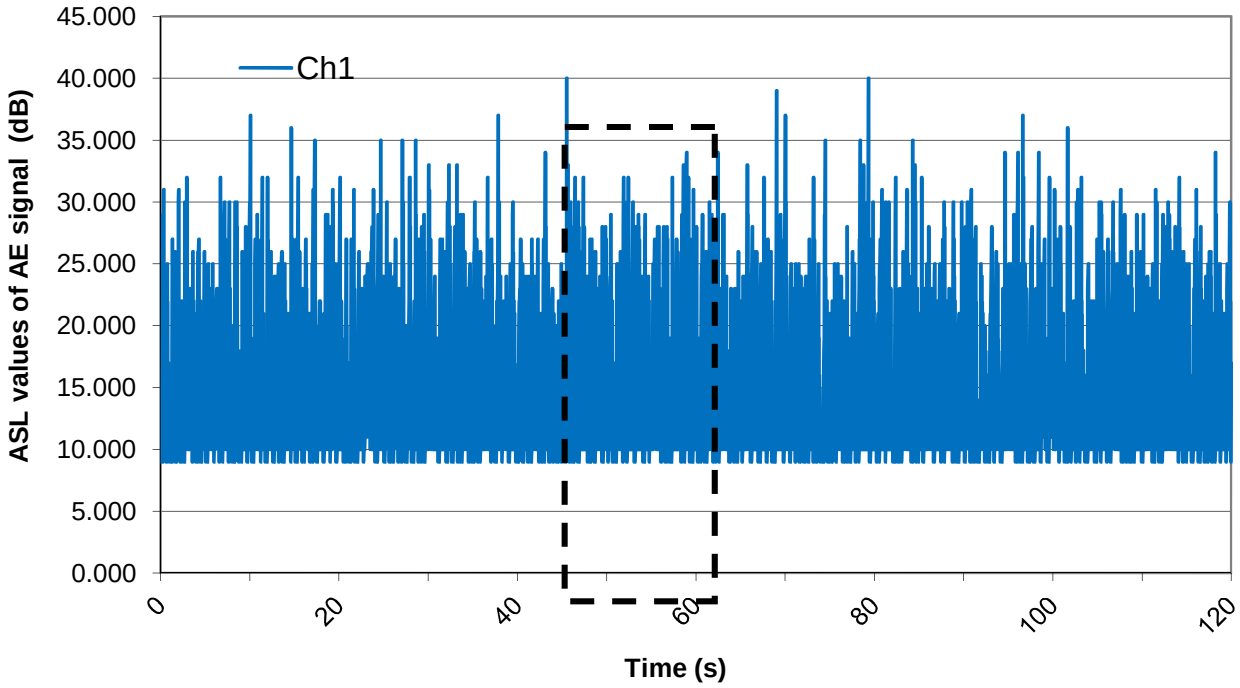

Figure D-3 ASL of AE levels at V_{SL}=1.1 ms^{-1} and V_{SG} = 0.8 ms^{-1}

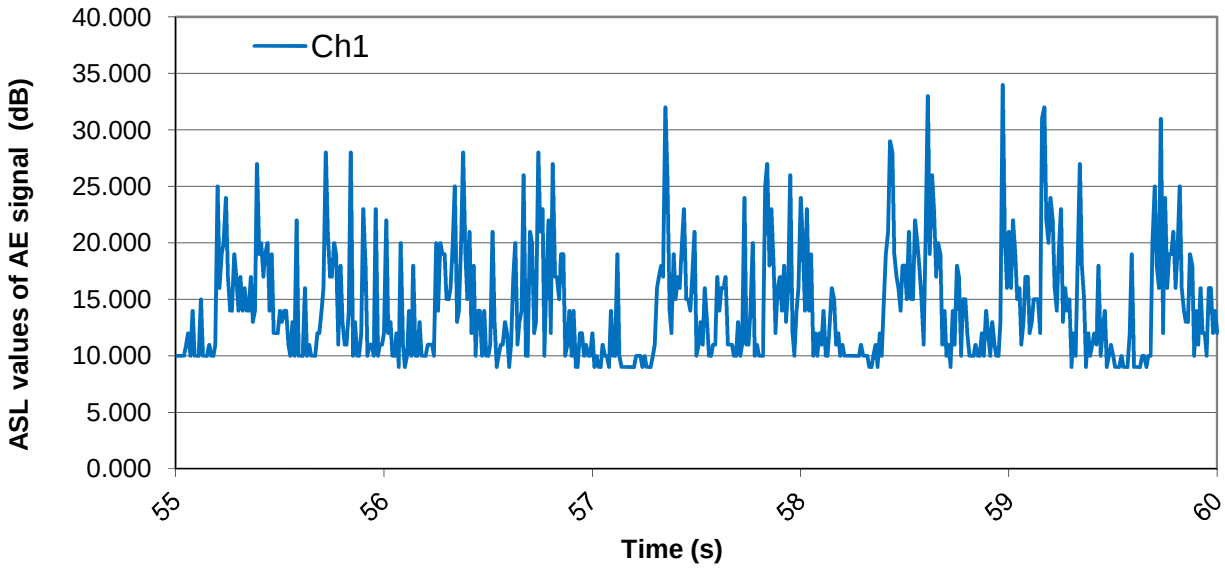

Figure D-4: ASL of AE levels of time 55-60 seconds of figure D-3

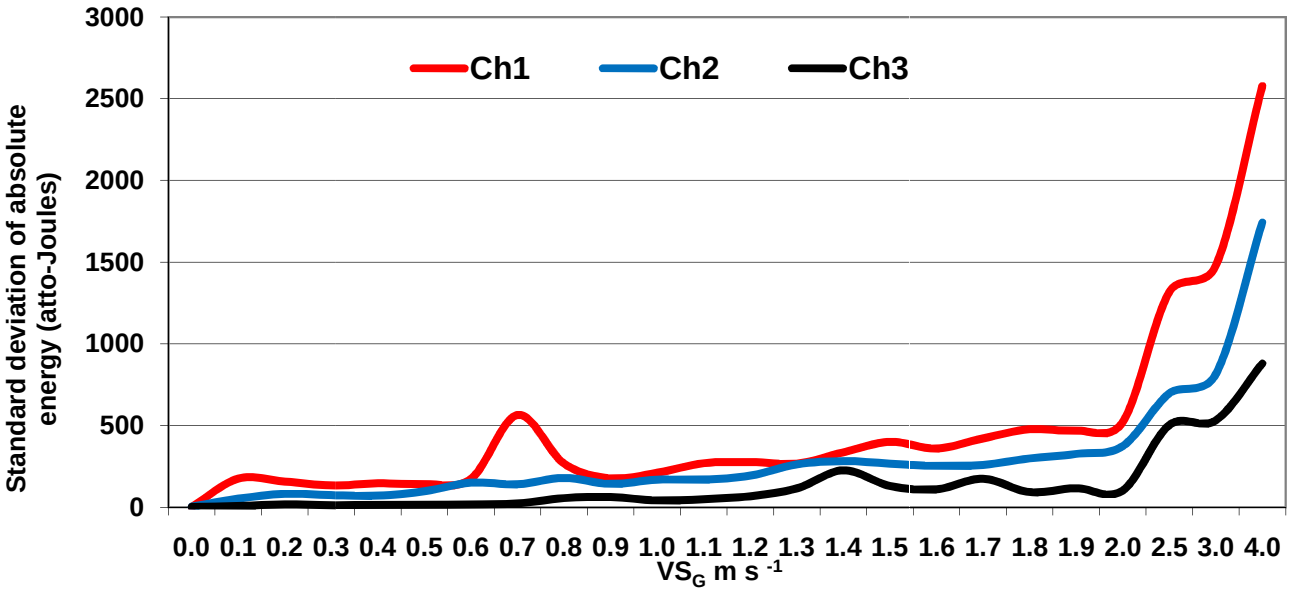

FigureD-5: Standard deviation of absolute energy of AE level for Varying V_{SG} and at V_{SL} =1.1ms^{-1}

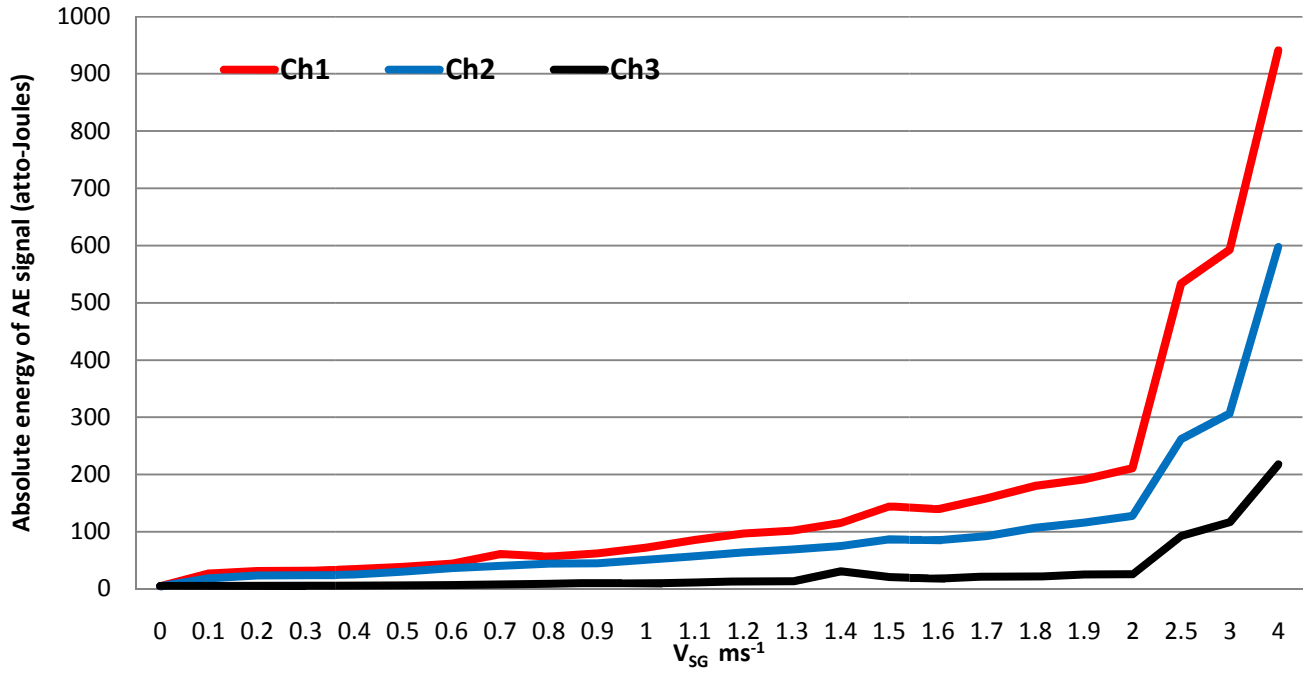

FigureD-6: Average values for absolute energy of AE signal for Varying V_{SG} and at V_{SL} =1.1ms^{-1}

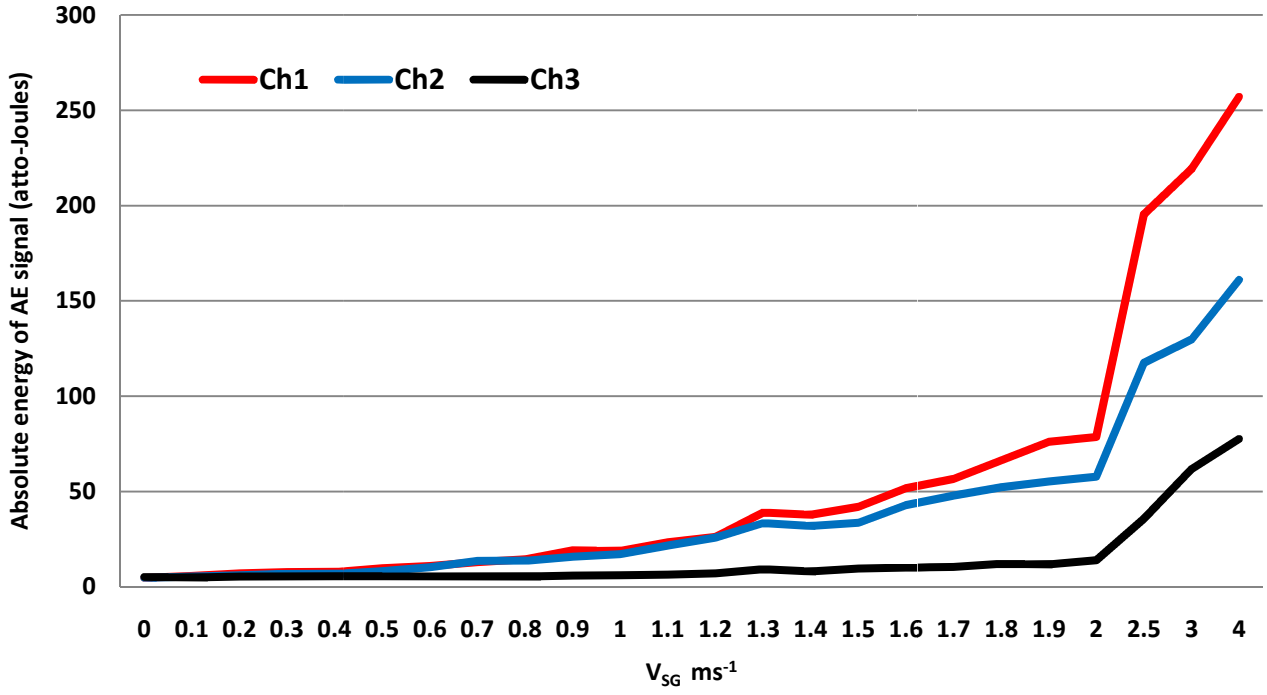

FigureD-7: Average values for absolute energy of AE signal for Varying V_{SG} and at V_{SL} =0.5ms^{-1}

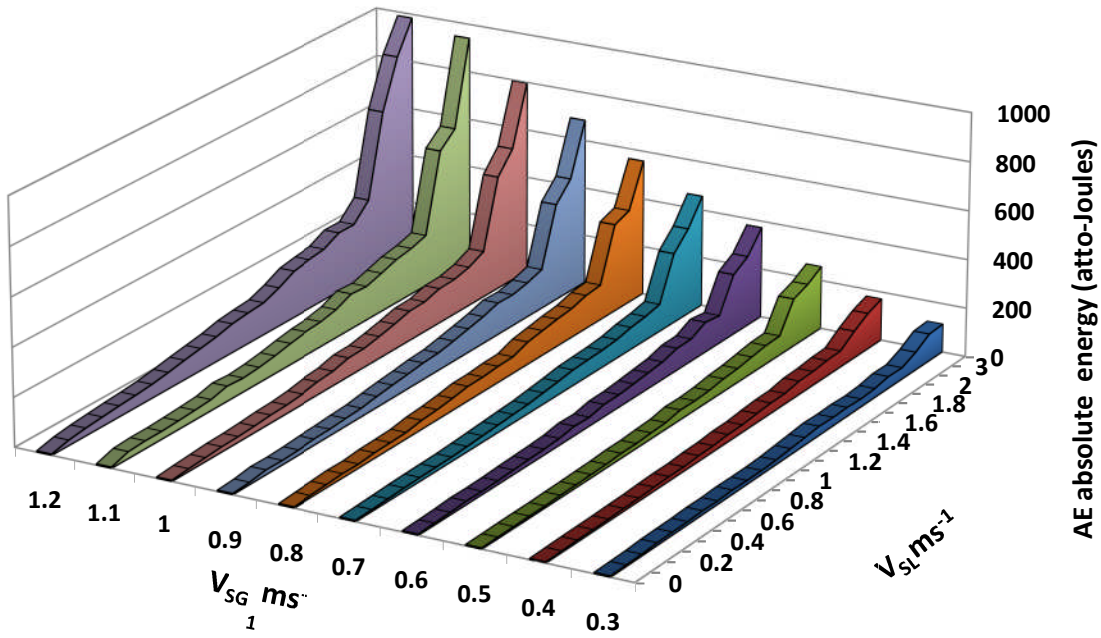

Figure D-8: Waterfall plot for AE abs. energy level acquired from the top steel pipe sensor for the Test Campaigns of initial investigative test rig

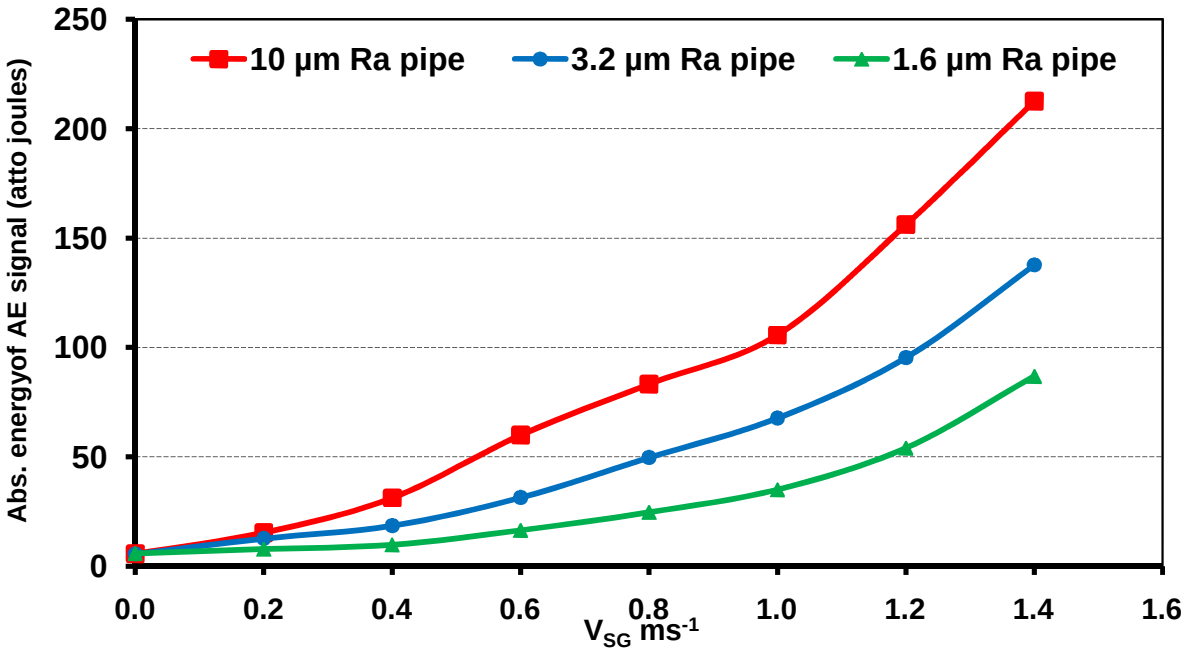

Figure D-9: AE energy of Ch1 from three surface roughness grades at V_{SL}=1.0 ms^{-1}

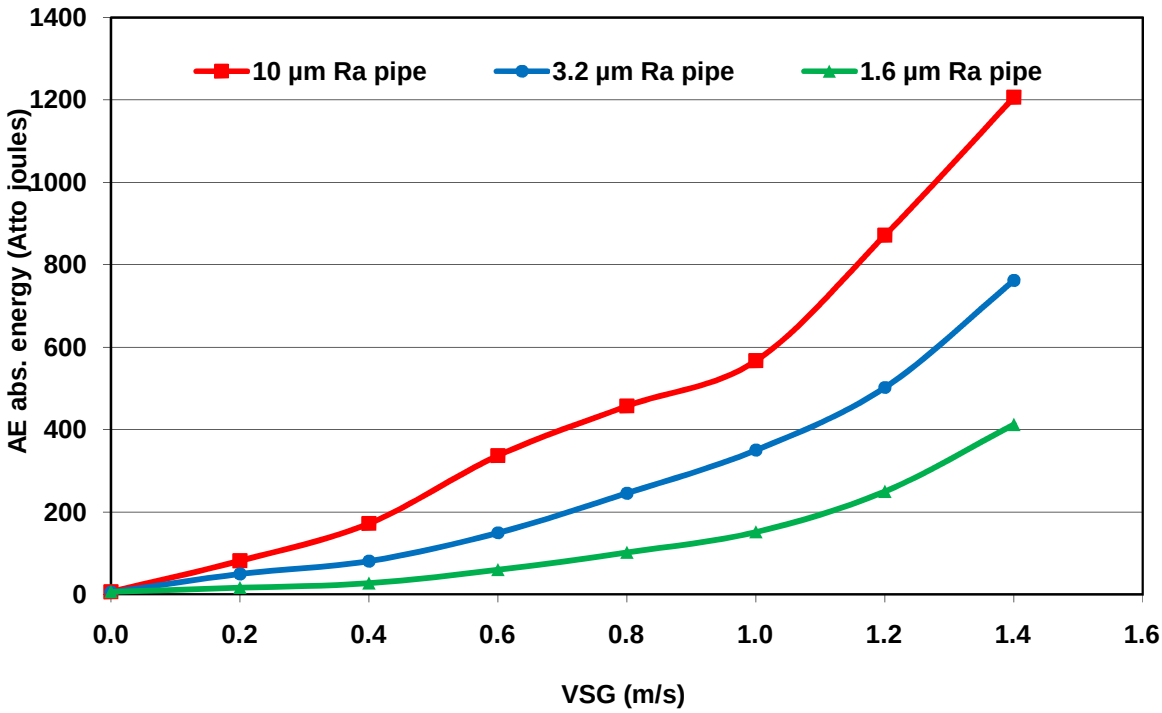

Figure D-10:**AE energy of Ch2 from three surface roughness grades at V_{SL}=1.0 ms^{-1}**